Multiterminal Source-Channel Coding

Rate and Outage Analysis

Wolf

Technische Universität Dresden

Multiterminal Source-Channel Coding: Rate and Outage Analysis

Albrecht Wolf

der Fakultät Elektrotechnik und Informationstechnik der
Technischen Universität Dresden
zur Erlangung des akademischen Grades

Doktoringenieur

(Dr.-Ing.)

genehmigte Dissertation

Vorsitzender:	Prof. Dr.-Ing. habil. Frank Ellinger
Gutachter:	Prof. Dr.-Ing. Dr. h.c. Gerhard Fettweis
	Prof. Dr. Markku Juntti

Tag der Einreichung: 04.02.2019
Tag der Verteidigung: 04.06.2019

Abstract

Cooperative communication is seen as a key concept to achieve ultra-reliable communication in upcoming fifth-generation mobile networks (5G). A promising cooperative communication concept is multiterminal source-channel coding, which attracted recent attention in the research community.

This thesis lays theoretical foundations for understanding the performance of multiterminal source-channel codes in a vast variety of cooperative communication networks. To this end, we decouple the multiterminal source-channel code into a multiterminal source code and multiple point-to-point channel codes. This way, we are able to adjust the multiterminal source code to any cooperative communication network without modification of the channel codes. We analyse the performance in terms of the outage probability in two steps: at first, we evaluate the instantaneous performance of the multiterminal source-channel codes for fixed channel realizations; and secondly, we average the instantaneous performance over the fading process. Based on the performance analysis, we evaluate the performance of multiterminal source-channel codes in three cooperative communication networks, namely relay, wireless sensor, and multi-connectivity networks. For all three networks, we identify the corresponding multiterminal source code and analyse its performance by the rate region for binary memoryless sources. Based on the rate region, we derive the outage probability for additive white Gaussian noise channels with quasi-static Rayleigh fading. We find results for the exact outage probability in integral form and closed-form solutions for the asymptotic outage probability at high signal-to-noise ratio.

The importance of our results is fourfold: (i) we give the ultimate performance limits of the cooperative communication networks under investigation; (ii) the optimality of practical schemes can be evaluated with respect to our results, (iii) our results are suitable for link-level abstraction which reduces complexity in network-level simulation; and (iv) our results demonstrate that all three cooperative communication networks are key technologies to

enable 5G applications, such as device to device and machine to machine communications, internet of things, and internet of vehicles.

In addition, we evaluate the performance improvement of multiterminal source-channel codes over other (non-)cooperative communications concepts in terms of the transmit power reduction given a certain outage probability level. Moreover, we compare our theoretical results to simulated frame-error-rates of practical coding schemes. Our results manifest the superiority of multiterminal source-channel codes over other (non-)cooperative communications concepts.

Kurzfassung

Kooperative Kommunikation gilt als Schlüsselkonzept der aufstrebenden fünften Generation mobiler Netzwerke (5G), um sehr zuverlässige Kommunikation zu ermöglichen. Multiterminal Source-Channel Codierung ist ein vielversprechendes Konzept der kooperativen Kommunikation, welchem in der Forschungsgemeinschaft momentan viel Aufmerksamkeit gewidmet wird.

Diese Dissertation beschäftigt sich mit den theoretischen Grundlagen des Leistungsvermögens von Multiterminal Source-Channel Codierung in verschiedenen Varianten kooperativer Kommunikationsnetzwerke. Zu diesem Zweck trennen wir den Multiterminal Source-Channel Code in einen Multiterminal Source Code und in mehrere Punkt-zu-Punkt Channel Codes. Dadurch können wir den Multiterminal Source Code an verschiedene kooperative Kommunikationsnetzwerke adaptieren, ohne die Channel Codes ändern zu müssen. Die Leistungsfähigkeit bezüglich der Ausfallwahrscheinlichkeit analysieren wir in zwei Schritten: zunächst beurteilen wir die unmittelbare Leistungsfähigkeit der Multiterminal Source-Channel Codes für feststehende Kanalrealisierung; weiterhin berechnen wir die mittlere unmittelbare Leistungsfähigkeit in Abhängigkeit des Schwundkanals. Aufbauend auf diese Leistungsfähigkeitsanalyse beurteilen wir die Leistungsfähigkeit von Multiterminal Source-Channel Codes in drei kooperativen Kommunikationsnetzwerken: Relay, Wireless Sensoren und Multi-Connectivity Netzwerke. Für alle drei Netzwerke identifizieren wir den korrespondierenden Multiterminal Source Code und analysieren seine Leistungsfähigkeit anhand der Ratenregionen für binäre gedächtnislose Quellen. Basierend auf dieser Ratenregion, können wir die Ausfallwahrscheinlichkeit für additive weiße gaußsche Rauschkanäle mit quasistatischem Rayleigh-Fading ableiten. Wir stellen für die exakte Ausfallwahrscheinlichkeit Werte in Integralform fest, für die asymptotische Ausfallwahrscheinlichkeit eine geschlossene Lösung bei hohem Signal-Rausch-Verhältnis.

Unsere Ergebnisse sind in vierfacher Weise relevant: (i) Wir berichten die ultimativen Leistungsgrenzen der untersuchten kooperativen Kommunikationsnetzwerke. (ii) Mit Hilfe unserer Ergebnisse kann die Optimalität von praktischen Codierungsschemata beurteilt werden. (iii) Unsere Ergebnisse können der Link-level Abstraktion dienen, wodurch die Komplexität von Simulationen auf Netzwerkebene reduziert wird. (iv) Unsere Ergebnisse zeigen, dass alle drei untersuchten kooperativen Kommunikationsnetzwerke

Schlüsseltechnologien darstellen, um 5G Applikationen zu ermöglichen, wie sie in der D2D- und M2M-Kommunikation, dem Internet der Dinge und Fahrzeugnetzwerken von Nöten sind.

Außerdem untersuchen wir die Leistungssteigerung durch Multiterminal Source-Channel Codierungen im Vergleich zu anderen (nicht-)kooperativen Kommunikationskonzepten im Hinblick auf die Reduktion der Übertragungsleistung bei bestimmten Ausfallwahrscheinlichkeiten. Darüber hinaus vergleichen wir unsere theoretischen Ergebnisse mit simulierten Paketfehlerhäufigkeiten von praktischen Codierungsschemata. Unsere Arbeit unterstreicht die Überlegenheit von Multiterminal Source-Channel Codierungen im Vergleich zu anderen (nicht-)kooperativen Kommunikationskonzepten.

Acknowledgement

First of all, I would like to express my deepest gratitude to my doctoral advisor, Gerhard Fettweis, who gave me continuous support and advice during my work and study at Vodafone Chair Mobile Communications Systems, TU Dresden. I would also like to thank Prof. Markku Juntti for reviewing this work as my second supervisor.

I am highly indebted to Meik Dörpinghaus and José Cândido Silveira Santos Filho for sharing their knowledge and wisdom on information and communication theory. Many of the results in this work were inspired during our fruitful discussions.

I further express my thanks to Tadashi Matsumoto, who brought my attention to the very interesting topic of multiterminal source-channel coding. Many results in this thesis are based on his research.

My special thanks goes to my colleagues and co-authors Philipp Schulz, Nick Schwarzenberg, Diana Cristina González, Maximilian Matthé, and Lin Zhou. I enjoyed the fruitful discussions about research problems and our collaborative work has broaden my horizon.

Contents

Introduction 1

1.1 Motivation and Background

The evolution of fifth-generation mobile networks (5G) is driven by a wide variety of new emerging application scenarios, like device to device (D2D) and machine to machine (M2M) communications, internet of things (IoT), internet of vehicles (IoV), etc. [ARS16]. The applications requirements range from enhanced data rates and energy efficiency to high reliability and low latency [Mal16].

As a first step, we discuss some applications and their requirements in detail:

1. *Scenarios with high reliability and challenging channel conditions:* Providing connectivity everywhere, including highways and remote low-populated areas, in order to enable IoV applications, is a challenging task. The high speed of the cars and the rich scattering environment lead to dispersive channels, which impair reliable communication. Moreover, dynamic topology changes can compound the communication [Zho13].

2. *Scenarios with high reliability and energy efficiency:* For IoT applications, such as environmental monitoring, sensor nodes are usually densely deployed in a field, periodically collecting local data from a certain physical or environmental phenomenon of interest, and reliably reporting those observations to a fusion center (FC). However, the operational lifetime of wireless sensors is essentially determined by their battery life, since they are equipped with small embedded batteries which in the majority of scenarios are difficult to charge or replace [AY07]. Consequently, energy efficiency is a critical requirement for environment monitoring.

3. *Scenarios with high reliability and low latency:* An application example is to wirelessly control a robot in a factory hall [Ehr+17], where the robot receives motion control updates at a regular time interval. Depending on the robot task, round-trip latency of less than $1\,\mathrm{ms}$ and application error-rates down to 10^{-9} [Sch+17] are demanded. Again, the

rich scattering environment of a factory hall impairs reliable wireless communication.

Suitable wireless networks of all three applications face a common challenge: ensure reliable communication at any time, while obeying additional constraint(s), e.g., low latency or energy efficiency. Subsequently, we introduce suitable communication networks to cope with theses requirements.

Cooperative Communication   Cooperative communication in wireless networks has proved to be an effective technique that enables single-antenna users to share their antennas in order to create a virtual multiple-input multiple-output (MIMO) system, and thus, providing some type of diversity in wireless networks [Li09]. In general, diversity is a prevalent way to mitigate fading effects yielding reliable communication. Microdiversity [Mol12], including time, spatial and frequency diversity, is well suited to combat small-scale fading. However, microdiversity might not be suitable for combating large-scale fading, which is created by shadowing effects. Shadowing is almost independent of the frequency band, and therefore frequency diversity proves then ineffective. Spatial diversity could be used, but the correlation distances for large-scale fading can be greater than ten or even hundred meters. Thus, macrodiversity [Mol12], where large distances between antennas exist, proves more appropriate to combat large-scale fading.

For all three applications mentioned before, cooperative communication networks are known to exploit some type of diversity yielding reliable communications over fading channels.

Relay Network   For application 1), IoV communications based on relaying are a promising solution to ensure reliability at acceptable levels via macrodiversity. A prominent concept for relay networks is decode-and-forward (DF), where the relay decodes the received message from the source and than re-encodes it before transmitting the message to the destination. The decoded message is discarded by the relay whenever an error is detected [BH06]. However, by allowing erroneous messages to be forwarded to the destination, an improved error rate performance can be achieved, as shown in [AM12], a concept referred to as lossy forwarding (LF) (the notion of allowable intra-link errors between source and relay was first introduced in [GFZ05]). The principle of LF is based on multiterminal source-channel codes (MSCCs). The central idea is that an erroneous relay message is still somewhat correlated to the source message, thus serving as valuable side information in the decoding
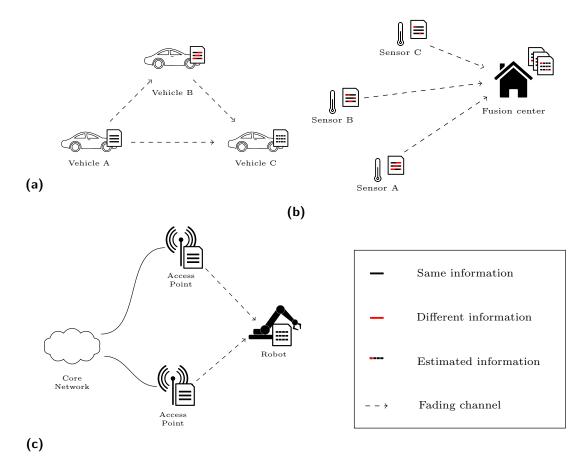
Fig. 1.1. Cooperative communication networks provide some type of diversity to mitigate fading effects yielding reliable communication. In this thesis, we consider three cooperative communication networks, namely, (a) relay network, (b) wireless sensor network, and (c) multi-connectivity network.

process at the destination. A schematic diagram of a relay network is shown in Fig. 1.1a.

Wireless Sensor Network For application 2), the sensors are in general densely concentrated, with each cluster presenting an elevated degree of spatial correlation among the measured data [JP04]. The presence of mutually correlated sensing data can be exploited by MSCCs, to improve the reliability of wireless sensor networks (WSNs) via macrodiversity, which in turn leads to a higher energy efficiency compared to non-cooperative concepts. A schematic diagram of WSN is shown in Fig. 1.1b

Multi-Connectivity Network For application 3), multi-connectivity (MCo) is a promising tool for boosting the reliability and capacity of wireless networks [Öhm17]. At first, it provides a flexible communication framework that can trade diversity for multiplexing via multiple routes to the destination (see Fig. 1.1c). Secondly, MCo networks can use spatial and frequency macrodiversity, such that multiple copies of the same information can, in the best case, be delivered within a single time slot. Concepts such as selection combining (SC), maximal-ratio combining (MRC), and MSCC can be used to exploit the diversity.

In all three cooperative communication networks MSCCs can be used to exploit the diversity yielding an improved performance. This great range of application make MSCCs a promising concept for 5G, and thus, MSCCs attracted recent attention in the research community.

Ultimately, communication concepts are evaluated based on their fundamental performance limits. These limits are a prevalent way to understand the communication concept itself, the interplay between system parameters, and to evaluate practical coding schemes. To the best of our knowledge, the fundamental performance limits of MSCCs for the referred networks have been unknown so far.

1.2 Outline

This thesis contributes fundamental limits of the MSCC reliability performance in the referred cooperative communication networks. We quantify the reliability performance in terms of the outage probability of MSCCs based on an approach proposed by Matsumoto et al [CAM13a; Zho+14].

To this end, we decouple the MSCC into one multiterminal source code and multiple point-to-point channel codes, which is optimal for parallel channels and infinite blocklength [XL07]. This source-channel separation is quite appealing from a practical standpoint, since it implies that the multiterminal source coding can be performed without channel knowledge and the point-to-point channel coding without knowledge of the source correlation. The multiterminal source code defines the minimum set of rates (a.k.a. the rate region) at which the terminal encoders can communicate with the destination decoder while still conveying enough information for lossless reconstruction of the sources. The rate region differs for the referred cooperative communication networks. The first major contribution of this thesis is to identify

and derive the exact rate region for the cooperative communication networks under investigation.

In this work we consider parallel additive white Gaussian noise (AWGN) channels with quasi-static Rayleigh fading. The outage probability is an important concept in fading channels, which provides a way to characterize the performance of communication systems. For point-to-point communication, an outage event occurs if the instantaneous channel capacity is less than the desired rate. The same is true for multipoint-to-point communication, i.e., an outage event occurs if the set of the instantaneous channel capacities is outside the rate region. The second major contribution of this thesis is to derive the outage probability for parallel AWGN channels with quasi-static Rayleigh fading for the cooperative communication networks under investigation. We find results for the exact outage probability in integral form and closed-form solutions for the asymptotic outage probability at high signal-to-noise ratio (SNR).

Our results are a good performances indicator to evaluate the reliability of MSCC in light of ultra-reliable applications. In fact, we derive simple and insightful closed-form expressions depending on system parameters that can be easily used to assess or optimize practical cooperative communication deployments. To this end, a high SNR analysis turns out to be a strong candidate, as it offers a simple yet in-depth characterization of the system performance's general trend. Furthermore, our results are well suited for physical layer abstraction, which reduces computational complexity in higher layer simulations.

The remainder of this thesis is structured as follows.

- In Chapter 2, we give an unified solution framework, which enables the analysis of all three cooperative communication networks under investigation in the subsequent chapters. At first, we review the relevant network information theoretical concepts for the performance analysis. Secondly, we define a general MSCC, which can be adapted to the referred cooperative communication networks. Thirdly, we introduce the channel model and define the outage probability. Fourthly, we outline a practical distributed turbo code (DTC), which can be deployed in all three cooperative communication networks. Finally, we comprehensively outline our main contributions in this thesis.

- Chapters 3-5 are the main part of this thesis. Each chapter corresponds to one cooperative communication network:

  - Chapter 3: Relay Network

  - Chapter 4: Wireless Sensor Network

  - Chapter 5: Multi-Connectivity Network

  In each chapter, we review the related work including the MSCC under investigation and baseline (non-)cooperative communication concepts. We then define the system model and formulate the problem statement. Subsequently, we adapt our unified solution framework to the corresponding cooperative communication network and carry out the rate region and outage probability analysis. We then compare the MSCC results of each cooperative communication network to its baseline, quantify the performance gain, and illustrate our result by some numerical examples. In addition, we compare the theoretical results to the practical simulation results of the DTC. At the end of each chapter the key findings are summarized.

- During the research process, some new questions arose in regard to underlying assumptions of the theoretical approach and practical implementations. In Chapter 6 we address the following questions for MCo: How does correlation of the fading channels degrade the performance? What is the impact of typical receiver imperfections such as channel estimation and packet detection? How realistic are the theoretical performance improvements in real cellular networks?

- Finally, the thesis is concluded in Chapter 7.

1.3 Notation

In this thesis, random variables (RVs) and their realizations are denoted in capital (e.g., X) and lowercase (e.g., x) letters, respectively. All sets (e.g., alphabets of RVs) are denoted in calligraphic letter (e.g., $\mathcal{X}$), and its cardinality, by $|\mathcal{X}|$. Moreover, $X^n := (X(1), \ldots, X(n))$ denotes a random vector of length n. The probability mass function (pmf) and probability density function (pdf) of the discrete and continuous RV X are denoted by $p_X(x)$ and $f_X(x)$, respectively. The pmf and pdf are simply denoted by $p(x)$ and $f(x)$, respectively, whenever this notation is unambiguous.

We use $\mathbb{R}$, $\mathbb{R}_+$ and $\mathbb{N}$ to denote the sets of real numbers, non-negative real numbers, and natural numbers, respectively. Given any two integers $a, b \in \mathbb{N}$, we use $[a : b]$ to denote the inclusive collection of all integers between a and b, i.e., $[a : b] := \{c : c \in \mathbb{N}, a \leq c \leq b\}$.

Finally, we denote the probability of an event $\mathcal{E}$ as $\Pr\{\mathcal{E}\}$, the mutual information as $I(\cdot; \cdot)$, the entropy as $H(\cdot)$, the natural logarithm as $\ln(\cdot)$, the binary logarithm as $\mathrm{ld}(\cdot)$, the binary entropy function as $h(p) = -p\,\mathrm{ld}(p) - (1 - p)\,\mathrm{ld}(1 - p)$, the binary convolution as $a_1 * a_2 = a_1(1 - a_2) + (1 - a_1)a_2$, and the multivariate binary convolution as $a_1 * ... * a_N = a_1 * (... * (a_{N-1} * a_N)...)$, which is a *cascaded* binary convolution. For two functions $f(x)$ and $g(x)$, the notation $f(x) = \Theta(g(x))$ means that $k_1 g(x) \leq f(x) \leq k_2 g(x), \exists k_1 > 0, \exists k_2 > 0, \exists x_0, \forall x > x_0$, and $f(x) = O(g(x))$ means that $f(x) \leq kg(x), \exists k > 0, \exists x_0, \forall x > x_0$.

General Problem and Unified Solution Framework

<div style="text-align: right">2</div>

The performance analysis of wireless transmissions over fading channels is often established in two steps:

- At first, given that the channel realization is constant over the transmission of a frame, the performance of the wireless transmission is expressed as a function of a random instantaneous SNR Γ, drawn from pdf $f_\Gamma(\gamma)$.

- Secondly, if the instantaneous channel performance is less than the transmission rate, an outage event occurs. The outage probability is determined by integration over pdf $f_\Gamma(\gamma)$ on condition that an outage event occurs.

In this chapter, the necessary background knowledge for the performance analysis of cooperative communications systems which operate over fading channels is reviewed.

Sections 2.1-2.3 are dedicated to review the key concepts that allow for an analysis of the instantaneous performance. At first, we summarize some classical results of distributed lossless compression, namely, the Slepian-Wolf theorem and the many-help-one theorem by Gelfand and Pinsker. Shannon's channel coding theorem is briefly discussed in the context of parallel channels. Secondly, we introduce the multiterminal source-channel coding setup and review the corresponding source-channel separation theorem by Xiao and Lue.

Sections 2.4-2.6 introduce relevant concepts to evaluate the average performance. We introduce parallel AWGN channels with quasi-static Rayleigh fading and then define the exact and asymptotic outage probability.

Subsequently, in Section 2.7, we present a practical coding scheme to evaluate the frame-error-rates via Monte-Carlo simulations.

Finally, we outline the main contributions of this thesis in Section 2.8.
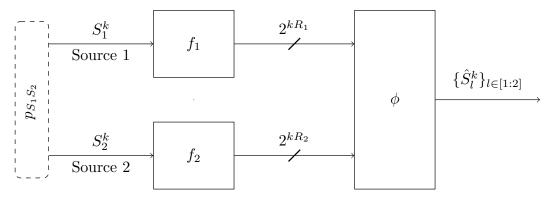
Fig. 2.1. Distributed lossless compression system. We are interested in the optimal rate region at which the distributed encoders can reliably communicate (i.e., lossless compression of all sources) with the decoder.

2.1 Distributed Lossless Compression

Distributed lossless compression has a rich history. Slepian and Wolf [SW73] were the first to characterise the problem of distributed encoding of multiple correlated sources. In their seminal paper, the rate region for the lossless distributed encoding of two correlated sources was derived. A simple proof of the Slepian-Wolf result with extension to an arbitrary number of correlated sources was presented by Cover [Cov75]. Wyner [Wyn75], and Ahlswede and Körner [AK75] considered a different problem, in which an auxiliary RV (i.e., side information) was introduced to expand the rate region of a lossless single-source coding problem. In that setup, coded (or partial) side information was available at the decoder.

Wyner and Ziv [WZ76] presented a generalization to lossy single-source coding with uncoded side information. This was the first characterization of a multiterminal rate-distortion function. Berger [Ber77] and Tung [Tun78] extended the Slepian-Wolf problem to the lossy distributed encoding of an arbitrary number of correlated sources. In those two works, inner and outer bounds for the multiterminal rate-distortion region were presented, which do not coincide in general.

The theorems of distributed lossless compression, which were established in the referred previous work and are necessary in the analysis for our work, are summarized in this section.

2.1.1 Slepian-Wolf Problem

Slepian and Wolf [SW73] considered a source coding problem where the decoder aims at perfectly reproducing two correlated discrete memoryless sources (DMSs) which are independently compressed at two terminals (see Fig. 2.1). Let us formally define the code.

Definition 1. *An (k, M_1, M_2)-code consists of*

- *two encoders*

$$f_l : \mathcal{S}_l^k \to [1 : M_l], \forall l \in [1 : 2], \ and \tag{2.1}$$

- *a decoder*

$$\phi : \prod_{l \in [1:2]} [1 : M_l] \to \prod_{l \in [1:2]} \mathcal{S}_l^k. \tag{2.2}$$

Given an (k, M_1, M_2)-code, the source estimates can be expressed as

$$(\hat{S}_1^k, \hat{S}_2^k) = \phi(\{f_l(S_l^k)\}_{l \in [1:2]}) \tag{2.3}$$

and the probability of error for a distributed lossless source code is defined as

$$P_{\mathrm{e}}^{(k)} := \Pr\left\{\{S_l^k\}_{l \in [1:2]} \neq \{\hat{S}_l^k\}_{l \in [1:2]}\right\}. \tag{2.4}$$

The pair $\{R_l\}_{l \in [1:2]}$ will be called an admissible combination of coding rates for $\{S_l\}_{l \in [1:2]}$ if there exists an (k, M_1, M_2)-code for which $M_l \leq 2^{kR_l}, l \in [1 : 2]$, and $\lim_{k \to \infty} P_{\mathrm{e}}^{(k)} = 0$. The optimal rate region, hereafter denoted as $\mathcal{R}_{\mathrm{SW}}$, is the set of all admissible combinations of rates $\{R_l\}_{l \in [1:2]}$, which was characterized by Slepian and Wolf.

Theorem 1. (Slepian-Wolf theorem [SW73]) *The optimal rate region for distributed lossless source coding of two DMSs $\{S_l\}_{l \in [1:2]}$, drawn from a joint pmf $p_{S_1 S_2}(s_1, s_2)$, is the set of rate pairs $\{R_l\}_{l \in [1:2]}$ given by*

$$\mathcal{R}_{SW} = \Big\{(R_1, R_2) :$$
$$R_1 \geq H(S_1|S_2),$$
$$R_2 \geq H(S_2|S_1),$$
$$R_1 + R_2 \geq H(S_1, S_2)\Big\}. \tag{2.5}$$
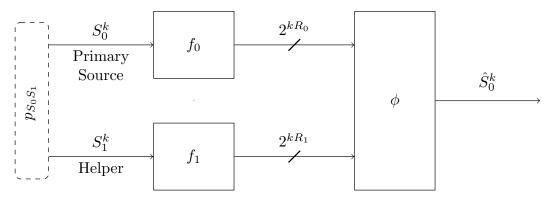
Fig. 2.2. Distributed lossless compression system with a helper. We are interested in the optimal rate region at which the distributed encoders can reliably communicate (i.e., lossless compression of the primary source) with the decoder. The encoder of the helper provides side information for decoding.

The Slepian-Wolf theorem is proved based on *random binning* [EGK11], which is a key concept of distributed lossless compression for partitioning the outcomes of the random sources. A simple proof of the Slepian-Wolf result with extension to an arbitrary number of sources was presented by Cover in [Cov75].

Theorem 2. (Generalized Slepian-Wolf theorem [Cov75]) *The optimal rate region for distributed lossless source coding of L DMSs $\{S_l\}_{l \in [1:L]}$, drawn from a joint pmf $p_{S_1 \ldots S_L}(s_1, \ldots, s_L)$, is the set of rate pairs $\{R_l\}_{l \in [1:L]}$ given by*

$$\mathcal{R}_{SW} = \Big\{ (R_1, \ldots, R_L) :$$
$$\sum_{l \in \mathcal{V}} R_l \geq H\left(\{S_l\}_{l \in \mathcal{V}} | \{S_l\}_{l \in \mathcal{V}^c}\right), \forall \mathcal{V} \subseteq [1:L] \Big\}, \tag{2.6}$$

where $\mathcal{V}^c$ denotes the complement of $\mathcal{V}$.

2.1.2 Many-Help-One Problem

Consider the distributed compression system depicted in Fig. 2.2, where only one of the two sources is to be recovered losslessly and the encoder for the other source (helper) provides *coded side information* to the decoder to help the first encoder's rate. In literature, this setup is referred to as source coding with coded side information.

The definitions of a code, proofs, and optimal rate region are the same as for the distributed lossless source coding setup in Section 2.1.1, except that the probability of error is defined as

$$P_{\mathrm{e}}^{(k)} := \Pr \left\{ S_0^k \neq \hat{S}_0^k \right\}. \tag{2.7}$$

The optimal rate region for the source coding problem with coded side information, hereafter denoted as $\mathcal{R}_{\mathrm{WAK}}$, was derived by Wyner [Wyn75], amd Ahlswede and Körner [AK75].

Theorem 3. (Wyner-Ahlswede-Körner theorem [Wyn75; AK75]) *Let $\{S_l\}_{l\in[0:1]}$ be two DMSs. The optimal rate region $\mathcal{R}_{WAK}$ for distributed lossless source coding of S_0 with the helper observing S_1, drawn from a joint pmf $p_{S_0 S_1}(s_0, s_1)$, is given by the convex closure of set of all $\{R_l\}_{l\in[0:1]}$ satisfying the following conditions:*

- *There exists a discrete auxiliary RV U_1 taking values in $\mathcal{U}_1$ such that (S_0, S_1, U_1) satisfies the Markov chain $S_0 \rightarrow S_1 \rightarrow U_1$.*

- $|\mathcal{U}_1| \leq |\mathcal{S}_1| + 1$.

- $R_0 \geq H(S_0|U_1)$ *and* $R_1 \geq I(S_1; U_1)$.

The idea that a decoder wishes to reproduce a primary source with the help of an auxiliary source, introduced by Wyner [Wyn75], and Ahlswede and Körner [AK75], can intuitively extended to an arbitrary number of auxiliary sources $(S_1, ..., S_L)$, a.k.a. helpers. Finding the rate region of such a system defines the so-called many-help-one problem. This problem has been recognized as a highly challenging one and only a few particular solutions are known to date. Gelfand and Pinsker [GP79] determined the rate region when the auxiliary sources are discrete and conditionally independent if the primary source is given[1]. Hereafter, this case is referred to as the conditionally independent (CI) condition. The joint pmf of $\{S_l\}_{l\in[0:L]}$ satisfies

$$p_{S_0 S_1 ... S_L}(s_0, s_1, ..., s_L) = p_{S_0}(s_0) \prod_{l\in[1:L]} p_{S_l|S_0}(s_l|s_0). \tag{2.8}$$

---

[1]The system model for the many-help-one problem is a special case of the system model for the lossless chief executive officer (CEO) problem investigated in [GP79] by Gelfand and Pinsker. In the CEO problem, the primary source is not encoded but rather observed from multiple helpers. Clearly, Gelfand and Pinsker's rate region is non-empty if and only if $H(S_0|S_1, \ldots, S_L) = 0$ (this condition was referred to therein as "completeness of observations"). According to [GP79], the rate region can be given by taking into account the "completeness of observations" for the encoding of the primary source [Ooh08].
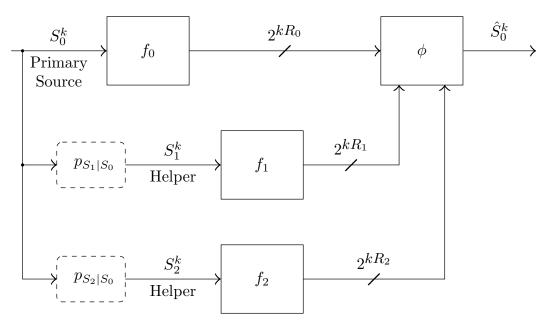
Fig. 2.3. System model for lossless many-help-one problem with two independently degraded helpers (i.e., $L = 2$). We are interested in the optimal rate region at which the distributed encoders can reliably communicate (i.e., lossless compression of the primary source) with the decoder. The helpers are conditionally independent given the primary source and their encoders provide side information for decoding.

Fig. 2.3 illustrates the lossless many-help-one system model with two helpers (i.e., $L = 2$).

Theorem 4. *(Gelfand-Pinsker theorem [GP79]) Let $\{S_l\}_{l \in [0:L]}$ be $(L + 1)$ DMSs. The optimal rate region $\mathcal{R}_{GP}$ for distributed lossless source coding of S_0 with helpers observing independently degraded sources $\{S_l\}_{l \in [1:L]}$, drawn from a joint pmf $p_{S_0 \ldots S_L}(s_0, \ldots, s_L)$ satisfying the CI condition in (2.8), is given by the convex closure of the set of all rates $\{R_l\}_{l \in [0:L]}$ satisfying the following conditions:*

1. *There exists an L-tuple $\{U_l\}_{l \in [1:L]}$ of discrete auxiliary RVs taking values in $\mathcal{U}_1 \times \ldots \times \mathcal{U}_L$ such that $\{S_0, S_l, U_l\}_{l \in [1:L]}$ satisfies the Markov chains $U_1 \ldots U_L \to S_1 \ldots S_L \to S_0$ and $U_l \to S_l \to S_{\bar{l}} \to U_{\bar{l}}, \forall l \in [1 : L], l \neq \bar{l}$.*

2. $|\mathcal{U}_l| \leq |\mathcal{S}_l| + (L + 1)2^{L-1} + 1, \forall l \in [1 : L].$

3. $R_0 \geq H(S_0 | U_1, \ldots, U_L)$ *and*
   $\sum_{l \in \mathcal{V}} R_l \geq I\left(\{S_l\}_{l \in \mathcal{V}}; \{U_l\}_{l \in \mathcal{V}} | \{U_l\}_{l \in \mathcal{V}^c}\right),$ *where*
   $\forall \mathcal{V} \subseteq [1 : L]$ *and* $\mathcal{V}^c = [1 : L] \backslash \mathcal{V}.$

2.2 Parallel Channel Coding

We now consider a dual setting that transmits the compressed messages (e.g., $\{m_l \in [1 : M_l]\}_{l\in[1:L]}$ in Definition 1) over a noisy parallel channel with L sub-channels. At first, let us consider a point-to-point communication system, where the sender wishes to reliably communicate a message $m \in [1 : M]$ in n channel uses to a receiver over a noisy channel. For doing so, the sender encodes the message into a codeword X^n. At the receiver, the decoder obtains the estimate $\hat{m}$ of the message from the received codeword Y^n. The channel coding problem is to find the highest rate $R = \mathrm{ld}(M)/n$ at which the encoder can reliably communicate, i.e., the probability of decoding error can be made arbitrarily small with the decoder. The highest rate is referred to as the channel capacity. In this section, we introduce the concept of parallel channels and define the capacity region, based on the channel coding theorem.

Let X_l^n and Y_l^n be sequences of n complex channel input and output symbols, respectively. The parallel channel is described by a pmf

$$p_{Y_1...Y_L|X_1...X_L}(y_1, ..., y_L|x_1...x_L) = \prod_{l\in[1:L]} p_{Y_l|X_l}(y_l|x_l). \tag{2.9}$$

We define cost functions associated with the channel inputs for all sub-channels as

$$\rho_l : \mathcal{X} \to \mathbb{R}_+, \forall l \in [1 : L]. \tag{2.10}$$

The sequence of input channel symbols X_l^n needs to satisfy cost constraints

$$\mathbb{E}\left[\rho_l(X_l)\right] \leq P_l, \forall l \in [1 : L], \tag{2.11}$$

where

$$\rho_l(X_l) := \frac{1}{n} \sum_{i\in[1:n]} \rho_l(X_l(i)) \tag{2.12}$$

for some $\{P_l\}_{l\in[1:L]} > 0$. Let

$$C_l(P_l) = \max_{p_{X_l}(x_l):\mathbb{E}[\rho_l(X_l)]\leq P_l} I(X_l; Y_l) \tag{2.13}$$
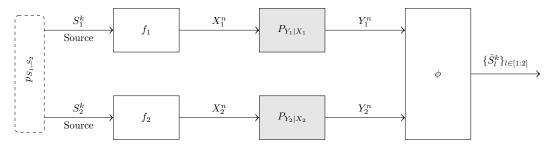
Fig. 2.4. Multiterminal source-channel setup. We are interested in the optimal cost constraints tuple at which the distributed encoders can reliably communicate (i.e., lossless compression of all sources) with the decoder over parallel channels.

be the lth channel capacity of a discrete memoryless channel (DMC) $p_{Y_l|X_l}(y_l|x_l)$. The channel coding theorem states the condition on the rate R_l with respect to $C_l(P_l)$ as follows.

Theorem 5. *(Channel coding theorem [Sha48]) For a DMC, all rates R_l below capacity $C_l(P_l)$ are achievable, i.e., the probability of error approaches zero for $n \to \infty$. Conversely, in order to guarantee reliable communication, the rate R_l must satisfy the condition $R_l \leq C_l(P_l)$.*

The capacity region $\mathcal{C}\left(\{P_l\}_{l\in[1:L]}\right)$ of the parallel channel under cost constraint $\{P_l\}_{l\in[1:L]}$ is defined by

$$\mathcal{C}\left(\{P_l\}_{l\in[1:L]}\right) := \left\{(R_1, ..., R_L) : 0 \leq R_l \leq C_l(P_l), \forall l \in [1:L]\right\}. \qquad (2.14)$$

2.3 Multiterminal Source-Channel Coding

In this section, we consider a joint source-channel coding setup with distributed sources. Fig. 2.4 illustrates a multiterminal source-channel setup where L transmitters wish to communicate k symbols of uncompressed correlated sources $\{S_l\}_{l\in[1:L]}$ over a parallel DMC $\prod_{l\in[1:L]} p_{Y_l|X_l}(y_l|x_l)$ in n transmissions so that the receivers can perfectly reconstruct the source symbols. A prevalent way, in this setup, is to perform source and channel encoding as well as channel and source decoding separately. For point-to-point communication with memoryless source and memoryless channel, Shannon proved that such strategy is asymptotically optimal, i.e., for $k \to \infty$, which is called Shannon's source-channel separation theorem. The theorem for a multiterminal setup was proven by Xiao and Lue.

Let us formally define the multiterminal source-channel code.

Definition 2. *An $(k, n, P_1, ..., P_L)$-code consists of*

- *L encoders*

$$f_l : \mathcal{S}_l^k \to \mathcal{X}_l^n, \ \forall \, l \in [1 : L], \ and \qquad (2.15)$$

- *a decoder*

$$\phi : \prod_{l \in [1:L]} \mathcal{Y}_l^n \to \prod_{l \in [1:L]} \mathcal{S}_l^k, \qquad (2.16)$$

such that

$$\mathbb{E}\left[\rho_l(X_l)\right] \leq P_l, \forall l \in [1 : L]. \qquad (2.17)$$

Given an $(k, n, P_1, ..., P_L)$-code, the source estimates can be expressed as

$$\{\hat{S}_l^k\}_{l \in [1:L]} = \phi(\{Y_l^n\}_{l \in [1:L]}) \qquad (2.18)$$

and the probability of error $P_e^{(k)}$ is defined as in (2.4) or (2.7).

The L-tuple $\{P_l\}_{l \in [1:L]}$ will be called an admissible combination for $\{S_l\}_{l \in [1:L]}$ if, for fixed k/n and sufficiently large k, there exists an $(k, n, P_1, ..., P_L)$-code which satisfies the cost constraints in (2.17) and $\lim_{k \to \infty} P_e^{(k)} = 0$.

Xiao and Lue [XL07] proved that separated source and channel coding, i.e., multiterminal source coding and multiple point-to-point channel codes, is asymptotically optimal ($k \to \infty$) for the multiterminal source-channel setup.

Theorem 6. *(Multiterminal source-channel separation theorem [XL07]) Let k/n be a fixed source-channel coding rate and $k \to \infty$. Then, the cost constraints L-tuple $\{P_l\}_{l \in [1:L]}$ is admissible if and only if*

$$\mathcal{C}\left(\{P_l\}_{l \in [1:L]}\right) \cap (k/n) \cdot \mathcal{R} \neq \emptyset. \qquad (2.19)$$

Remark 1: Note that Theorem 6 holds for any rate region $\mathcal{R}$, including the Slepian-Wolf and Many-Help-One rate regions in Theorem 2 and Theorem 4.

Remark 2: Although Theorem 6 was proven for DMSs and DMCs, it also holds for Gaussian sources with mean square error (MSE) criterion and
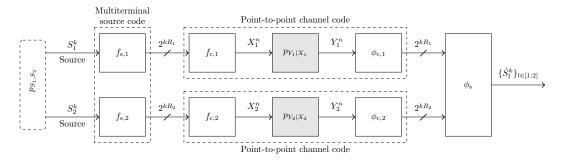
Fig. 2.5. Separation of multiterminal source-channel setup into one multiterminal source code and multiple point-to-point channel codes. This source-channel separation is quite appealing, since it implies that the multiterminal source coding can be performed without channel knowledge and the point-to-point channel coding without knowledge of the source correlation.

AWGN channels [XL07]. The result was provided by Oohama [Ooh97], where Berger-Tung's achievable rate region [Ber77; Tun78] was extended to Gaussian sources[2].

Throughout this thesis, we denote $R_c = k/n$ as the spectral efficiency, measured in source samples per channel symbol. The separation of the multiterminal source-channel code is depicted in Fig. 2.5. We use the subscript "s" and "c" to indicate the source and channel code, respectively.

2.4 Channel Model

As motivated in the Introduction, we consider delay-constrained communication systems operating over a slowly-varying fading channel. In such a scenario, it is plausible to assume that the duration of each transmitted codeword (sequence of n channel symbols) is smaller than the coherence time of the channel. Thus, that the random fading coefficients stay constant over the duration of each codeword [BPS98]. We shall refer to this channel model as *quasi-static fading channel*. Throughout this thesis, we consider L parallel AWGN channels with independent quasi-static Rayleigh fading.

---

[2]The Slepian-Wolf problem and the Many-Help-One problem are special cases of the Berger-Tung problem [EGK11].

2.4.1 AWGN Channel

Let X_l^n and Y_l^n be the input and output of a time-discrete channel. The output is the sum of the input and the noise N_l^n, i.e.,

$$Y_l^n = X_l^n + N_l^n.$$ (2.20)

The Gaussian RVs in N_l^n are independent and identically distributed (i.i.d.) with zero-mean and variance of $\sigma_N^2 = N_0/2$ per dimension, i.e., $N_l(i) \sim \mathcal{N}(0, \sigma_N^2)$, for $i \in [1:n]$.

As stated in Theorem 5, the channel capacity defines the maximum number of bits per dimension that could be reliably transmitted through a noisy channel. The AWGN channel capacity for an one-dimensional channel with input sequence X_l^n and cost constraint $\mathbb{E}\left[\rho_l(X_l) = \frac{1}{n} \sum_{i \in [1:n]} |X_l(i)|^2\right] \leq \sigma_X^2$ (referred to as average power constraint) and zero-mean Gaussian noise with variance σ_N^2 is [Sha48; Sha59b]

$$C_\psi = \frac{1}{2} \operatorname{ld}\left(1 + \frac{\sigma_X^2}{\sigma_N^2}\right).$$ (2.21)

Let us define the function $\psi(x) := \operatorname{ld}(1 + x)$. In practical communication systems, it is common to assume a circularly symmetric complex Gaussian channel with independent real and imaginary part. Thus, the noise variance is separated in real and imaginary component each, i.e., $\sigma_N^2 = N_0/2$ per dimension. For a complex Gaussian channel with average power constraint $\sigma_X^2 = P_l/2$ for real and imaginary component each, the capacity is

$$C_\psi = \psi\left(\frac{P_l}{N_0}\right).$$ (2.22)

2.4.2 Quasi-Static Rayleigh Fading Channel

In a quasi-static Rayleigh fading channel, the change in the received signal power over time due to multi-path fading and shadowing (a.k.a. channel gain) is also considered. The received sequence at the receiver is defined as

$$Y_l^n = A_l \cdot X_l^n + N_l^n,$$ (2.23)

where A_l represents the channel gain, which remains constant over the transmission of one sequence of n symbols, but varies sequence by sequence. The channel gain can be modeled as a zero-mean, circularly symmetric complex Gaussian RV with unit variance, i.e., $A_l \sim \mathcal{CN}(0, 1)$. The channel state information (CSI) is assumed to be known at the receiver.

Let us define the instantaneous received SNR by

$$\Gamma_l := |A_l|^2 \bar{\Gamma}_l \qquad (2.24)$$

with the average received SNR $\bar{\Gamma}_l$ being obtained as

$$\bar{\Gamma}_l = \frac{P_l}{N_0} \cdot d_l^{-\eta}, \qquad (2.25)$$

for $l \in [1 : L]$, where d_l is the distance between transmitter and receiver and η is the path loss exponent.

The received SNR of the lth fading channel is exponentially and independently distributed according to the pdf

$$f_{\Gamma_l}(\gamma_l) = \frac{1}{\bar{\Gamma}_l} \exp\left(-\frac{\gamma_l}{\bar{\Gamma}_l}\right). \qquad (2.26)$$

Based on the assumption of independent fading, the joint pdf of the parallel fading channel can be factorized to

$$f_{\Gamma_1 \ldots \Gamma_L}(\gamma_1, \ldots, \gamma_L) = \prod_{l \in [1:L]} f_{\Gamma_l}(\gamma_l). \qquad (2.27)$$

Given an L-tuple SNR realization $\{\gamma_l\}_{l \in [1:L]}$, drawn independently from (2.27), the instantaneous capacity region for the parallel AWGN channel with quasi-static Rayleigh fading can be specialized to

$$\mathcal{C}_\psi\left(\{\gamma_l\}_{l \in [1:L]}\right) = \left\{(R_1, \ldots, R_L) : 0 \leq R_l \leq \psi(\gamma_l), \forall l \in [1 : L]\right\}. \qquad (2.28)$$
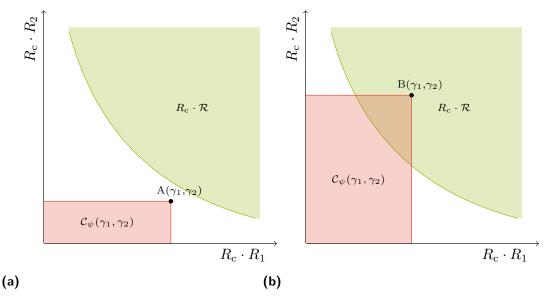
Fig. 2.6. Rate region $\mathcal{R}$ and capacity region $\mathcal{C}_\psi(\gamma_1, \gamma_2)$: (a) outage event, and (b) non-outage event. If the rate and capacity region do not intersect, an outage event occurs and vice versa.

2.5 Outage Probability

The outage probability is an important concept for fading channels, which provides a way to characterize the performance of communication systems in non-ergodic fading scenarios. As L is finite, the parallel fading channel is non-ergodic, i.e., L is not large enough to average over channel variations. In this section, we combine the previous results to define the outage probability of cooperative communication networks operating over fading channels, an approach proposed by Matsumoto et al in [CAM13a; Zho+14].

Combining Theorem 6 and the assumption of L parallel AWGN channels with independent quasi-static Rayleigh fading, the outage probability is given by the integration over the joint pdf $f_{\Gamma_1...\Gamma_L}(\gamma_1, ..., \gamma_L)$ under the condition that Theorem 6 is not fulfilled, i.e.,

$$P^{\text{out}} = \Pr\left[\mathcal{C}_\psi\left(\{\Gamma_l\}_{l\in[1:L]}\right) \cap R_{\text{c}} \cdot \mathcal{R} = \emptyset\right]. \tag{2.29}$$

Fig. 2.6 qualitatively illustrates the rate region $\mathcal{R}$ and capacity region $\mathcal{C}_\psi(\gamma_1, \gamma_2)$ for $L = 2$. Let us assume a received SNR realization, i.e., the pairs (γ_1, γ_2). The maximal achievable rates over the parallel channel are the pair $(\psi(\gamma_1), \psi(\gamma_2))$. In Fig. 2.6 we marked two different pairs at point A and point B. Since the maximal achievable rate pair at point A is outside the rate region $R_{\text{c}} \cdot \mathcal{R}$, an outage event occurs, i.e., $\lim_{k\to\infty} P_{\text{e}}^{(k)} > 0$. The

maximal achievable rate pair at point B is inside the rate region $R_{\mathrm{c}} \cdot \mathcal{R}$, i.e., there exists a code such that $\lim_{k \to \infty} P_{\mathrm{e}}^{(k)} = 0$. The outage probability is the integration over the joint pdf $f_{\Gamma_1 \dots \Gamma_L}(\gamma_1, \dots, \gamma_L)$ under the condition that the maximal achievable rate pair of the capacity region $\mathcal{C}_\psi(\Gamma_1, \Gamma_2)$ is outside the rate region $R_{\mathrm{c}} \cdot \mathcal{R}$.

2.6 Asymptotic Outage Probability

In this work, we evaluate the reliability performance by analyzing the exact outage probability. Unfortunately, a closed-form solution of the exact outage probability in (2.29) cannot be found for the cooperative communication networks considered in this work. On the other hand, the asymptotic outage probability at high SNR offers a simple characterization for the reliability performance. Especially for ultra reliable communications, operating in the medium- to high-SNR region, the asymptotic outage probability is a well-suited performance indicator. In the literature, the asymptotic outage probability is given depending on the so-called *coding gain* G_{c} and *diversity gain* d (see, e.g., [WG03]), as

$$\tilde{P}^{\mathrm{out}} = \left(G_{\mathrm{c}} \cdot \bar{\Gamma}\right)^{-G_{\mathrm{d}}}, \tag{2.30}$$

where $\bar{\Gamma}$ is the average received SNR. The diversity gain G_{d} determines the slope of the outage probability versus the average SNR curve in a log-log scale, at high SNR. On the other hand, the coding gain G_{c} (in dB), determines the shift of the outage probability in relative SNR to a benchmark outage probability (e.g., $\bar{\Gamma}^{-G_{\mathrm{d}}}$). Fig. 2.7 illustrates the relationship between the exact and asymptotic outage probability as well as the coding and the diversity gains.

2.7 Distributed Turbo Code

In this thesis, we are also interested in real link-level evaluations. One way to exploit the correlation of the sources in a practical communication system is the concept of DTCs, initially published in [AM12]. Fig. 2.8 illustrates a DTC for $L = 2$. The link-level performance can be quantified by frame-error-rates (FERs) in Monte-Carlo simulations. For sufficiently large frame length n, the outage probability is the lowest achievable FER known [NFR07]. We now outline the DTC in [AM12].
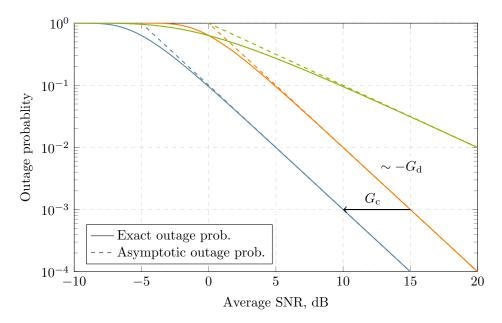
Fig. 2.7. Exact and asymptotic outage probability with the respective diversity and coding gains. The asymptotic outage probability offers a simple yet in-depth characterization of the system performance's general trend. The diversity gain G_d is defined as the slope of the outage probability versus the average SNR curve, at high SNR. The coding gain G_c is the shift of the outage probability in relative SNR to a benchmark outage probability.

2.7.1 Convolutional Encoder

As proposed in [AM12] each binary source sequence S_l^k is encoded by a twofold serially concatenated code. At first, a systematic non-recursive convolutional code (SNRCC) is applied, and secondly, an accumulator with a systematic recursive convolutional code (SRCC) and doping ratio P_ACC. The introduction of the accumulator to the coding scheme prevents an error floor of the decoder [PS06]. Finally the modulated sequence X_l^n generated by some modulation scheme is transmitted via an AWGN channel with quasi-static Rayleigh fading.

2.7.2 Joint Turbo Decoder

Each turbo decoder in Fig. 2.8b has two matching BCJR algorithms [Bah+74] to decode the SNRCC and SRCC applied at the encoder. The basic idea of DTC is to exchange information among all turbo decoders via a global iteration, and thus exploit the correlation of the sources. The joint turbo decoder (JTD) can be partitioned as follows:
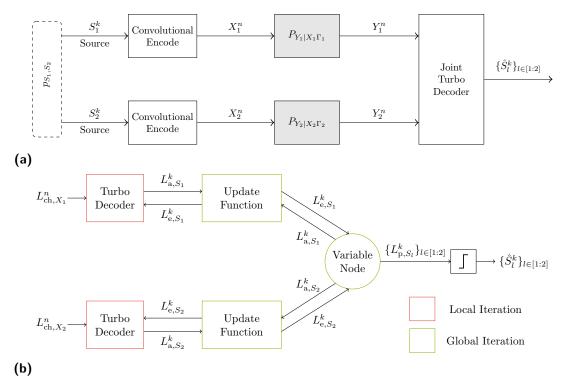
Fig. 2.8. Distributed turbo code: (a) a schematic diagram, and (b) joint turbo decoder. The code consists of distributed convolutional encoders and a joint turbo decoder. The joint turbo decoder alternately performs a local and global iteration. Local iteration: each turbo decoder individually performs a decoding iteration. Global iteration: all turbo decoders exchange LLRs via the update functions and variable node. The update function evaluates the exchanged LLRs based on the source correlation.

1. **Initialization** | It is assumed that the JTD has perfect knowledge of the CSI. Hence, the channel log likelihood ratios (LLRs) of X_l^n can be calculated as

$$\{L_{\mathrm{ch},X_l}(i)\}_{i\in[1:n]} = \left\{ \ln \frac{\Pr\{X_l(i) = 0 | Y_l(i) = y_l(i), \Gamma_l = \gamma_l\}}{\Pr\{X_l(i) = 1 | Y_l(i) = y_l(i), \Gamma_l = \gamma_l\}} \right\}_{i\in[1:n]}. \tag{2.31}$$

For example, if we consider binary phase shift keying (BPSK) modulation, where bit "0" is mapped to "$+\sqrt{P_l}$" and bit "1" is mapped to "$-\sqrt{P_l}$", the channel LLR for the ith symbol is calculated as follows

$$L_{\mathrm{ch},X_l}(i) = \ln \frac{\frac{1}{\sqrt{2\pi\sigma_N^2}} \exp\left(-\frac{|\Re(y_l(i)) - a_l\sqrt{P_l}|^2}{2\sigma_N^2}\right)}{\frac{1}{\sqrt{2\pi\sigma_N^2}} \exp\left(-\frac{|\Re(y_l(i)) + a_l\sqrt{P_l}|^2}{2\sigma_N^2}\right)} \tag{2.32}$$

$$= \frac{4a_l\sqrt{P_l}}{2\sigma_N^2} \Re(y_l(i)) = \frac{4a_l\sqrt{P_l}}{N_0} \Re(y_l(i)). \tag{2.33}$$

$\Re(\cdot)$ takes the real part of a complex value in its argument.

2. **Local Iteration** | Each turbo decoder then performs an update using the channel information L_{ch,X_l}^n and the *extrinsic* LLR L_{e,S_l}^k from the global iteration. Due to non existing *extrinsic* LLRs in the first iteration only the channel information is included. The decoder provides the *a priori* LLR L_{a,S_l}^k to the global iteration.

3. **Global Iteration** | From a general perspective a source with a high correlation (measured by the crossover probability ϵ_l) shares a greater amount of mutual information with the other sources. Therefore, the source sequence contains a more significant amount of valuable information compared to a source sequence with a low correlation [RA12]. To account for this, the update function $f_c(\cdot, \cdot)$ [AM12] performs an evaluation of the source sequence reliability. If the crossover probability ϵ_l is low, the LLR of source l will be promoted and vice versa. The update of the *extrinsic* LLR is calculated as

$$\{L_{\mathrm{e},S_l}(i)\}_{i\in[1:k]} = \{f_c(L_{\mathrm{a},S_l}(i),\epsilon_l)\}_{i\in[1:k]} \tag{2.34}$$

$$= \left\{ \ln \frac{(1-\epsilon_l)\cdot\exp(L_{\mathrm{a},S_l}(i))+\epsilon_l}{(1-\epsilon_l)+\epsilon_l\cdot\exp(L_{\mathrm{a},S_l}(i))} \right\}_{i\in[1:k]}. \tag{2.35}$$

Information among the turbo decoders is exchanged at the variable node, where the *a priori* LLR L_{a,S_l}^k is obtained by the sum of all other source *extrinsic* LLRs, i.e.,

$$L_{\mathrm{a},S_l}^k = \sum_{\bar{l}\in[1:L]\setminus\{l\}} L_{\mathrm{e},S_{\bar{l}}}^k. \tag{2.36}$$

L_{a,S_l}^k is then fed back to the update function. The update function again evaluates the *extrinsic* information from the other sources with the crossover probability, as seen in (2.34). Each turbo decoder obtains an updated *extrinsic* LLR L_{e,S_l}^k.

4. **Hard Decision** | The JTD estimates $\{\hat{S}_l^k\}_{l\in[1:L]}$ by interpreting the sign of *a posteriori* LLR $L_{\mathrm{p},S_l}^k = L_{\mathrm{a},S_l}^k + L_{\mathrm{e},S_l}^k$ for $l \in [1:L]$.

$$\hat{S}_l(i) = \begin{cases} 1, & L_{\mathrm{p},S_l}(i) < 0 \\ 0, & L_{\mathrm{p},S_l}(i) \geq 0 \end{cases} \tag{2.37}$$

The decoding process is performed in an iterative manner between step 2) and 3) and at the convergence point completed by 4). For a detailed explanation of the DTC, the authors refer to [AM12].

2.8 Main Contributions of this Thesis

Our research investigates MSCCs from the perspective of exploiting correlation among multiple sources in three cooperative networks:

(1) **Relay network**

(2) **Wireless sensor network**

(3) **Multi-connectivity network**

Our major contributions for all three networks are as follows:

A **Rate region** Although the corresponding rate regions for our cooperative communication networks are known (see Theorem 2 and Theorem 4), their specialization to binary sources remains surprisingly challenging. In this work, we derive exact rate regions and tight bounds for Theorem 2 and Theorem 4, when specialized to sources that are binary, uniformly distributed, and interrelated through symmetric channels.

B **Exact outage probability** Based on the derived rate regions, we establish the exact outage probability, defined in (2.29), for network (2) and network (3). For network (1), we find an upper bound for the exact outage probability, based on the rate region's inner bound. Unfortunately, a closed-from solution of the exact outage probability remains unknown, but the integral form can be evaluated via numerical simulations.

C **Asymptotic outage probability** For network (2) and network (3) we are able to derive the asymptotic outage probability and, thus, can give the exact coding and diversity gains (see (2.30)). We show by numerical examples that the provided asymptotes approach the exact solutions already at low-to-medium SNR. Unfortunately, the asymptotic outage probability for network (1) could not be found.

D SNR gain We quantify the performance gain of MSCCs compared to other cooperative or non-cooperative communication concepts based on the derived outage probability results. Eventually, we are interested in the transmit power reduction of one system compared to another system, which we refer to as *SNR gain*. Based on the SNR gain we answer some fundamental questions, for instance,

(i) Given a target (fixed) spectral efficiency, how much transmit power can be saved while achieving the same outage probability at high SNR?

(ii) Given a target (fixed) outage probability, how much transmit power can be saved while achieving the same throughput at high SNR?

(iii) How those savings vary with the level of the target metric and with the number of connections and topology?

E Outage probability vs. frame-error-rate We evaluate the error-rate performance of the DTC, presented in Section 2.7, for all three networks by Monte-Carlo simulation and compare its performance to the outage probability.

F Further practical constraints During the process, some new questions arose in regard to underlying assumptions of our theoretical approach and practical implementations. Accordingly, for network (3), we addressed the following additional points:

(i) In Section 2.4.2, the received SNRs are independently distributed (see (2.9)). However, it is often the case that the fading is correlated due to insufficient physical separation of the antennas or frequency bands. To better understand the influence of correlated fading, we extend the joint pdf in (2.26) by correlation parameters and derive exact and asymptotic outage probabilities.

(ii) We also assume the SNR to be known at the receiver (see Section 2.4.2). In practical receiver implementations, the SNR is estimated from training data in the preamble. The estimation accuracy depends on the preamble design, which in turn can influence the overall system performance. Likewise dependent on preamble design, packet detection is a major concern for receiver implementations. Therefore, the impact of SNR estimation and

packet detection for cooperative communications should be evaluated. To this end, we consider the error-rate performance of the physical layer of the wireless local area network (WLAN) standard (IEEE 802.11a), where SNR estimation and packet detection are included.

(iii) We are interested in the actual gain of implementing cooperative communications into cellular networks. Therefore, we apply our analysis to real field channel measurements and thereby illustrate the potential of cooperative communications in actual cellular networks.

2.9 Bibliographical Notes

Parts of the content in this thesis were presented at conferences and published in journals. The detail is as follows:

- The content of Chapter 3: **Relay Network** was presented at the IEEE 56th Annual Allerton Conference on Communication, Control, and Computing [Wol+18a][3] and published in the IEEE Wireless Communications Letters [Wol+17b][4].

- The content of Chapter 4: **Wireless Sensor Network** was published in the IEEE Communications Letters [Wol+16][5].

- The content of Chapter 5: **Multi-Connectivity Network** was presented at the IEEE 2017 Global Communications Conference [Wol+17a][4] and published in the IEEE Transactions on Communications [Wol+19][6].

In the above publications, the author of this thesis had the main responsibility, i.e., derivation of the analytical results, implementation of the simulation frameworks, and drafting the manuscripts.

- The content of Chapter 6: **Further Practical Constraints** was published in the IEEE Transactions on Communications [Wol+19][6], were the author of this thesis had the main responsibility; and was presented at the IEEE 2018 European Conference on Networks and Communications [Sch+18][3], and published in two diploma theses [Sch17; Che19],

---

[3]© 2018 IEEE
[4]© 2017 IEEE
[5]© 2016 IEEE
[6]© 2019 IEEE

where the author of this thesis provided the main idea and supervised the work.

Besides these publications, the author published other conference papers [WMF15; Wol+15; Wol+18b] and co-authored several conference papers [Ter+16; Gon+16; ZWM18; Sch+19b] and several journal papers [Gon+17; Gon+18; San+18; ZWM19; Sch+19a] in the relevant area during his doctoral study.

Personal use of this material is permitted. Permission from IEEE must be obtained for all other uses, in any current or future media, including reprinting/republishing this material for advertising or promotional purposes, creating new collective works, for resale or redistribution to servers or lists, or reuse of any copyrighted component of this work in other works.

Relay Network $\qquad$ 3

Although the rate region for the lossless many-help-one problem with independently degraded helpers is already "solved", its solution is given in terms of a convex closure over a set of auxiliary random variables. Thus, for any such problem in particular, an optimization over the set of auxiliary random variables is required to truly solve the rate region. Providing the solution is surprisingly difficult even for an example as basic as binary sources. In this chapter, we derive a simple and tight inner bound on the rate region's lower boundary for the lossless many-help-one problem with independently degraded helpers when specialized to sources that are binary, uniformly distributed, and interrelated through symmetric channels. Based on the rate region we obtain an upper bound on the outage probability of a LF multirelay system. The outage probability provides the ultimate performance limit of the system reliability. In addition, for comparison, we derive the outage probability of a DF multirelay system, which discards any intra-link errors (IEs). We show that, the more relays are employed, the more advantageous it is to forward the IEs, as opposed to discarding them.

3.1 Related Work

In DF, the decoded message is discarded by the relay whenever an error is detected [BH06]. On the other hand, by allowing IEs to be forwarded to the destination, an improved end-to-end performance can be achieved, as shown in [AM12] for a classic topology with one source, one relay, and one destination (the notion of allowable intra-link errors was first introduced in [GFZ05]). The central idea is that an erroneous relay message is still somewhat correlated to the source message, thus serving as valuable side information in the decoding process at the destination. Based on the theorems of source coding with side information [Wyn75; AK75] and source-channel separation [EGK11, Theorem 3.7], the outage probability of a LF relaying system was derived in [Zho+14] for a classic three-node topology, assuming that all the links undergo block Rayleigh fading. In that work, LF was shown to outperform DF, analyzed in [BH06]. An excellent tutorial on LF can be found in [He+18].

One may want to extend the outage analysis in [Zho+14] to two or more relays. This is an important extension, because in the harsh environment

of potential applications (e.g., fifth-generation vehicular networks) parallel routes (i.e., multiple relays) may be required to keep connectivity at an acceptable level. In principle, such an extended analysis could be attained based on the rate region for the distributed encoding of one primary source (S_0) and multiple auxiliary ones ($S_1, ..., S_L$). This is the so-called many-help-one problem, which is still open in its general form. Only a few particular solutions are known to date. Körner and Marton [KM79] addressed a two-help-one problem where the primary source is a modulo-two sum of correlated binary auxiliary sources. Gelfand and Pinsker [GP79] determined the rate region when the auxiliary sources are discrete and conditionally independent, given the primary source. Motivated by the Gelfand-Pinsker result, Oohama [Ooh05] determined the rate-distortion region for the same setup but Gaussian sources. Tavildar [TVW10] derived the rate-distortion region for Gaussian sources with a correlation model following a tree-like structure. For other works on the many-help-one problem, see [Ooh08] and the references therein.

While the characterization given by Gelfand and Pinsker [GP79] (see Theorem 4) is elegant and quite general, it presents a practical disadvantage: the solution relies on auxiliary RVs whose statistics are unknown in advance. Thus, the numerical characterization of the region of achievable rates for any particular joint distribution of $(S_0, S_1, ..., S_L)$ requires an optimization over all admissible conditional distributions for the auxiliary RVs $(U_1, ..., U_L)$. Gelfand and Pinsker [GP79] showed that the rate region remains unchanged if the alphabet size of the auxiliary RVs is bounded by $|\mathcal{U}_l| \leq |\mathcal{S}_l| + (L+1)2^{L-1} + 1$. However, with an increasing number of helpers the bound on the alphabet size increases, and so does the complexity of the optimization problem. Jana [Jan09] showed that the cardinality of the auxiliary RVs can be tightly bounded by $|\mathcal{U}_l| \leq |\mathcal{S}_l|$ for a broad class of multiterminal source coding problems, including the many-help-one problem. But still, the optimization problem remains surprisingly challenging, even for binary sources.

In [Gu+07], the one-help-one problem (a.k.a. source coding with coded side information) was considered with binary sources which are related through a binary symmetric channel (BSC). It was then shown that the rate region is achieved if and only if the auxiliary RV and the helper are related through a BSC as well.
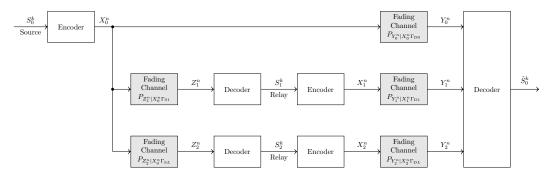
Fig. 3.1. Lossy forwarding multirelay system with two relays (i.e., $L = 2$). The source wishes to reliably transmit information to the destination with the aid of multiple relays over parallel fading channels. We are interested in the outage probability.

3.2 System Model

We consider a dual-hop relaying system in which one source cooperates with L half-duplex relays to transmit information to one destination, as shown in Fig. 3.1. We assume that all the channels undergo independent quasi-static Rayleigh fading and additive white Gaussian noise with mean power N_0 (see Section 2.4.2). For convenience, we reproduce the pdf of the received SNRs in (2.26) with slightly different notations. The pdf of the received SNR of all the links is exponentially distributed, given by

$$f_{\Gamma_\nu}(\gamma) = \frac{1}{\bar{\Gamma}_\nu} \exp\left(-\frac{\gamma}{\bar{\Gamma}_\nu}\right), \tag{3.1}$$

where $\nu \in \{S0, S1, \ldots, SL, D1, \ldots, DL\}$, $\bar{\Gamma}_{D0} := (P_S/N_0)d_{D0}^{-\eta}$ is the average received SNRs of the source-to-destination link, $\bar{\Gamma}_{Sl} := (P_S/N_0)d_{Sl}^{-\eta}$ for $l \in [1:L]$ are the average received SNRs of the source-to-relay links, $\bar{\Gamma}_{Dl} := (P_{Dl}/N_0)d_{Dl}^{-\eta}$ for $l \in [1:L]$ are the average received SNRs of relay-to-destination links; including the respected path loss $d_\nu^{-\eta}$, and P_S and P_{Dl} stand for the transmit powers at source and lth relay, respectively. The CSI is assumed to be known at the receiver.

The system model has one binary memoryless source (BMS), denoted as $[S_0(i)]_{i=1}^\infty$, with i denoting discrete time. The k-sample source sequence shall be represented in vector form as $S_0^k = [S_0(1), S_0(2), ..., S_0(k)]$. When appropriate, for simplicity, we shall drop the temporal index, denoting the source output simply as S_0. The source S_0 takes values from a binary set $\{0, 1\}$ with uniform probabilities, i.e., $p_{S_0}(s_0 = 0) = p_{S_0}(s_0 = 1) = 0.5$.

The relaying system operates on a time-division multiple access basis, with the transmission process being accomplished in four steps, as follows. At

first, the source sequence S_0^k is encoded to the transmit source sequence X_0^n, i.e., the encoder maps $\mathcal{S}_0^k \to \mathcal{X}_0^n$, and broadcasted to the destination and all relays. Secondly, each relay decodes its received relay sequence Z_l^n to the binary relay sequence S_l^k, i.e., the lth decoder maps $\mathcal{Z}_l^n \to \mathcal{S}_l^k$. The relay sequences S_l^k for $l \in [1:L]$, differ from the original source sequence S_0^k according to certain first-hop crossover probabilities $\epsilon_l := \Pr\{S_0 \neq S_l\}$, which depend on the instantaneous received SNRs between the primary source and the lth relay, $\Gamma_{\mathrm{S}l}$. Thirdly, the relay sequence S_l^k is decoded to X_l^n, i.e., the lth encoder maps $\mathcal{S}_l^k \to \mathcal{X}_l^n$, and transmitted to the destination. Lastly, all received sequences Y_l^n for $l \in [0:L]$ are jointly decoded to retrieve S_0^k, i.e., the decoder maps $\prod_{l \in [0:L]} \mathcal{Y}_l^n \to \mathcal{S}_0^k$, we denote its estimate as $\hat{S}_0^k$. The probability of error $\mathrm{P}_{\mathrm{e}}^{(k)} = \Pr\left\{S_0^k \neq \hat{S}_0^k\right\}$ (see (2.7)) depends on the instantaneous received SNRs between the primary source and destination $\Gamma_{\mathrm{S}0}$, and relays and destination, $\Gamma_{\mathrm{D}l}$ for $l \in [1:L]$.

3.3 Problem Statement and Approach

Eventually, we are interested in the outage probability of the LF multirelay system, i.e.,

$$P_{\mathrm{LF},L}^{\mathrm{out}} = \Pr\left\{\mathcal{C}_\psi\left(\{\Gamma_{\mathrm{D}l}\}_{l \in [0:L]}\right) \cap R_{\mathrm{c}} \cdot \mathcal{R}_{\mathrm{GP}} = \emptyset\right\}. \tag{3.2}$$

Note that the rate region $\mathcal{R}_{\mathrm{GP}}$ depends on the first-hop crossover probabilities $\{\epsilon_l\}_{l \in [1:L]}$, and thus on the received SNRs between the primary source and the L relays, $\{\Gamma_{\mathrm{S}l}\}_{l \in [1:L]}$.

In order to derive the outage probability in (3.2), we first consider the rate region $\mathcal{R}_{\mathrm{GP}}$ when specialized to source and helpers that are binary, uniformly distributed, and interrelated through BSCs. Next, we determine the crossover probability depending on the instantaneous received first-hop crossover probability based on Shannon's source-channel separation theorem [EGK11, Theorem 3.7]. Finally, we then determine the outage probability by averaging over all received SNRs.

3.4 Rate Region

In this section, we investigate the many-help-one problem when specialized to source and helpers that are binary, uniformly distributed, and interrelated through BSCs. Motivated by the results in [Gu+07], we assume the helpers and auxiliary RVs are also interrelated through BSCs, thereby deriving a simple and tight inner bound on the rate region's lower boundary for the investigated problem. The more degraded the helpers, the tighter the inner bound, as indicated from our numerical examples.

3.4.1 Background

Recall the many-help-one rate region $\mathcal{R}_{\text{GP}}$ in Theorem 4 and the CI condition in (2.8). In order to reduce its complexity, Jana showed in [Jan09, Lemma 2.2] that the computational complexity of Theorem 4 can be reduced, i.e., the cardinality of the auxiliary RVs can be tightly bounded by $|\mathcal{U}_l| \leq |\mathcal{S}_l|, \forall l \in [1:L]$, for a broad class of multiterminal source coding problems, including the lossless many-help-one problem[1].

Even after the above reduction of cardinality, the optimization problem at hand remains highly complicated. Take, for instance, the case of $L = 2$. To compute the lower convex boundary of $\mathcal{R}_{\text{GP}}$, we need to minimize the Lagrangian function

$$
\begin{aligned}
H(S_0|U_1, U_2) &+ \mu_1 I(S_1; U_1|U_2) + \mu_2 I(S_2; U_2|U_1) \\
&+ \mu_3 I(S_1, S_2; U_1, U_2),
\end{aligned} \tag{3.3}
$$

over $p_{U_1|S_1}(u_1|s_1)$ and $p_{U_2|S_2}(u_2|s_2)$, with $\mu_1, \mu_2, \mu_3 > 0$. Yet, the function in (3.3) is in general neither convex nor concave over $p_{U_1|S_1}(u_1|s_1)$ and $p_{U_2|S_2}(u_2|s_2)$. For example, $H(S_0|U_1, U_2)$ is concave while $I(S_1; U_1|U_2)$ is convex over $p_{U_1|S_1}(u_1|s_1)$. Therefore, the optimization is surprisingly difficult even in the simplest case where all the sources are binary RVs.

---

[1] The framework provided by Jana includes the lossless many-help-one problem, when $(M, J, L) = (\text{any}, 1, 0)$ and S is deterministic. In [Jan09], M is the number of sources, J is the number of sources which are reconstructed lossless, L is the number of sources which are reconstructed within some distortion constraint, and S is some side information.

3.4.2 Binary Symmetric Case

In this section, we consider the case where the source S_0 is binary and uniformly distributed, i.e., $p_{S_0}(0) = p_{S_0}(1) = 1/2$, and related to the helpers $S_l, l \in [1:L]$, via BSCs, i.e., $\epsilon_l := p_{S_l|S_0}(0|1) = p_{S_l|S_0}(1|0)$. Let us define the binary asymmetric channel (BAC) between the helpers and auxiliary RVs by the crossover probabilities $\alpha_l := p_{U_l|S_l}(1|0)$ and $\beta_l := p_{U_l|S_l}(0|1)$ for $l \in [1:L]$. Fig. 3.2 shows a schematic diagram of all RVs and the respective crossover probabilities for $L = 2$. The optimization problem can be formulated as follows: for fixed ϵ_l, determine all sets of $\{\alpha_l, \beta_l\}_{l \in [1:L]}$ which are on the lower convex boundary of the optimal rate region in Theorem 4. This optimization problem cannot be solved in closed form. Instead, a solution can be given within a target precision by means of an exhaustive numerical search.

Alternatively, driven by the results in [Gu+07], we derive an inner bound on the rate region's lower boundary based on the assumption of BSCs between the helpers and the auxiliary RVs, i.e., $\kappa_l = \alpha_l = \beta_l$ for $l \in [1:L]$. Importantly, later on we show by numerical examples that the proposed inner bound can be tight, mainly as the helpers turn out to be more degraded. In the following, we first examine the special case with two helpers and then extend our results to an arbitrary number of helpers.

Two Helpers

Theorem 7. *If (S_0, S_1, S_2) is a 3-tuple of binary RVs and their joint pmf satisfies (2.8), with $p_{S_0}(0) = p_{S_0}(1) = 1/2$, $p_{S_l|S_0}(0|1) = p_{S_l|S_0}(1|0) = \epsilon_l$, and $p_{U_l|S_l}(0|1) = p_{U_l|S_l}(1|0) = \kappa_l$ for some $0 \leq \epsilon_l \leq 1/2, l \in [1:2]$, then an inner bound on the rate region's lower boundary is given by*

$$
\begin{aligned}
\{(R_0, R_1, R_2) : \\
R_0 &= h(\epsilon_1 * \kappa_1) + h(\epsilon_2 * \kappa_2) - h(\epsilon_1 * \kappa_1 * \epsilon_2 * \kappa_2), \\
R_1 &= h(\epsilon_1 * \kappa_1 * \epsilon_2 * \kappa_2) - h(\kappa_1), \\
R_2 &= h(\epsilon_1 * \kappa_1 * \epsilon_2 * \kappa_2) - h(\kappa_2), \\
R_1 + R_2 &= 1 + h(\epsilon_1 * \kappa_1 * \epsilon_2 * \kappa_2) - h(\kappa_1) - h(\kappa_2), \\
(\kappa_1, \kappa_2) &\in [0, 0.5]^2 \}.
\end{aligned}
\tag{3.4}
$$
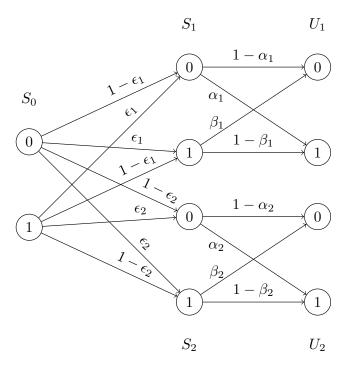
Fig. 3.2. The binary symmetric case with two helpers (i.e., $L = 2$). The primary source S_0 and helpers $\{S_1, S_2\}$ are related via BSCs (with crossover probability ϵ_l) and the helpers $\{S_1, S_2\}$ and auxiliary RVs $\{U_1, U_2\}$ are related via BACs (with crossover probabilities α_l and β_l).

Proof. Given symmetric channels and uniformly distributed source symbols, the following holds:

$$H(S_0) = H(S_l) = H(U_l) = 1, \tag{3.5}$$

$$H(U_l|S_0) = H(S_0|U_l), \tag{3.6}$$

$$H(U_1|U_2) = H(U_2|U_1), \tag{3.7}$$

for $l \in [1:2]$. The information measures in (3.3) can be reformulated as

$$
\begin{aligned}
H(S_0|U_1, U_2) &= H(S_0) + H(U_1|S_0) + H(U_2|S_0, U_1) \\
&\quad - H(U_1) - H(U_2|U_1) \tag{3.8} \\
&= H(U_1|S_0) + H(U_2|S_0) - H(U_2|U_1), \tag{3.9} \\
I(S_l; U_l|U_{\bar{l}}) &= H(U_l|U_{\bar{l}}) - H(U_l|S_l, U_{\bar{l}}) \tag{3.10} \\
&= H(U_l|U_{\bar{l}}) - H(U_l|S_l), \tag{3.11} \\
I(S_1, S_2; U_1, U_2) &= H(U_1, U_2) - H(U_1, U_2|S_1, S_2) \tag{3.12} \\
&= H(U_1) + H(U_2|U_1) - H(U_1|S_1, S_2, U_2) \\
&\quad - H(U_2|S_1, S_2) \tag{3.13} \\
&= H(U_1) + H(U_2|U_1) - H(U_1|S_1) - H(U_2|S_2), \tag{3.14}
\end{aligned}
$$

where $l, \bar{l} \in [1:2]$, $l \neq \bar{l}$. The steps can be justified as follows: in (3.8) and (3.13) we used the chain rule of entropy; (3.9), (3.11), and (3.14) follow from from the Markov chain, i.e., $U_l \to S_l \to S_0 \to S_{\bar{l}} \to U_{\bar{l}}$, and the properties given in (3.5). As shown by Wyner in [Wyn73], the conditional entropy of two binary RVs A and B related by a BSC with crossover probability δ is given by $H(A|B) = h(\delta)$. For $U_l \to S_l \to S_0$ and $U_1 \to S_1 \to S_0 \to S_2 \to U_2$, the end-to-end crossover probabilities are given by $\epsilon_l * \kappa_l$ and $\epsilon_1 * \kappa_1 * \epsilon_2 * \kappa_2$, respectively. Using this along with (3.6) and (3.7), the conditional entropies in (3.9), (3.11), and (3.14) can be given by

$$H(U_1|S_0) + H(U_2|S_0) - H(U_2|U_1) = h(\epsilon_1 * \kappa_1) + h(\epsilon_2 * \kappa_2)$$
$$- h(\epsilon_1 * \kappa_1 * \epsilon_2 * \kappa_2), \qquad (3.15)$$

$$H(U_l|U_{\bar{l}}) - H(U_l|S_l) = h(\epsilon_1 * \kappa_1 * \epsilon_2 * \kappa_2) - h(\kappa_l), \qquad (3.16)$$

$$H(U_2|U_1) - H(U_1|S_1) - H(U_2|S_2) = h(\epsilon_1 * \kappa_1 * \epsilon_2 * \kappa_2) - h(\kappa_1) - h(\kappa_2). \qquad (3.17)$$

The inner bound is then generated as the auxiliary parameters are ranged over $(\kappa_1, \kappa_2) \in [0, 0.5]^2$. This completes the proof. $\qquad \square$

Extension to an Arbitrary Number of Helpers

Theorem 8. *If $(S_0, S_1, ..., S_L)$ is an $(L+1)$-tuple of binary RVs and their joint pmf satisfies (2.8), with $p_{S_0}(0) = p_{S_0}(1) = 1/2$, $p_{S_l|S_0}(0|1) = p_{S_l|S_0}(1|0) = \epsilon_l$, and $p_{U_l|S_l}(0|1) = p_{U_l|S_l}(1|0) = \kappa_l$ for some $0 \leq \epsilon_l \leq 1/2, l \in [1:L]$, then an inner bound on the rate region's lower boundary is given by*

$$\{(R_0, R_1, ..., R_L) :$$
$$R_0 = \sum_{l \in [1:L]} h\left(\epsilon_l * \kappa_l\right) - \eta(\{\epsilon_l * \kappa_l\}_{l \in [1:L]}),$$
$$\sum_{l \in \mathcal{V}} R_l = \eta(\{\epsilon_l * \kappa_l\}_{l \in [1:L]}) - \eta(\{\epsilon_l * \kappa_l\}_{l \in \mathcal{V}^c}) - \sum_{l \in \mathcal{V}} h(\kappa_l),$$
$$\forall \mathcal{V} \subset [1:L] \text{ and } \mathcal{V}^c = [1:L] \backslash \mathcal{V},$$
$$\sum_{l \in [1:L]} R_l = 1 + \eta(\{\epsilon_l * \kappa_l\}_{l \in [1:L]}) - \sum_{l \in [1:L]} h(\kappa_l),$$
$$\{\kappa_l\}_{l \in [1:L]} \in [0, 0.5]^L\}, \qquad (3.18)$$

where

$$\eta(\{\epsilon_l * \kappa_l\}_{l \in [1:L]}) \quad := - \sum_{\{u_l\}_{l \in [2:L]} \in \{0,1\}^{L-1}}$$

$$\times \Big(\sum_{s_0 \in \{0,1\}} p_{U_2...U_L|S_0}(u_2,...,u_l|s_0) p_{S_0|U_1}(s_0|0) \Big)$$

$$\times \operatorname{ld} \Big(\sum_{s_0 \in \{0,1\}} p_{U_2...U_L|S_0}(u_2,...,u_l|s_0) p_{S_0|U_1}(s_0|0) \Big)$$

(3.19)

for $L \geq 2$, with

$$p_{U_2...U_L|S_0}(u_2,...,u_l|s_0) = \prod_{l \in [2:L]} p_{U_l|S_0}(u_l|s_0) \tag{3.20}$$

$$= \prod_{l \in [2:L]} \{(1 - \epsilon_l * \kappa_l)\, \mathbb{1}(u_l = s_0) + (\epsilon_l * \kappa_l)\, \mathbb{1}(u_l \neq s_0)\}, \tag{3.21}$$

and

$$p_{S_0|U_1}(s_0|0) = \big[\, (1 - \epsilon_1 * \kappa_1)\, \mathbb{1}(s_0 = 0)$$
$$+ (\epsilon_1 * \kappa_1)\, \mathbb{1}(s_0 \neq 0)\big]. \tag{3.22}$$

For $L < 2$ we have $\eta(\{\epsilon_l * \kappa_l\}_{l \in [1:L]}) = 0$. In (3.21) and (3.22), $\mathbb{1}(\cdot)$ is the indicator function. In particular, for $L = 2$, $\eta(\{\epsilon_1 * \kappa_1, \epsilon_2 * \kappa_2\}) = h(\epsilon_1 * \kappa_1 * \epsilon_2 * \kappa_2)$.

Proof. See Appendix A.1. □

Theorem 7 and Theorem 8 provide closed-form solutions to evaluate the outage probability in the subsequent sections. We see that the inner bound on the rate region's lower boundary is given depending on the crossover probabilities of the BSCs between the primary source and the helpers. An increased crossover probability yields an increase in the rate constraints, which we demonstrate by numerical examples in Section 3.8.

3.5 Source-Relay Link Crossover Probability

Recall the quasi-static Rayleigh fading assumption (see Section 2.4), i.e., the fading coefficient stays constant over one transmission interval. Given a fixed fading coefficient, the source-relay transmission corresponds to a joint source-channel setup where the transmitter wishes to communicate k symbols of an uncompressed source S_l over a discrete memoryless channel $p_{Z_l|X_l}$ in n

transmissions so that the receivers can reconstruct the source symbols within a distortion constraint $\mathcal{D}_l$. A prevalent way, in this case, is to perform source and channel encoding as well as channel and source decoding separately. For point-to-point communication with memoryless source and memoryless channel, Shannon proved that such strategy is asymptotically optimal, i.e., for $k \to \infty$, which is called Shannon's source-channel separation theorem.

Theorem 9. *(Source-channel separation theorem [Sha59a]) Given a DMS S_l, an average distortion measure $d(s_l, \hat{s}_l)$ with rate-distortion function $R_l(\mathcal{D}_l)$ and a DMC with capacity C_l, the following statement holds.*

If $kR_l(\mathcal{D}_l) \le nC_l$, then there exists a sequence of joint source-channel codes such that

$$\limsup_{k \to \infty} \mathbb{E}\left\{d(S_l^k, \hat{S}_l^k)\right\} \le \mathcal{D}_l, \tag{3.23}$$

where k is the number of source samples and n is the number of channel input symbols. $R_l(D_l)$ is expressed in bits per source sample and the capacity C_l is in bits per channel input symbol.

Thus, the maximum achievable value of the transmission rate $R_l(\mathcal{D}_l)$ for each source-relay link is related to its respective received SNR $\Gamma_{\mathrm{D}l}$ by [Sha48], [EGK11, Theorem 3.7]

$$R_l(\mathcal{D}_l) = \frac{1}{R_{\mathrm{c}}} \cdot \psi\left(\Gamma_{\mathrm{S}l}\right), \tag{3.24}$$

where $\psi(\Gamma_{\mathrm{S}l}) := \mathrm{ld}(1 + \Gamma_{\mathrm{S}l})$ is the instantaneous complex AWGN channel capacity (see (2.22)). Based on Theorem 9, the AWGN channel can be modeled as a BSC, i.e., with the Hamming distortion measure and for a given $\Gamma_{\mathrm{S}l}$ value, the minimum distortion $\mathcal{D}_{l,\min}$ is equivalent to the crossover probability ϵ_l of a BSC [ZA06]. Thus, the crossover probability ϵ_l in Theorem 8 can be related to the corresponding received SNR by means of [Zho+14]

$$\epsilon_l(\Gamma_{\mathrm{S}l}) = \begin{cases} h^{-1}\left(1 - \dfrac{\psi(\Gamma_{\mathrm{S}l})}{R_{\mathrm{c}}}\right) & \text{for } 0 \le \Gamma_{\mathrm{S}l} < A_1, \\ 0 & \text{for } \Gamma_{\mathrm{S}l} \ge A_1, \end{cases} \tag{3.25}$$

for $L \in [1 : L]$, $A_1 := 2^{R_{\mathrm{c}}} - 1$, and $h^{-1}(\cdot)$ is the inverse binary entropy function. The achievability of ϵ_l depends on the existence of a code which is capacity-achieving for the source-destination and -relay links at the same time.

3.6 Outage Probability

In this section, we derive an upper bound on the outage probability of LF based on the derived inner bound of the Gelfand-Pinsker rate region in Theorem 8. Furthermore, we derive the exact and asymptotic outage probability of DF for comparison.

3.6.1 Lossy Forwarding

In Theorem 8, the auxiliary sources are assumed to be conditionally independent given the primary source. Note that this assumption perfectly matches the LF system depicted in Fig. 3.1, in which the decoded relay sequences are independently degraded replicas of the source sequence.

Recall the discussion in Section 2.5. On the one hand, we have the capacity region $\mathcal{C}_\psi \left(\{ \Gamma_{\mathrm{D}l} \}_{l \in [0:L]} \right)$ depending on the received SNRs of the source- and relay-destination links. On the other hand, we have the rate region $\mathcal{R}_{\mathrm{GP}} \left(\{ \Gamma_{\mathrm{S}l} \}_{l \in [1:L]} \right)$ depending on the received SNRs of the source-relay links. An outage event occurs, whenever the intersection of both regions is empty, see Theorem 6. Thus, for (3.2) we have

$$P_{\mathrm{LF},L}^{\mathrm{out}} = \Pr \left\{ \mathcal{C}_\psi \left(\{ \Gamma_{\mathrm{D}l} \}_{l \in [0:L]} \right) \cap R_{\mathrm{c}} \cdot \mathcal{R}_{\mathrm{GP}} \left(\{ \Gamma_{\mathrm{S}l} \}_{l \in [1:L]} \right) = \emptyset \right\} \tag{3.26}$$

$$= \Pr \left\{ \left\{ \frac{1}{R_{\mathrm{c}}} \psi(\Gamma_{\mathrm{D}l}) \right\}_{l \in [0:L]} \notin \mathcal{R}_{\mathrm{GP}} \left(\{ \Gamma_{\mathrm{S}l} \}_{l \in [1:L]} \right) \right\} \tag{3.27}$$

$$< \Pr \left\{ \left(\frac{1}{R_{\mathrm{c}}} \psi(\Gamma_{\mathrm{D}0}) \le \sum_{l \in [1:L]} h\left(\epsilon_l(\Gamma_{\mathrm{S}l}) * \kappa_l \right) - \eta(\{ \epsilon_l(\Gamma_{\mathrm{S}l}) * \kappa_l \}_{l \in [1:L]}) \right) \cup \right.$$

$$\bigcup_{\forall \mathcal{V} \subset [1:L]} \left(\frac{1}{R_{\mathrm{c}}} \sum_{l \in \mathcal{V}} \psi(\Gamma_{\mathrm{D}l}) \le \eta(\{ \epsilon_l(\Gamma_{\mathrm{S}l}) * \kappa_l \}_{l \in [1:L]}) \right.$$

$$\left. - \eta(\{ \epsilon_l(\Gamma_{\mathrm{S}l}) * \kappa_l \}_{l \in \mathcal{V}^{\mathrm{c}}}) - \sum_{l \in \mathcal{V}} h(\kappa_l) \right) \cup$$

$$\left(\frac{1}{R_{\mathrm{c}}} \sum_{l \in [1:L]} \psi(\Gamma_{\mathrm{D}l}) \le 1 + \eta(\{ \epsilon_l(\Gamma_{\mathrm{S}l}) * \kappa_l \}_{l \in [1:L]}) - \sum_{l \in [1:L]} h(\kappa_l) \right),$$

$$\left. \mathcal{V}^{\mathrm{c}} = [1:L] \backslash \mathcal{V}, 0 \le \kappa_l \le 0.5, \forall l \in [1:L] \right\}. \tag{3.28}$$

The above steps are justified as follows: (3.27) is a reformulation, where we determine the probability that the maximum achievable rates of the capacity region are outside the rate region (see Section 2.5); in (3.28) the

rate constrains from Theorem 8 are substituted accordingly. Since Theorem 8 is an inner bound on the rate region's lower boundary, the substitution yields an upper bound on the outage probability. The expression in (3.28) cannot be solved in closed form, thus requiring numerical evaluation.

3.6.2 Decode-and-Forward

In this section we derive the outage probability of a DF multirelay scheme. Unlike [BH06], instead of MRC, we assume a MSCC (in this context also known as joint decoding or parallel coding), which is optimal.

In DF, a relay forwards a sequence iff it is detected error free. The corresponding outage probability can be assessed in three stages: (1) we calculate the probability that the destination fails to recover the source sequence when received by the source-destination link and forwarded by a given subset of relays $\mathcal{V} \subseteq [1 : L]$; (2) we calculate the probability that the source sequence be forwarded by each such subset; and (3) we sum over the probabilities of all outage events, i.e., $\forall \mathcal{V} \subseteq [1 : L]$. Next we elaborate on these stages.

Stage (1): Slepian and Wolf [SW73] considered a source coding problem where the decoder aims at perfectly reproducing correlated sources that are separately encoded at different terminals (See Theorem 2). The Slepian-Wolf rate region is suitable for DF. With the assumption that a given subset of the relays $\mathcal{V}$, have perfectly reconstructed the source sequence, the Slepian-Wolf rate region for $1 + |\mathcal{V}|$ *identical* "sources" $S_0, S_{v_1}, ..., S_{v_{|\mathcal{V}|}}$ simplifies to

$$\mathcal{R}_{\text{SW},\mathcal{V}} = \left\{ (R_0, R_{v_1}, ..., R_{v_{|\mathcal{V}|}}) : \sum_{l \in \{0\} \cup \mathcal{V}} R_l \geq H(S_0) = 1 \right\}. \tag{3.29}$$

Note that $\mathcal{R}_{\text{SW},\mathcal{V}}$ is not dependent on the received SNRs of the source-relay links, given set $\mathcal{V}$. The corresponding outage probability can be derived as

$$P_{\text{DF},\mathcal{V}}^{\text{out}} = \Pr \left\{ \mathcal{C}_{\psi} \left(\{\Gamma_{\text{D}l}\}_{l \in \{0\} \cup \mathcal{V}} \right) \cap R_{\text{c}} \cdot \mathcal{R}_{\text{SW},\mathcal{V}} = \emptyset \right\} \tag{3.30}$$

$$= \Pr \left\{ 0 \leq \psi(\Gamma_{\text{D}0}) < R_{\text{c}}, 0 \leq \psi(\Gamma_{\text{D}v_1}) < R_{\text{c}} - \psi(\Gamma_{\text{D}0}), ..., \right.$$

$$\left. 0 \leq \psi(\Gamma_{\text{D}v_{|\mathcal{V}|}}) < R_{\text{c}} - \psi(\Gamma_{\text{D}0}) - \psi(\Gamma_{\text{D}v_1}) - ... - \psi(\Gamma_{\text{D}v_{|\mathcal{V}|-1}}) \right\} \tag{3.31}$$

$$= \Pr \left\{ 0 \leq \Gamma_{\text{D}0} < 2^{R_{\text{c}}} - 1, 0 \leq \Gamma_{\text{D}v_1} < 2^{R_{\text{c}} - \psi(\Gamma_{\text{D}0})} - 1, ..., \right.$$

$$\left. 0 \leq \Gamma_{\text{D}v_{|\mathcal{V}|}} < 2^{R_{\text{c}} - \psi(\Gamma_{\text{D}0}) - ... - \psi(\Gamma_{\text{D}v_{|\mathcal{V}|-1}})} - 1 \right\} \tag{3.32}$$

$$= \int_{\gamma_{\mathrm{D}0}=0}^{2^{R_{\mathrm{c}}}-1} \int_{\gamma_{\mathrm{D}v_1}=0}^{2^{R_{\mathrm{c}}-\psi(\gamma_{\mathrm{D}0})}-1} \cdots \int_{\gamma_{\mathrm{D}v_{|\mathcal{V}|}}=0}^{2^{R_{\mathrm{c}}-\psi(\gamma_{\mathrm{D}0})-\cdots-\psi(\gamma_{\mathrm{D}v_{|\mathcal{V}|-1}})}-1}$$

$$f_{\Gamma_{\mathrm{D}0}}(\gamma_{\mathrm{D}0}) f_{\Gamma_{\mathrm{D}v_1}}(\gamma_{\mathrm{D}v_1}) \ldots f_{\Gamma_{\mathrm{D}v_{|\mathcal{V}|}}}(\gamma_{\mathrm{D}v_{|\mathcal{V}|}}) \mathrm{d}\gamma_{\mathrm{D}v_{|\mathcal{V}|}} \ldots \mathrm{d}\gamma_{\mathrm{D}v_1} \mathrm{d}\gamma_{\mathrm{D}0}. \qquad (3.33)$$

The above steps are justified as follows: (3.30) follows directly from (3.29) and Theorem 6; in (3.31), after following similar reformulations as in (3.27) and (3.28), the sum constraint is separated into individual constraints; in (3.32) the bounds are transformed with $\psi^{-1}(y) = 2^y - 1$; in (3.33) the probability of outage is established in integral form with the assumption that the received SNRs Γ_ν, are independent. The pdf $f(\gamma_\nu)$ is given in (3.1). Although the outage expression in (3.33) cannot be solved in closed form, a simple asymptotic solution can be derived at high SNR as

$$P_{\mathrm{DF},\mathcal{V}}^{\mathrm{out}} \approx \int_{\gamma_{\mathrm{D}0}=0}^{2^{R_{\mathrm{c}}}-1} \int_{\gamma_{\mathrm{D}v_1}=0}^{2^{R_{\mathrm{c}}-\psi(\gamma_{\mathrm{D}0})}-1} \cdots \int_{\gamma_{\mathrm{D}v_{|\mathcal{V}|}}=0}^{2^{R_{\mathrm{c}}-\psi(\gamma_{\mathrm{D}0})-\cdots-\psi(\gamma_{\mathrm{D}v_{|\mathcal{V}|-1}})}-1}$$

$$\frac{1}{\bar{\Gamma}_{\mathrm{D}0}\bar{\Gamma}_{\mathrm{D}v_1}...\bar{\Gamma}_{\mathrm{D}v_{|\mathcal{V}|}}} \mathrm{d}\gamma_{\mathrm{D}v_{|\mathcal{V}|}} \ldots \mathrm{d}\gamma_{\mathrm{D}v_1} \mathrm{d}\gamma_{\mathrm{D}0} \qquad (3.34)$$

$$= \frac{A_{|\mathcal{V}|+1}}{\bar{\Gamma}_{\mathrm{D}0}\bar{\Gamma}_{\mathrm{D}v_1}...\bar{\Gamma}_{\mathrm{D}v_{|\mathcal{V}|}}} \qquad (3.35)$$

where

$$A_{|\mathcal{V}|+1}(R_{\mathrm{c}}) = (-1)^{|\mathcal{V}|+1} \left(1 - 2^{R_{\mathrm{c}}} \cdot e_{|\mathcal{V}|+1}\left(-R_{\mathrm{c}}\ln(2)\right)\right). \qquad (3.36)$$

Here, $e_L(x) = \sum_{l \in [0:L-1]} \frac{x^l}{l!}$ is the exponential sum function. For more details, we refer to the derivations in Appendix A.2.

Stage (2): From the assumption that the link channels are mutually independent, the probability that a given subset of the relays $\mathcal{V} \subseteq [1:L]$, have perfectly reconstructed the source sequence—whereas the remaining relays $\mathcal{T} = [1:L]\backslash\mathcal{V}$ have erroneously reconstructed it—can be formulated as

$$P_{\mathrm{R},\mathcal{V}}^{\mathrm{out}} = \int_{\gamma_{\mathrm{S}v_1}=A_1}^{\infty} \cdots \int_{\gamma_{\mathrm{S}v_{|\mathcal{V}|}}=A_1}^{\infty} \int_{\gamma_{\mathrm{S}t_1}=0}^{A_1} \cdots \int_{\gamma_{\mathrm{S}t_{|\mathcal{T}|}}=0}^{A_1}$$

$$f_{\Gamma_{\mathrm{S}1}}(\gamma_{\mathrm{S}1})...f_{\Gamma_{\mathrm{S}L}}(\gamma_{\mathrm{S}L})\mathrm{d}\gamma_{\mathrm{S}L}...\mathrm{d}\gamma_{\mathrm{S}1} \qquad (3.37)$$

$$= \prod_{l \in \mathcal{V}} \exp\left(-\frac{A_1}{\bar{\Gamma}_{\mathrm{S}l}}\right) \prod_{l \in \mathcal{T}} \left(1 - \exp\left(-\frac{A_1}{\bar{\Gamma}_{\mathrm{S}l}}\right)\right) \qquad (3.38)$$

$$\approx \frac{(A_1)^{|\mathcal{T}|}}{\bar{\Gamma}_{\mathrm{S}t_1}...\bar{\Gamma}_{\mathrm{S}t_{\mathcal{T}}}}. \qquad (3.39)$$

The above steps are justified as follows: in (3.37), the probability that the ith relay can perfectly reconstruct the source sequence is $\int_{A_1}^{\infty} f_{\Gamma_{\mathrm{S}l}}(\gamma_{\mathrm{S}l}) \mathrm{d}\gamma_{\mathrm{S}l}$ and the probability that the lth relay cannot perfectly reconstruct the source sequence is $\int_0^{A_1} f_{\Gamma_{\mathrm{S}l}}(\gamma_{\mathrm{S}l}) \mathrm{d}\gamma_{\mathrm{S}l}$, with A_1 being given as in (3.25); in (3.38), we use (3.1) to solve the integrations; in (3.39), a high-SNR approximation is obtained, based on the MacLaurin series of the exponential function, which leads to $\exp(-x_i) \approx 1 - x_i$ and $\prod_i (1 - x_i) \approx 1$ for $x_i \to 0$.

Stage (3): Finally, the outage probability of a DF multirelay scheme is assessed $\forall \mathcal{V} \subseteq [1 : L]$ as

$$P_{\mathrm{DF},L}^{\mathrm{out}} = \sum_{\forall \mathcal{V} \subseteq [1:L]} P_{\mathrm{DF},\mathcal{V}}^{\mathrm{out}} \cdot P_{\mathrm{R},\mathcal{V}}^{\mathrm{out}} \tag{3.40}$$

$$\approx \sum_{\forall \mathcal{V} \subseteq [1:L]} \frac{A_{|\mathcal{V}|+1}}{\bar{\Gamma}_{\mathrm{D}0}\bar{\Gamma}_{\mathrm{D}s_1}...\bar{\Gamma}_{\mathrm{D}s_{|\mathcal{V}|}}} \cdot \frac{(A_1)^{|\mathcal{T}|}}{\bar{\Gamma}_{\mathrm{S}t_1}...\bar{\Gamma}_{\mathrm{S}t_{\mathcal{T}}}}, \tag{3.41}$$

where $P_{\mathrm{DF},\mathcal{V}}^{\mathrm{out}}$ and $P_{F,\mathcal{V}}^{\mathrm{out}}$ are given in (3.33) and (3.38), and their approximations, in (3.35) and (3.39), respectively.

3.7 Lossy Forwarding vs. Decode-and-Forward

3.7.1 SNR Gain

Ultimately, we are interested in the transmit power reduction of LF over DF, referred to as the SNR gain. Due to the lacking LF outage probability closed-form solution we cannot draw conclusions on the SNR gain based on an analytical formula. However, we numerically evaluate the SNR gain in the following section.

3.7.2 Diversity Gain

Similar to the SNR gain, an analytical evaluation of the LF diversity gain is not feasible, due to the lacking asymptotic outage probability closed-form solution. However, from (3.41) we determine the diversity gain of DF. As one can easily see, each denominator in (3.41) is a multiplication of $L + 1$ average SNR values, thus the diversity gain of DF is $L + 1$ (see Section 2.6).

3.7.3 Channel Usage

In LF the relays may forward erroneous sequences to the destination, whereas in DF the relays discard such sequences. Thus, the LF scheme achieves a lower outage probability at the expense of a higher channel usage, in comparison to the DF scheme. In this section we quantify this extra channel usage. To this end, we define a channel use ratio, $R_{\mathrm{cu},L}$, as the average channel use of DF over the average channel use of LF, obtained as

$$R_{\mathrm{cu},L} = \underbrace{\frac{1}{L+1}}_{\text{LF}} \cdot \Big(\underbrace{\underbrace{1}_{\text{Pr[source transmits]}} + \sum_{\forall \mathcal{V} \subseteq [1:L]} |\mathcal{V}| \cdot \underbrace{P_{\mathrm{R},\mathcal{V}}^{\text{out}}}_{\text{Pr}[l\text{th relay transmits, } \forall l \in \mathcal{V}]} \Big)}_{\text{DF}}. \qquad (3.42)$$
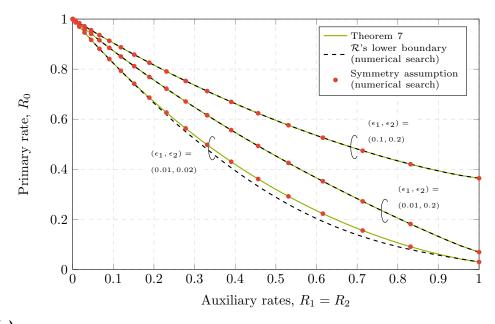
The above expression is justified as follows. For LF, the average channel use is $L+1$, since in this scheme all relays constantly forward the received source sequence to the destination. In contrast, for DF, any group of $|\mathcal{V}|$ relays forwards messages to the destination with a certain probability $P_{\mathrm{R},\mathcal{V}}^{\text{out}}$ given as in (3.38), $\forall \mathcal{V} \subseteq [1:L]$. In particular, at high SNR, $R_{\mathrm{cu},L}$ approaches one, because so does the probability that all relays perfectly recover the source sequence.

3.8 Numerical Examples

3.8.1 Rate Region

In this section we illustrate our inner bounds in Theorem 7 and Theorem 8 by numerical examples. We show results for $L \in \{2,3\}$ with different values of ϵ_l, $l \in [1:L]$. We check these analytical bounds by performing an exhaustive numerical search (under the assumption that the auxiliary RVs are connected to the helpers through symmetric channels). Also, for comparison, we assess the exact rate region's lower boundary by performing an exhaustive search without any restriction on the symmetry, i.e., the helpers and auxiliary RVs being related via binary asymmetric channels (BACs) with $\{\alpha_l, \beta_l\}_{l \in [1:L]} \in [0, 0.5]^{2L}$.

In Fig. 3.3a we show our results in Theorem 7 (green line), numerical-search results for a symmetric channel between S_l and U_l (red dots), and the rate region's lower boundary (black dashed line). We show results for $L = 2$ with $(\epsilon_1, \epsilon_2) = \{(0.01, 0.02), (0.01, 0.2), (0.1, 0.2)\}$ and symmetric auxiliary rates

(a)

(b)
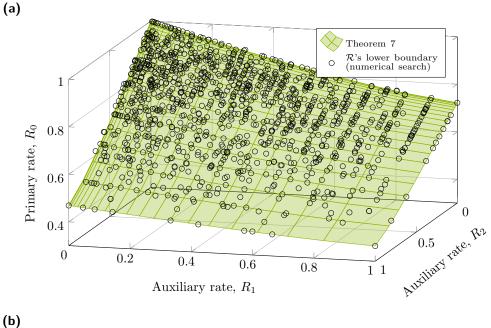
Fig. 3.3. Rate region $\mathcal{R}$: (a) symmetric rates $R_1 = R_2 \in [0,1]$ with $(\epsilon_1, \epsilon_2) \in \{(0.01, 0.02), (0.01, 0.2), (0.1, 0.2)\}$, and (b) $(R_1, R_2) \in [0,1]^2$ with $(\epsilon_1, \epsilon_2) \in \{(0.1, 0.2)\}$.

$R_1 = R_2 = R$, i.e., (R_0, R, R). The following can be observed: i) Theorem 7 matches the simulation results for symmetric channels, and (ii) Theorem 7 gives a tight inner bound on the rate region's lower boundary, especially for large values of ϵ_l, i.e., as the helpers turn out to be more degraded versions of the primary source. Fig. 3.3b shows the rate 3-tuples for $L = 2$ and $(\epsilon_1, \epsilon_2) = \{(0.1, 0.2)\}$. We show results of Theorem 7 (green plane) and
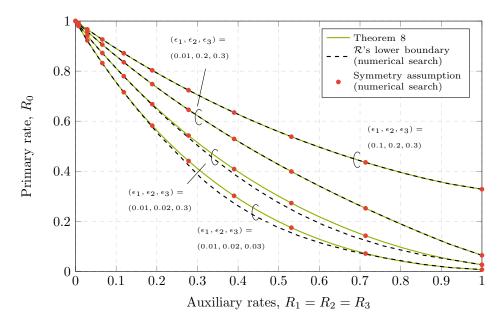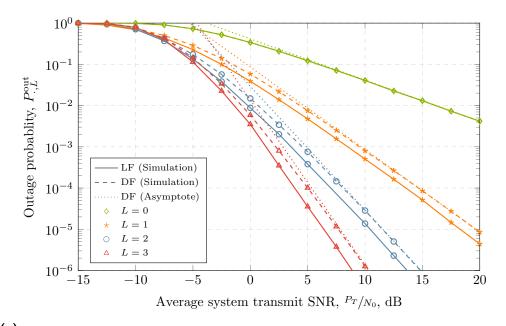
Fig. 3.4. Rate region $\mathcal{R}$: symmetric rates $R_1 = R_2 = R_3 \in [0, 1]$ with $(\epsilon_1, \epsilon_2, \epsilon_3) \in \{(0.01, 0.02, 0.03), (0.01, 0.02, 0.3), (0.01, 0.2, 0.3), (0.1, 0.2, 0.3)\}$.

the rate region's lower boundary (black dots). The same conclusions as in Fig. 3.3a can be made by careful evaluation of a variety of setups.

In Fig. 3.4 we show our results in Theorem 8 (green line), numerical-search results for a symmetric channel between S_l and U_l (red dots), and the rate region's lower boundary (black dashed line). We show results for $L = 3$ with $(\epsilon_1, \epsilon_2, \epsilon_3) \in \{(0.01, 0.02, 0.03), (0.01, 0.02, 0.3), (0.01, 0.2, 0.3), (0.1, 0.2, 0.3)\}$ and symmetric auxiliary rates $R_1 = R_2 = R_3 = R$, i.e., (R_0, R, R, R). The same conclusions as for $L = 2$ can be drawn.

3.8.2 Outage Probability

In this section, we illustrate the derived outage probabilities and channel use ratios. The outage probability's upper bound of LF is assessed via Monte-Carlo simulation—or, equivalently, via numerical integration, from (3.28); the outage probability of DF is assessed in an asymptotic fashion, from (3.41), as well as via Monte-Carlo simulation—or, equivalently, via numerical integration, from (3.33) and (3.38) into (3.40). The channel use ratio is assessed analytically, from (3.42). We assume a binary phase-shift keying modulation and a channel-code rate of $1/2$, so that $R_{\mathrm{c}} = 0.5$. Moreover, we assume the average channel power gain of a given link equals $d^{-\eta}$, with d denoting the link distance and η being the path-loss exponent. For illustration purposes, we consider $\eta = 3.5$ and that all relays are located halfway between source

(a)

(b)
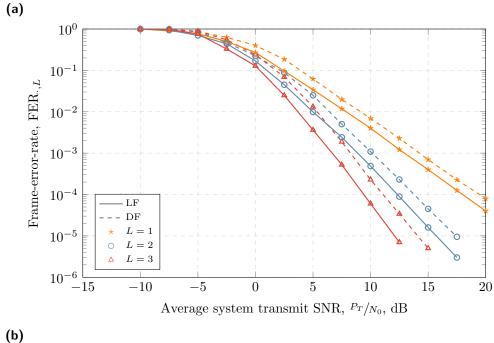
Fig. 3.5. Lossy forwarding vs. decode-and-forward: (a) outage probability, and (b) frame-error-rate.

and destination. We define an average system transmit SNR as P_T/N_0, where P_T is a total amount of power equally allocated among the source and all relays.

Fig. 3.5a depicts the outage probability of the LF (upper bound) and DF (exact and asymptotic) schemes versus the average system transmit SNR. Fig. 3.6 depicts the corresponding channel use ratio. In the examples, we consider the use of no, one, two, and three relays, i.e., $L \in \{0, 1, 2, 3\}$. The
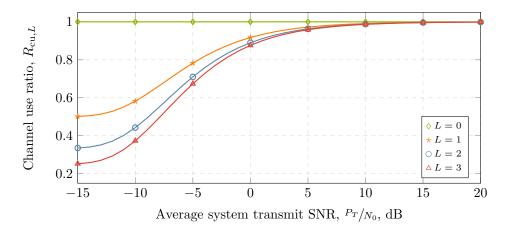
Fig. 3.6. Lossy forwarding vs. decode-and-forward: channel use.

figures attest that LF outperforms DF in terms of outage probability, becoming more advantageous as the number of relays increases. On the other hand, such an improvement requires an extra cost in terms of channel usage, mainly at low SNR. In addition, we conclude that both schemes achieve a diversity gain of $L + 1$.

Fig. 3.5b depicts the FER of the LF and DF schemes, versus the average system transmit SNR, as achieved by the DTC in [AM12], see Section 2.7. Note that we consider one, two, and three relays, i.e., $L \in \{1, 2, 3\}$. We used the following simulation parameters:

- Frame length: $n = 1000$ channel symbols

- Generator polynomial of SNRCC: $G_{\text{SNRCC}} = ([3, 1])_8$

- Generator polynomial of SRCC: $G_{\text{SRCC}} = ([3, 1]3)_8$

- Doping ratio of ACC: $P_{\text{ACC}} = 8$ (source), $P_{\text{ACC}} = 16$ (relays)

- Local iterations: 15

- Global iterations: 3

- Path-loss exponent: $\eta = 3.52$

- Relays are located halfway between source and destination

We then compared the FER of LF to that of DF. In order to unambiguously evaluate the effect of allowing intra-link errors, we adopted for DF the same coding scheme we adopted for LF — except that only error-free relay sequences are forwarded in the former. In addition, we compared the FER simulation results with the outage probability expressions derived befor. The

figures attest that the LF scheme outperforms the DF scheme in terms of both outage probability and FER, becoming more advantageous as the number of relays increases. From those figures we conclude that the coding structure in [AM12] is clearly suboptimal, since the FER curves are loosely above the outage ones. This suboptimality may be caused by the following: i) finite frame length, ii) simple convolutional code, iii) decoding without iteration at the relay, and iv) extrinsic information exchange between decoders at the receiver might not be optimal. Nevertheless, we conclude that despite the additional complexity of practical MSCC implementations, the concept is well suited to achieve ultra-reliable communications in relay networks.

3.9 Summary

In this chapter, we evaluated the potential of MSCCs in relay networks. In particular, we considered two different systems, namely, LF and DF. In DF, the decoded message is discarded by the relay whenever an error is detected. In contrast, in LF, the relay forwards even an erroneous message to the destination. Ultimately, we were interested in fundamental limits of both systems and their performance differences.

For LF, we faced two major challenges in order to derive fundamental limits. At first, we had to specialize the rate region for the many-help-one problem with independently degraded helpers to sources that are binary, uniformly distributed, and interrelated through symmetric channels. Providing the solution was surprisingly difficult even for this basic scenario, since an optimization over auxiliary RVs with unknown statistics was required. Nevertheless, we derived a simple and tight inner bound of the rate region's lower boundary based on reasonable assumptions about the auxiliary RVs' statistics. The inner bound is given as a function of the BSC crossover probabilities between source and helpers. Numerical results indicated that the derived inner bound proves increasingly tight as the helpers become more degraded. Secondly, we found an outage probability's upper bound based on our derived inner bound on the rate region's lower boundary. The outage probability's upper bound could not be solved in closed form, thus requiring numerical evaluation.

Unlike existing work for DF, instead of MRC, we found fundamental limits for MSCCs. To this end, we derived the exact outage probability in integral form based on the corresponding rate region. The exact outage probability could not be solved in closed form, but a simple asymptotic solution was derived at high SNR.

From our results we concluded the following in regard to the performance of MSCCs in relay networks. With every additional relay, the diversity gain increases, which in turn leads to an increased system reliability. Therefore, MSCCs are a preeminent way to achieve reliably communication in relay networks. Our results are analytically described depending on the number of relays, the spectral efficiency, the topology, and the SNR, and thus, can be used to assess or optimize practical cooperative communication deployments. From the numerical examples, we concluded that LF outperforms DF in terms of outage probability, becoming more advantageous as the number of relays increases. On the other hand, such an improvement requires an extra cost in terms of channel usage, mainly at low SNR. Furthermore, we compared our theoretical results to a practical DTC. A gap between the outage probability and FER curves revealed the limitations of the DTC. Nevertheless, at high SNR, the curves exhibit the same slope, thus indicating the same diversity gain.

Wireless Sensor Network | 4

It is well known that MSCCs can improve the reliability and energy efficiency of WSNs by exploiting the correlation among sensing data. In this chapter, we quantify the communication performance of MSCCs in terms of outage probability, which is the ultimate performance limit with regard to the system reliability. We derive simple, yet accurate analytical outage probability results, in which the number of connections, the spectral efficiency, the path loss, and the SNR are incorporated, giving new insights into the potentials of MSCCs. These are our main contributions: (1) derivation of the distributed lossless compression (DLC) rate region for BMSs that are interrelated through BSCs; (2), derivation of the exact and asymptotic outage probability for MSCC, based on the corresponding rate region; and (3) quantifying the performance improvement of MSCC over non-cooperative coding in terms of SNR gain.

4.1 Related Work

As shown in [AM12; XLC04; RG07], the presence of mutually correlated sensing data can be exploited with MSCC to improve the reliability of WSNs, which in turn leads to a higher energy efficiency. In [RG07], a suboptimal power allocation scheme was proposed. In that scheme, the data are encoded separately at each node and jointly decoded at the FC by pairs of nodes. In [CAM13b], capitalizing on Slepian-Wolf's correlated source coding theorem [SW73], an asymptotically optimal power allocation was derived for a classical three-node relaying system containing intra-link errors. A theoretical investigation on the outage probability of such a system was presented in [Zho+14].

4.2 System Model

We consider a clustered network as shown in Fig. 4.1, consisting of L sensor nodes, dispensing BMSs, denoted as $[S_l(i)]_{i=1}^{\infty}$, for $l \in [1:L]$, with i denoting discrete time. The k-sample source sequence shall be represented in vector form as $S_l^k = [S_l(1), S_l(2), ..., S_l(k)]$. When appropriate, for simplicity, we shall drop the temporal index, denoting the source output simply as S_l. The source S_l takes values from a binary set $\{0, 1\}$ with uniform probabilities, i.e., $p_{S_l}(s_l = 0) = p_{S_l}(s_l = 1) = 0.5$. As argued before, these sequences are
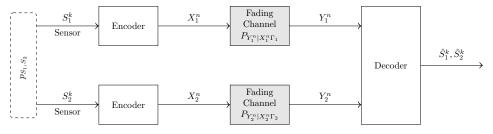
Fig. 4.1. System model of a clustered wireless sensor network with two sensors (i.e., $L = 2$). Multiple sensors monitor a physical phenomenon and transmit their correlated data to a common fusion center over parallel fading channels. The fusion center exploits the correlated sensor data to improve the decoding performance. We are interested in the outage probability, i.e., probability that at least one sensor data cannot reliably decoded.

mutually correlated, with the correlation coefficient between S_i and S_j being expressed as

$$\rho_{l,j} = \frac{\mathbb{E}[S_i S_j] - \mathbb{E}[S_i]\mathbb{E}[S_j]}{\sqrt{\text{Var}[S_i]\text{Var}[S_j]}}. \tag{4.1}$$

Since the source sequences are binary and uniformly distributed, it follows that $\mathbb{E}[S_l] = 0.5$ and $\text{Var}[S_l] = 0.25, \forall l \in [1 : L]$. In order to calculate the correlation term $\mathbb{E}[S_i S_j]$, we introduce an auxiliary binary uniformly distributed source, S_0, from which each source S_l is generated through an independent binary symmetric channel with crossover probability ϵ_l[1]. Consequently, $\mathbb{E}[S_i S_j]$ can be computed in terms of the corresponding crossover probabilities as

$$
\begin{aligned}
\mathbb{E}[S_i S_j] =& p_{S_0}[s_0 = 0]p_{S_i S_j | S_0}[s_i = 1, s_j = 1 | s_0 = 0] \\
&+ p_{S_0}[s_0 = 1]p_{S_i S_j | S_0}[s_i = 1, s_j = 1 | s_0 = 1] \\
=& 0.5\epsilon_i\epsilon_j + 0.5(1 - \epsilon_i)(1 - \epsilon_j),
\end{aligned}
\tag{4.2}
$$

and using this in (4.1) the correlation coefficient can finally be obtained as

$$\rho_{l,j} = 4\epsilon_i\epsilon_j - 2(\epsilon_i + \epsilon_j) + 1. \tag{4.3}$$

Each source sequence S_l^k is encoded to the transmit source sequence X_l^n, i.e., the lth encoder maps $\mathcal{S}_l^k \to \mathcal{X}_l^n$, and transmitted to the FC over parallel fading channels. In this work, we consider quasi-static Rayleigh fading and AWGN with mean power N_0 (see Section 2.4.2). For convenience, we reproduce

---

[1]Although the auxiliary sequence may be regarded as a representation of the original phenomenon being monitored, as well as the binary symmetric channels may be regarded as a model for the imperfect sensing mechanism, these have been introduced here merely as a mathematical artifice to yield mutually correlated binary sequences.

the pdf of the received SNRs in (2.26). The pdf of the received SNR Γ_l is given by

$$f_{\Gamma_l}(\gamma_l) = \frac{1}{\bar{\Gamma}_l} \exp\left(-\frac{\gamma_l}{\bar{\Gamma}_l}\right), \tag{4.4}$$

with the average SNR $\bar{\Gamma}_l$ being obtained as

$$\bar{\Gamma}_l = \frac{P_l}{N_0} \cdot d_l^{-\eta}, \tag{4.5}$$

where P_l is the transmit power at the lth sensor, d_l is the distance between the lth sensor and the FC, and η is the path loss exponent. The CSI is assumed to be known at the receiver. All received sequences Y_l^n for $l \in [1:L]$ are jointly decoded to retrieve $\{S_l^k\}_{l\in[1:L]}$, i.e., the decoder maps $\prod_{l\in[1:L]} \mathcal{Y}_l^n \to \prod_{l\in[1:L]} \mathcal{S}_l^k$, we denote the estimates as $\{\hat{S}_l^k\}_{l\in[1:L]}$. The probability of error $P_e^{(k)} := \Pr\left\{\{S_l^k\}_{l\in[1:L]} \neq \{\hat{S}_l^k\}_{l\in[1:L]}\right\}$ (see (2.4)) depends on the instantaneous received SNRs Γ_l for $l \in [1:L]$.

4.3 Problem Statement and Approach

In this work, we want to quantify the communication performance by the outage probability given by

$$P_{\mathrm{WSN},L}^{\mathrm{out}} = \Pr\left\{\mathcal{C}_\psi\left(\{\Gamma_l\}_{l\in[1:L]}\right) \cap R_{\mathrm{c}} \cdot \mathcal{R}_{\mathrm{SW}} = \emptyset\right\}. \tag{4.6}$$

In order to derive the outage probability in (4.6), we first consider the rate region $\mathcal{R}_{\mathrm{SW}}$ when specialized to sources that are binary, uniformly distributed, and interrelated via correlation coefficients. The multiple sensing information sequences may be considered as correlated sources and, thus, Slepian-Wolf's theorem can reason the performance gain of a MSCC scheme, which we specialize to the referred case. We then determine the exact outage probability by averaging over all received SNRs and find the exact coding gain via a high-SNR analysis.

4.4 Rate Region

Recall the Slepian-Wolf rate region $\mathcal{R}_{\mathrm{SW}}$ in Theorem 2. According to that theorem, all sequences S_l^k can be recovered error-free iff the rates R_l, $l \in [1 : L]$, satisfy the following inequality constraints:

$$\sum_{l \in \mathcal{V}} R_l \geq H\left(\{S_l\}_{l \in \mathcal{V}} | \{S_l\}_{l \in \mathcal{V}^c}\right)$$

$$= H\left(\{S_l\}_{l \in [1:L]}\right) - H\left(\{S_l\}_{l \in \mathcal{V}^c}\right), \qquad (4.7)$$

with

$$H\left(\{S_l\}_{l \in \mathcal{V}}\right) = - \sum_{\{s_l\}_{l \in \mathcal{V}} \in \{0,1\}^{|\mathcal{V}|}} p_{S_{v_1} \dots S_{v_{|\mathcal{V}|}}}\left(s_{v_1}, \dots, s_{v_{|\mathcal{V}|}}\right)$$

$$\times \operatorname{ld} p_{S_{v_1} \dots S_{v_{|\mathcal{V}|}}}\left(s_{v_1}, \dots, s_{v_{|\mathcal{V}|}}\right) \qquad (4.8)$$

for all subsets $\mathcal{V} \subseteq [1 : L]$ and complementary sets $\mathcal{V}^c = [1 : L] \backslash \mathcal{V}$. The probabilities required in (4.8) can be obtained as

$$p_{S_{v_1} \dots S_{v_{|\mathcal{V}|}}}\left(s_{v_1}, \dots, s_{v_{|\mathcal{V}|}}\right) = \frac{1}{2}\left[\prod_{l \in \mathcal{V}} p_{E_l}(s_l) + \prod_{l \in \mathcal{V}} (1 - p_{E_l}(s_l))\right], \qquad (4.9)$$

where $p_{E_l}(\cdot)$ is an auxiliary pmf associated to the crossover model for the lth sensor, defined by

$$p_{E_l}(s_l) := (1 - \epsilon_l)\delta(s_l) + \epsilon_l \delta(s_l - 1). \qquad (4.10)$$

4.5 Outage Probability

In this section, we derive the exact and asymptotic outage probability of MSCC based on the derived rate region. Furthermore, we derive the exact and asymptotic outage probability of a non-cooperative scheme for comparison.

4.5.1 Multiterminal Source-Channel Code

For a reliable WSN, it is required that all sensing information sequences are fully recovered. Therefore, a system outage occurs if at least one sequence S_l^k cannot be decoded error-free. Recall the discussion in Section 2.5. On the one hand, we have the capacity region $\mathcal{C}_\psi\left(\{\Gamma_l\}_{l\in[1:L]}\right)$ depending on the received SNRs. On the other hand, we have the rate region $\mathcal{R}_{\mathrm{SW}}$. An outage event occurs, whenever the intersection of both regions is empty, see Theorem 6. Thus, for (4.6) we have

$$P_{\mathrm{WSN},L}^{\mathrm{out}} = 1 - \Pr\left\{\bigcap_{\forall \mathcal{V}\subseteq[1:L]}\left(\sum_{l\in\mathcal{V}}\psi(\Gamma_l) \geq R_{\mathrm{c}}H\left(\{S_l\}_{l\in\mathcal{V}}|\{S_l\}_{l\in\mathcal{V}^c}\right)\right)\right\}. \quad (4.11)$$

The steps can be justified similarly as (3.26)-(3.28).

Next we derive the asymptotic outage probability in two steps: (i) we show that a reduced set of constraints suffices for a high-SNR asymptotic analysis, and (ii) we calculate the asymptotic outage probability based on the resulting SNR constraints.

(i) Reduction of constraints at high SNR We begin by decomposing the outage probability into two probability terms, for convenience, as shall become apparent soon. The first term, $P_{\mathrm{WSN},1}^{\mathrm{out}}$, is the probability that at least one of the L single-rate constraints in (4.7) is violated, i.e.,

$$P_{\mathrm{WSN},1}^{\mathrm{out}} = 1 - \Pr\left\{\{\psi(\Gamma_l) \geq R_{\mathrm{c}}H_l\}_{l\in[1:L]}\right\}, \quad (4.12)$$

where $H_l := H\left(S_l|\{S_{\bar{l}}\}_{\bar{l}\in[1:L]\setminus\{l\}}\right)$ is the entropy of the lth information sequence conditioned on all remaining sequences, being calculated as in (4.7)-(4.10). Since a subset of the rate constraints in (4.7) have been ignored in (4.12), the latter does not include all possible outage events, such that

$$P_{\mathrm{WSN},L}^{\mathrm{out}} = P_{\mathrm{WSN},1}^{\mathrm{out}} + \delta, \quad (4.13)$$

where the term $\delta \geq 0$ accounts for those additional outage events. Interestingly, it turns out that, as the SNR increases, δ converges faster to zero than $P_{\mathrm{WSN},1}^{\mathrm{out}}$, and thus, playing no role at high-SNR. Indeed, as shown in [WG03] under a different context, the asymptotic outage behavior of a transmission link depends exclusively on the SNR distribution in the vicinity of the origin. In our case, we have an L-variate rate (or SNR, equivalently) distribution, so that it suffices to cover the probability masses in the vicinity of the L

coordinate axes. Notice that this is fulfilled in (4.12). Therefore, the asymptotic outage probability, $\tilde{P}_{\text{WSN},L}^{\text{out}}$, reduces to $P_{\text{WSN},1}^{\text{out}}$. Rearranging $\psi(x) = y$ to $x = 2^y - 1$, which can be readily used to rewrite (4.12) as

$$\tilde{P}_{\text{WSN},L}^{\text{out}} = 1 - \Pr[\{\Gamma_l \geq A_l(R_{\text{c}})\}_{l\in[1:L]}], \tag{4.14}$$

where $A_l(R_{\text{c}}) := 2^{R_{\text{c}}H_l} - 1$ reflects the amount of correlation among the sensors.

(ii) Calculation of asymptotic outage probability   Since the received SNRs at the sensors are mutually independent, (4.14) can be evaluated as a product of L one-dimensional integrals, which, with the use of (4.4), gives

$$\tilde{P}_{\text{WSN},L}^{\text{out}} = 1 - \prod_{l\in[1:L]} \int_{\gamma_l=A_l(R_{\text{c}})}^{\infty} \frac{1}{\bar{\Gamma}_l} \exp\left(-\frac{\gamma_l}{\bar{\Gamma}_l}\right) d\gamma_l,$$

$$= 1 - \prod_{l\in[1:L]} \exp\left(-\frac{A_l(R_{\text{c}})}{\bar{\Gamma}_l}\right). \tag{4.15}$$

We further simplify the above formula due to the high-SNR assumption, by using the MacLaurin series for exponential functions $\exp(-x_i) \approx 1 - x_i$ and expanding the resulting product as $\prod_i (1 - x_i) \approx 1 - \sum_i x_i$, for $x_i \to 0$. As a result, the asymptotic outage probability is reduced to the strikingly compact form

$$\tilde{P}_{\text{WSN},L}^{\text{out}} = \sum_{l\in[1:L]} \frac{A_l(R_{\text{c}})}{\bar{\Gamma}_l}, \tag{4.16}$$

where $G_{\text{c,WSN}} = 1/A_l(R_{\text{c}})$ is the coding gain of MSCC. The diversity gain is merely one, as we can easily see from the denominators (see Section 2.6).

4.5.2 Non-Cooperative Coding

In this section we derive the outage probability of a non-cooperative coding for comparison. The lth source can be decoded error-free iff $\psi(\Gamma_l) \geq H(S_l)$ [CT06]. The outage probability can be obtained as

$$P_{\text{NC},L}^{\text{out}} = 1 - \Pr\left\{ \bigcap_{l\in[1:L]} \psi(\Gamma_l) \geq R_{\text{c}}H(S_l) \right\} \tag{4.17}$$

$$= 1 - \prod_{l\in[1:L]} \Pr\{\Gamma_l \geq B(R_{\text{c}})\} \tag{4.18}$$

$$=1 - \prod_{l\in[1:L]_{\gamma_l=B(R_c)}} \int_{}^{\infty} \frac{1}{\bar{\Gamma}_l} \exp\left(-\frac{\gamma_l}{\bar{\Gamma}_l}\right) d\gamma_l \tag{4.19}$$

$$=1 - \prod_{l\in[1:L]} \exp\left(-\frac{B(R_c)}{\bar{\Gamma}_l}\right) \tag{4.20}$$

$$\approx \sum_{l\in[1:L]} \frac{B(R_c)}{\bar{\Gamma}_l}, \tag{4.21}$$

from which $G_{c,NS} = 1/B(R_c)$, with $B(R_c) := 2^{R_c} - 1$, is the coding gain of non-cooperative coding. The steps can be justified in a similar fashion as (4.15)-(4.16).

4.6 SNR Gain

The SNR gain of MSCC with respect to non-cooperative coding can be defined as the corresponding asymptotic reduction in SNR while achieving the same outage probability. To ensure a fair comparison between different setups, we equally allocate the total transmit power P_T to all sensors, such that $P_l = P_T/L, \forall l \in [1 : L]$. However, this assumption is non-essential and other system setups can be evaluated from our formulas with some effort. We evaluate the required total average SNR $\bar{\Gamma} = \sigma_{(\cdot)}(\tilde{P}^{\text{out}})$ in the high-SNR regime. Based on (4.16) and (4.21), the average transmit SNR of the two schemes can asymptotically be written as

$$\sigma_{NS}(\tilde{P}^{\text{out}}) = \frac{P_T}{N_0} = \frac{L\sum_{l\in[1:L]} B(R_c) \cdot d_l^\eta}{\tilde{P}^{\text{out}}} \tag{4.22}$$

and
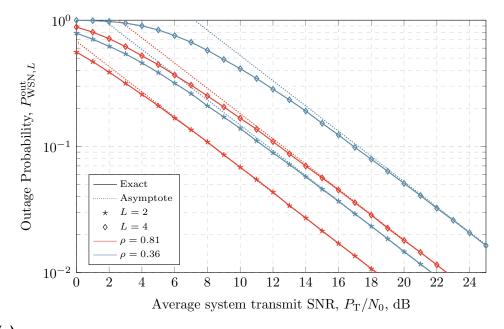
$$\sigma_{WSN}(\tilde{P}^{\text{out}}) = \frac{P_T}{N_0} = \frac{L\sum_{l\in[1:L]} A_l(R_c) \cdot d_l^\eta}{\tilde{P}^{\text{out}}}. \tag{4.23}$$

Finally, using (4.22) in (4.23), we obtain the SNR gain as the ratio between the required average SNRs for MSCC and non-cooperative coding as

$$G_{WSN} = \frac{\sum_{l\in[1:L]} B(R_c) \cdot d_l^\eta}{\sum_{l\in[1:L]} A_l(R_c) \cdot d_l^\eta}. \tag{4.24}$$

Once again, notice that the SNR gain in (4.24) is ultimately written in terms of the conditional entropies of the various sensors, their distances to the FC, and the path loss exponent.

4.7 Numerical Examples

(a)

(b)
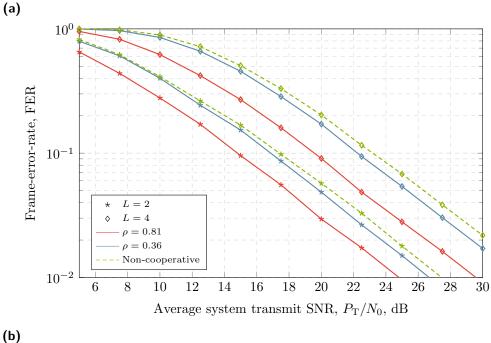
Fig. 4.2. MSCC performance: (a) outage probability, and (b) FER, with $L \in \{2, 3, 4\}$, $\rho \in \{0.36, 0.81\}$, and $R_c = 0.5$.

In this Section, we illustrate and discuss the performance of the investigated system through numerical examples. We consider binary phase-shift keying and a channel code rate of $R_c = 0.5$. Moreover, we assume that the sensors are identically correlated, i.e., $\rho_{l,j} = \rho$. We equally allocate the total transmit power P_T to all channels, such that $P_l = P_T/L, \forall l \in [1 : L]$. Furthermore,
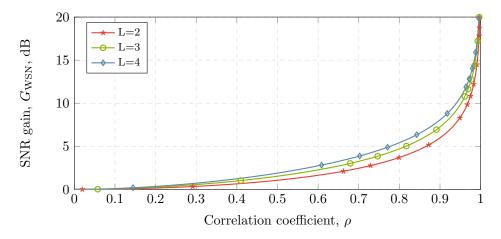
Fig. 4.3. MSCC performance: SNR gain over non-cooperative system with $L \in \{2, 3, 4\}$, $\rho \in [0, 1]$, and $R_c = 0.5$.

we normalize all distances to one. We define the average system transmit SNR as P_T/N_0. In what follows, we use $H_L := H(\{S_l\}_{l \in [1:L]})$ to denote the joint entropy of all information sequences. For simplicity, we call it system entropy.

Fig. 4.2a depicts the outage probability of MSCC (Monte-Carlo simulation of (4.11) and our asymptote in (4.16)) versus the average system transmit SNR P_T/N_0. We show results for $L \in \{2, 3, 5\}$ and $\rho \in \{0.36, 0.81\}$. We can observe the following: (i) the asymptote is very tight at medium and high SNR; (ii) for a fixed correlation coefficient, additional sensors manifests itself as a horizontal shift of the outage probability; and (iii) an increase in the correlation coefficient manifests itself as a vertical shift of the outage probability.

Fig. 4.3 depicts the SNR gain of MSCC —G_{WSN} given in (4.24)— over non-cooperative sensing, versus the correlation coefficient ρ. We observe that the SNR gain increases with the number of sensors and correlation coefficient. Interestingly, we see that the SNR gain increases significantly, if the correlation coefficient approaches one.

Fig. 4.2b depicts the FER of the MSCC schemes, versus the average system transmit SNR, as achieved by the DTC in [AM12], see Section 2.7. We used the following simulation parameters:

- Frame length: $n = 1000$ channel symbols

- Generator polynomial of SNRCC: $G_{SNRCC} = ([3, 1])_8$

- Generator polynomial of SRCC: $G_{SRCC} = ([3, 1]3)_8$
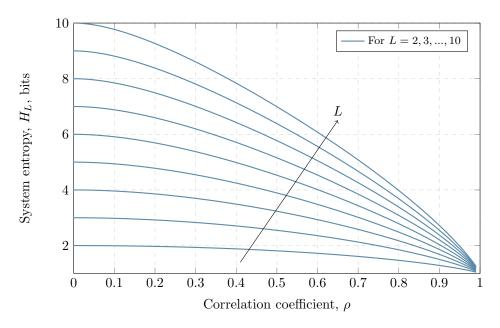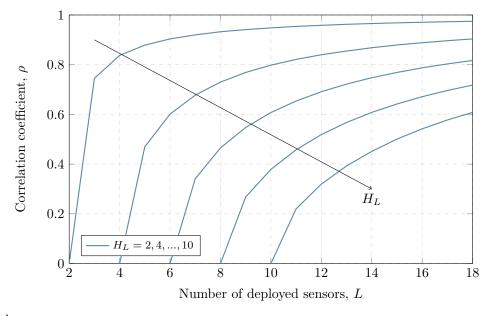
Fig. 4.4. System entropy vs. correlation coefficient for different numbers of sensors.

- Doping ratio of ACC: $P_{\text{ACC}} = 1$

- Local iterations: 15

- Vertical iterations: 3

We compare the FER of MSCC to that of a non-cooperative scheme. In order to unambiguously evaluate the effect of exploiting correlation, we adopted for the non-cooperative scheme the same coding scheme for MSCC — except that no information exchange between turbo decoders is performed. In addition, we compare the FER simulation results with the outage probability expressions derived before. The figures attest that the MSCC scheme outperforms the non-cooperative scheme in terms of both outage probability and FER, becoming more advantageous as the correlation coefficient increases. We see that an increased correlation coefficient manifests itself as a vertical shift of the FER curves. The gains of the FERs are similar to our analytically derived SNR gains. However, from those figures we conclude that the coding structure in [AM12] is clearly suboptimal, since the FER curves are loosely above the outage ones. This suboptimality may be caused by the following: i) limited frame length, ii) simple convolutional code, and iii) extrinsic information exchange between decoders at the receiver might not be optimal. Nevertheless, we conclude that practical MSCC implementations outperform non-cooperative concepts and therefore are well suited to achieve reliable communications in WSNs.
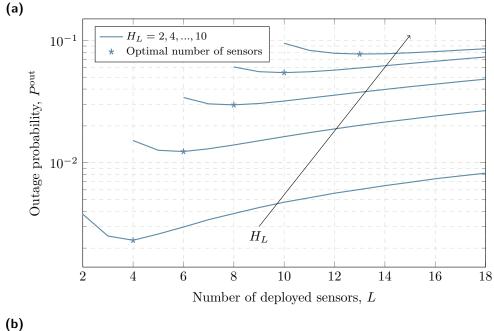
Fig. 4.5. (a) Correlation coefficient vs. number of sensors for different system entropies, and (b) outage probability vs. numbers of sensors for different system entropies at $P_{\mathrm{T}}/N_0 = 35\,\mathrm{dB}$.

As shown in Sections 4.2 and 4.4, the system entropy depends on the number of sensors and on the correlation coefficient between them. These analytical results are plotted in Fig. 4.4 and, under a rearranged perspective, also in Fig. 4.5 (a). The lower the correlation coefficient or the higher the number of sensors, the higher is the system entropy. In practice, the system entropy is usually determined by the total amount of information inherent to the physical phenomenon being monitored in a certain area, regardless of the

amount of sensors being deployed within that area. Following this, we now fix the system entropy for different numbers of sensors by adjusting the correlation coefficient accordingly. The resulting asymptotic outage probability in (4.16) is depicted in Fig. 4.5 (b) for $P_\mathrm{T}/N_0 = 35\,\mathrm{dB}$. As expected, the higher the system entropy, the higher is the outage probability, since the SNR requirements intensify. More interestingly, for each value of system entropy, an optimal number of sensors (asterisk markers) exists that minimizes the outage probability. Such behaviour indicates a trade-off between less correlation (L small) and more rate constraints (L large).

4.8 Summary

In WSN sensors are in general densely deployed to monitor a physical phenomenon. Therefore, the monitored sensor data has some degree of correlation. In this chapter, we were interested in the performance gain, if MSCCs exploit this correlation to improve the system reliability. Ultimately, we were interested in fundamental limits of MSCCs and their performance difference to non-cooperative communication concepts.

The derivation of the MSCC's fundamental limits were based on three key steps. At first, we introduced an auxiliary RV yielding an unambiguous correlation model between all BMSs. Secondly, we specialized the Slepian-Wolf rate region to the referred BMSs which we then interrelated through BSCs. Thirdly, based on the rate region, we derived the exact outage probability in integral form. The exact outage probability could not be solved in closed form, thus requiring numerical evaluation. Nevertheless, we found that a reduced set of rate constrains is sufficient to derive a simple asymptotic outage probability in closed form, at high SNR.

From our results we concluded the following in regard to the performance of MSCCs in WSNs. With every additional sensor, the coding gain increases, which in turn leads to an increased system reliability. However, the performance improvement is heavily dependent on the correlation among the sensor data. In contrast to relay networks, the diversity gain does not increase with additional sensors. Furthermore, the asymptotic analysis turned out to be well suited to assess or optimize practical cooperative communication deployments, as it offers a simple yet in-depth characterization of the system performance's general trend. We illustrated this based on a comparison between the analytical outage probability results and FERs of a practical DTC.

Finally, we quantified the performance improvement over non-cooperative concepts in terms of the SNR gain. This comparison showed that the additional complexity of MSCCs is an acceptable expense, considering the reliability improvement.

Multi-Connectivity Network $\Big|$ 5

MCo is considered to be a key strategy for enabling reliable transmissions and enhanced data rates in fifth-generation mobile networks, as it provides multiple links from source to destination. In this chapter, we quantify the performance limits of MCo in terms of outage probability and throughput. Outage probability and throughput provide, respectively, ultimate performance limits of system reliability and data rate. For doing so, we establish a simple, yet accurate analytical framework at high SNR, in which the number of links, the spectral efficiency, the path loss, and the SNR are incorporated, giving new insights into the potentials of MCo as compared with single-connectivity (SCo). These are our main contributions: (1) finding the exact coding gain of the outage probability for parallel AWGN channels with quasi-static Rayleigh fading; (2) quantifying the performance improvement of MCo over SCo in terms of SNR gain; and (3) comparing optimal and suboptimal combining schemes for MCo at the receiver side, namely multiterminal source-channel coding, selection combining, and maximal-ratio combining, also in terms of SNR gain. Multiterminal source-channel coding is also referred to as joint decoding in the context of MCo, which we use likewise in this chapter.

5.1 Related Work

Recently, research on ultra-reliable low latency communications (URLLC) is emerging considerably, focusing on the analysis of micro- and macrodiversity and its impact on reliability. In [Poc+15], MCo solutions that utilize micro- as well as macrodiversity were evaluated in system simulations to illustrate how the signal-to-interference-plus-noise ratio and the outage probability can be improved. In [Kir+15], the impairments of correlated fading were evaluated and the trade-offs between power consumption, link usage, and outage probability were given. In another work, multi-radio access-technology architectures were compared regarding their latency, which is significantly improved by MCo techniques [NP16]. For other works on MCo for URLLC, see [Öhm17] and the references therein. The major underlying concepts of MCo solutions, namely micro- and macrodiversity, have been extensively studied, and their effects on the outage probability are well understood [Mol12]. However, in the aforementioned studies, only linear (suboptimal) combining
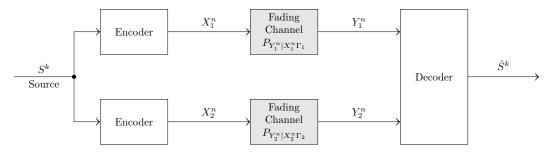
Fig. 5.1. Multi-connectivity system model. The source wishes to reliably transmit information to the destination over parallel fading channels. We are interested in the outage probability.

schemes, namely SC and MRC, have been considered. In particular, joint decoding (JD), which is optimum, remains open for investigation. Herein we help fill this gap.

Deriving the outage probability of JD for parallel fading channels has been recognized as a highly challenging problem. An important result is to evaluate the diversity-multiplexing tradeoff (DMT) of fading channels. The DMT states that by doubling the SNR, we get both a decrease in outage probability by the factor of $2^{-G_{\mathrm{d}}(G_{\mathrm{r}})}$, yielding an increase in reliability, and an increase in throughput of G_{r} bits per channel use, i.e., the DMT describes the slope and the pre-log factor of the outage probability and throughput, respectively, at infinite SNR. This concept was first proposed by Zheng and Tse for MIMO channels [ZT03]. The corresponding results for parallel fading channels can be found in [TV05]. For finite-SNR the DMT of MIMO channels was proposed in [Nar06] under correlated fading. However, the DMT analysis does not fully characterize the outage probability, and thus is not suitable to analyse the transmit power reduction of MCo over SCo. In [Bai+13], a tight upper and lower bound on the outage probability based on the outage exponent analysis is given but it involves heavy computational efforts as the results include the incomplete Gamma function and Meijer's G-function. The exact solution of the coding gain of JD remains unknown. In addition, neither the DMT analysis in [ZT03; TV05] nor the outage exponent analysis in [Bai+13] considers macrodiversity.

5.2 System Model

The system model, as illustrated in Fig. 5.1, has one BMS, denoted as $[S(t)]_{t=1}^{\infty}$, with the k-sample sequence being represented in vector form as $S^k = [S(1), S(2), ..., S(k)]$. When appropriate, for simplicity, we shall drop

the temporal index of the sequence, denoting the source merely as S. By assumption S takes values in a binary set with uniform probabilities, i.e., $p_S[s = 0] = p_S[s = 1] = 0.5$. Therefore, the entropy of the sequence is

$$\frac{1}{k} \cdot H(S^k) = H(S) = 1. \tag{5.1}$$

The source sequence S^k is encoded at L encoders, i.e., the lth encoder maps $\mathcal{S}^k \to \mathcal{X}_l^n$. The lth transmit sequence, denoted as X_l^n, is sent to the destination over parallel fading channels. The decoder at the destination retrieves the source sequence S^k from the received sequences $Y_l^n, l \in [1 : L]$, i.e., the decoder maps $\prod_{l \in [1:L]} \mathcal{Y}_l^n \to \mathcal{S}^k$.

As discussed in Section 2.4, we assume that the sequences X_l^n, $l \in [1 : L]$, are transmitted over parallel AWGN channels with quasi-static Rayleigh fading and mean power N_0. The pdf of the received SNR Γ_l is given in (2.26), which we reproduce here for convenience:

$$f_{\Gamma_l}(\gamma_l) = \frac{1}{\bar{\Gamma}_l} \exp\left(-\frac{\gamma_l}{\bar{\Gamma}_l}\right), \quad \text{for } \gamma_l \geq 0, \tag{5.2}$$

with the average SNR $\bar{\Gamma}_l$ being obtained as

$$\bar{\Gamma}_l = (P_l/N_0) \cdot d_l^{-\eta}, \tag{5.3}$$

where P_l is the transmit power of the lth channel, d_l is the distance between transmitter and the receiver, and η is the path loss exponent. The channel state information is assumed to be exclusively known at the receiver.

5.3 Problem Statement and Approach

In this work, we aim to quantify the communication performance using the outage probability given by

$$P_{\text{JD},L}^{\text{out}} = \Pr\left\{\mathcal{C}_\psi\left(\{\Gamma_l\}_{l \in [1:L]}\right) \cap R_{\text{c}} \cdot \mathcal{R}_{\text{SW}} = \emptyset\right\}. \tag{5.4}$$

In order to derive the outage probability in (5.4), we first consider the rate region $\mathcal{R}_{\text{SW}}$ when specialized to identical sources that are binary and uniformly distributed. We then determine the exact outage probability by averaging over all received SNRs and find the exact coding gain via high-SNR analysis.

5.4 Outage Probability

In this section, we establish the exact outage probability of JD in integral form. More importantly, we derive in closed form a corresponding asymptotic expression for the high-SNR regime. In addition, we reproduce known bounds on the JD outage probability given in [TV05; Bai+13], as well as the exact and asymptotic outage probabilities of SC and MRC [DG08; CYV05], which we require later on for comparison.

5.4.1 Joint Decoding

If all sources are identical, the Slepian-Wolf setup corresponds to the MCo system model, i.e., the Slepian-Wolf rate region in Theorem 2 simplifies to

$$\mathcal{R}_{\text{SW}} = \Big\{(R_1, ..., R_L) : \sum_{l \in [1:L]} R_l \geq H(S)\Big\}. \tag{5.5}$$

The outage probability for JD is given by the probability that the intersection between the capacity region $\mathcal{C}_\psi\left(\{\Gamma_l\}_{l\in[1:L]}\right)$ and the simplified Slepian-Wolf region $\mathcal{R}_{\text{SW}}$ in (5.5) is empty, i.e.,

$$P_{\text{JD},L}^{\text{out}} = \Pr\Big[\sum_{l\in[1:L]} \psi(\Gamma_l) < R_{\text{c}}\Big] \tag{5.6}$$

$$= \Pr\big[0 \leq \psi(\Gamma_1) < R_{\text{c}}, 0 \leq \psi(\Gamma_2) < R_{\text{c}} - \psi(\Gamma_1), ...,$$
$$0 \leq \psi(\Gamma_L) < R_{\text{c}} - \psi(\Gamma_1) - \psi(\Gamma_2) - ... - \psi(\Gamma_{L-1})\big] \tag{5.7}$$

$$= \Pr\big[0 \leq \Gamma_1 < 2^{R_{\text{c}}} - 1, 0 \leq \Gamma_2 < 2^{R_{\text{c}} - \psi(\Gamma_1)} - 1, ...,$$
$$0 \leq \Gamma_L < 2^{R_{\text{c}} - \psi(\Gamma_1) - \psi(\Gamma_2) - ... - \psi(\Gamma_{L-1})} - 1\big] \tag{5.8}$$

$$= \int_{\gamma_1=0}^{2^{R_{\text{c}}}-1} \int_{\gamma_2=0}^{2^{R_{\text{c}}-\psi(\gamma_1)}-1} ... \int_{\gamma_L=0}^{2^{R_{\text{c}}-\psi(\gamma_1)-\psi(\gamma_2)-...-\psi(\gamma_{L-1})}-1}$$
$$f(\gamma_1)f(\gamma_2)...f(\gamma_L)\mathrm{d}\gamma_L...\mathrm{d}\gamma_2\mathrm{d}\gamma_1. \tag{5.9}$$

The steps are justified as follows: (5.6) is a reformulation, where we determine the probability that the maximum achievable rates of the capacity region are outside the rate region (see Section 2.5); in (5.7) the sum constraint is separated into individual constraints; in (5.8) the bounds are transformed with $\psi^{-1}(y) = 2^y - 1$; in (5.9) the probability of outage is established in integral form with the assumption that the received SNRs $\Gamma_l, \forall l \in [1 : L]$, are independent. The pdf $f(\gamma_l)$ is given in (5.2). Although the outage expression

in (5.9) cannot be solved in closed form, a simple asymptotic solution can be derived at high SNR as

$$P_{\text{JD},L}^{\text{out}} \approx \int_{\gamma_1=0}^{2^{R_c}-1} \int_{\gamma_2=0}^{2^{R_c-\psi(\gamma_1)}-1} \cdots \int_{\gamma_L=0}^{2^{R_c-\psi(\gamma_1)-\psi(\gamma_2)-\ldots-\psi(\gamma_{L-1})}-1}$$

$$\frac{1}{\prod_{l\in[1:L]} \bar{\Gamma}_l} \mathrm{d}\gamma_L \ldots \mathrm{d}\gamma_2 \mathrm{d}\gamma_1 \tag{5.10}$$

$$= \frac{A_L(R_c)}{\prod_{l\in[1:L]} \bar{\Gamma}_l} \quad \text{where} \tag{5.11}$$

$$A_L(R_c) = (-1)^L \left(1 - 2^{R_c} \cdot e_L\left(-R_c \ln(2)\right)\right). \tag{5.12}$$

Here, $e_L(x) = \sum_{l\in[0:L-1]} \frac{x^l}{l!}$ is the exponential sum function. For more details, we refer to the derivations in Appendix A.2. The Lth root of the inverse numerator $G_{c,\text{JD}} = 1/\sqrt[L]{A_L(R_c)}$ is commonly termed the coding gain [WG03]. The diversity gain is L, as we see from the denominator (see Section 2.6).

In contrast to the asymptotic solution in (5.11), a lower bound for (5.9) is given by [TV05, Ch. 9.1.3]

$$P_{\text{JD},L}^{\text{out}} \geq [\Pr[0 \leq \psi(\Gamma) < R_c/L]]^L = \left[1 - \exp\left(-\frac{A_1(R_c/L)}{\bar{\Gamma}}\right)\right]^L, \tag{5.13}$$

for $\bar{\Gamma}_1 = \ldots = \bar{\Gamma}_L = \bar{\Gamma}$ and $A_1(R_c/L) = 2^{R_c/L} - 1$. Note that the lower bound is based on the assumption that an outage event occurs if the channel capacity of each fading channel cannot support the spectral efficiency R_c/L, i.e., each fading channel is allocated an equal share of the information.

In [Bai+13], based on the outage exponent analysis, a lower and an upper bound are given by

$$P_{\text{JD},L}^{\text{out}} \begin{cases} \geq & P_{\text{JD},L}^{\text{out,lower}} = a \exp\left(L\left[\left(\psi\left(\bar{\Gamma}\right) - \frac{R_c}{L}\right) E_{1,1}\left(\bar{\Gamma}\right) + E_{1,0}\left(\bar{\Gamma}\right)\right.\right. \\ & \left.\left. + \frac{E_0(\bar{\Gamma})}{L} + o(L)\right]\right), \\ \leq & P_{\text{JD},L}^{\text{out,upper}} = b \exp\left(L\left[\left(\psi\left(\bar{\Gamma}\right) - \frac{R_c}{L}\right) E_{1,1}\left(\bar{\Gamma}\right) + E_{1,0}\left(\bar{\Gamma}\right)\right.\right. \\ & \left.\left. + \frac{E_0(\bar{\Gamma})}{L} + o(L)\right]\right) \end{cases} \tag{5.14}$$

where a and b are constants, with $a \leq b$. $P_{\text{JD},L}^{\text{out,lower}}$ and $P_{\text{JD},L}^{\text{out,upper}}$ are referred to as the lower and upper outage exponents, respectively. The exact reliability functions $E_{1,1}\left(\bar{\Gamma}\right)$, $E_{1,0}\left(\bar{\Gamma}\right)$, and $E_0\left(\bar{\Gamma}\right)$ are given in [Bai+13]. According to [Bai+13], the outage probability differs for $R_c/L < C_{\text{ergodic}}$ and $R_c/L \geq C_{\text{ergodic}}$, where $C_{\text{ergodic}} = \lim_{L\to\infty} C_{\text{JD}}(\Gamma_1, \ldots, \Gamma_L)/L = \mathbb{E}\left[\psi(1+\Gamma)\right]$ is

the ergodic capacity. The derivations of (5.14) are mainly based on large deviations theory and Meijer's G-function [GR14; DZ10]. For more details on the outage exponent analysis, refer to [Bai+13].

In contrast to the bounds in (5.13) and (5.14), our asymptotic solution in (5.11) offers a simple, yet accurate solution at high SNR. The outage exponent analysis in (5.14) can achieve tight bounds on the outage probability, but the calculations involve the incomplete Gamma function and Meijer's G-function, which makes any further analytical derivations on the SNR gain, DMT, and throughput rather involved. As [Bai+13] did not explicitly consider the properties of the asymptotic outage probability, the exact solution of the coding gain remained unknown. The lower bound in (5.13) is a simple solution, but not tight, as we show later on. On the other hand, our asymptotic solution in (5.11) offers a remarkable simple asymptotical description of the outage probability at high SNR. Especially for URLLC, high-SNR results are well suited, as we are interested in frame error rates below 10^{-5}. Note that, more generally than (5.13) and (5.14), our solution also allows for different average SNRs, which is of practical relevance, if the signals are transmitted from or to different BSs. We detail this comparison via numerical examples in Section 5.9.

5.4.2 Linear Combining

For SC [DG08], at each time instance only the channel with the maximum rate $\psi(\Gamma_{\max}) = \psi\left(\max\left(\Gamma_1, ..., \Gamma_L\right)\right)$ is selected. If $\psi(\Gamma_{\max})$ does not satisfy the rate constraint for lossless compression, see, e.g., [CT06, Theorem 10.3.1] an outage occurs.

The outage probability for SC can be derived as follows [DG08, (2.42)]:

$$P_{\mathrm{SC},L}^{\mathrm{out}} = \Pr\left[\psi(\max\left(\Gamma_1, ..., \Gamma_L\right)) < R_{\mathrm{c}}\right] \tag{5.15}$$

$$= \prod_{i=1}^{L} \int_{\gamma_l=0}^{2^{R_{\mathrm{c}}}-1} f(\gamma_l)\mathrm{d}\gamma_l \tag{5.16}$$

$$= \prod_{l\in[1:L]} \left(1 - \exp\left(-\frac{A_1(R_{\mathrm{c}})}{\bar{\Gamma}_l}\right)\right), \tag{5.17}$$

with $A_1(R_{\mathrm{c}}) = 2^{R_{\mathrm{c}}} - 1$. The steps are justified as follows: (5.15) is given by the rate constraint of lossless compression and source channel separation theorem; (5.16) follows similar arguments as in (5.6), (5.8), and (5.9), respectively, and the multiple integral can be rewritten as the product of single

integrals, since the integral domain is normal and the SNRs are independent; (5.17) is the closed-form solution of the integral in (5.16). An asymptotic solution at high SNR can be derived by using the MacLaurin series of the exponential function $\exp(-x_l) \approx 1 - x_l$ for $x_l \to 0$, giving [DG08, (2.43)]

$$P_{\text{SC},L}^{\text{out}} \approx \frac{(A_1(R_{\text{c}}))^L}{\prod_{l \in [1:L]} \bar{\Gamma}_l}, \tag{5.18}$$

from which $G_{\text{c,SC}} = 1/A_1(R_{\text{c}})$ is the coding gain of SC.

For MRC [DG08], all received symbols are coherently added. The sum of all symbols is then decoded. To calculate the outage probability of MRC we define an auxiliary RV, namely, the total received SNR, as

$$\Gamma_{\text{MRC}} = \sum_{l \in [1:L]} \Gamma_l. \tag{5.19}$$

We have to distinguish between two cases:

Identical received average SNRs   For $\bar{\Gamma}_1 = ... = \bar{\Gamma}_L = \bar{\Gamma}$ the pdf of the total received SNR is given by [DG08, (2.30)]

$$f_{\Gamma_{\text{MRC}}}(\gamma_{\text{MRC}}) = \frac{\gamma_{\text{MRC}}^{(L-1)}}{(L-1)! \cdot \bar{\Gamma}^L} \exp\left(-\frac{\gamma_{\text{MRC}}}{\bar{\Gamma}}\right). \tag{5.20}$$

The outage probability can be then calculated as [DG08, (2.31)-(2.33)]

$$P_{\text{MRC},L}^{\text{out}} = \Pr\left[0 \leq \psi(\Gamma_{\text{MRC}}) < R_{\text{c}}\right] \tag{5.21}$$

$$= \int_{\gamma_{\text{MRC}}=0}^{2^{R_{\text{c}}}-1} f(\gamma_{\text{MRC}}) \mathrm{d}\gamma_{\text{MRC}} \tag{5.22}$$

$$= 1 - \exp\left(-\frac{A_1(R_{\text{c}})}{\bar{\Gamma}}\right)\left(\sum_{l \in [1:L]} \frac{\left(\frac{A_1(R_{\text{c}})}{\bar{\Gamma}}\right)^{(l-1)}}{(l-1)!}\right). \tag{5.23}$$

The steps can be justified similarly to (5.15)-(5.16). The closed form of the integral in (5.22) is given in [DG08, (2.33)]. An asymptotic solution can be derived at high SNR [CYV05, (16)] as

$$P_{\text{MRC},L}^{\text{out}} \approx \frac{1}{L!}\left(\frac{A_1(R_{\text{c}})}{\bar{\Gamma}}\right)^L, \tag{5.24}$$

from which $G_{\text{c,MRC}} = \sqrt[L]{L!}/A_1(R_{\text{c}})$ is the coding gain of MRC.

Different received average SNRs   For $\bar{\Gamma}_1 \neq ... \neq \bar{\Gamma}_L$ the pdf of the total received SNR is given by [Bib13, Proposition 3.1]

$$f_{\Gamma_{\mathrm{MRC}}}(\gamma_{\mathrm{MRC}}) = \sum_{l \in [1:L]} \bar{\Gamma}_l^{L-2} \exp\left(-\frac{\gamma_{\mathrm{MRC}}}{\bar{\Gamma}_l}\right) \prod_{\substack{m \in [1:L] \\ m \neq l}} \frac{1}{\bar{\Gamma}_l - \bar{\Gamma}_m}. \tag{5.25}$$

The outage probability can be then calculated as

$$P_{\mathrm{MRC},L}^{\mathrm{out}} = \Pr\left[0 \leq \psi(\Gamma_{\mathrm{MRC}}) < R_{\mathrm{c}}\right] \tag{5.26}$$

$$= \int_{\gamma_{\mathrm{MRC}}=0}^{2^{R_{\mathrm{c}}}-1} \sum_{l \in [1:L]} \bar{\Gamma}_l^{L-2} \exp\left(-\frac{\gamma_{\mathrm{MRC}}}{\bar{\Gamma}_l}\right) \prod_{\substack{m \in [1:L] \\ m \neq l}} \frac{1}{\bar{\Gamma}_l - \bar{\Gamma}_m} \mathrm{d}\gamma_{\mathrm{MRC}} \tag{5.27}$$

$$= \sum_{l \in [1:L]} \bar{\Gamma}_l^{L-1} \left(1 - \exp\left(-\frac{A_1(R_{\mathrm{c}})}{\bar{\Gamma}_l}\right)\right) \prod_{\substack{m \in [1:L] \\ m \neq l}} \frac{1}{\bar{\Gamma}_l - \bar{\Gamma}_m}. \tag{5.28}$$

The steps can be justified similarly to (5.15)-(5.17). No further simplification based on high SNRs can be achieved for (5.28). However, the asymptotic solution of identical received average SNRs in (5.24) gives a upper bound at high SNR for (5.28) by replacing $\bar{\Gamma}^L$ with $\prod_{l \in [1:L]} \bar{\Gamma}_l$ yielding

$$P_{\mathrm{MRC},L}^{\mathrm{out}} \lesssim \frac{1}{L!} \frac{(A_1(R_{\mathrm{c}}))^L}{\prod_{l \in [1:L]} \bar{\Gamma}_l}. \tag{5.29}$$

For more details on this upper bound, we refer to the derivations in Appendix A.3.

5.4.3 Single-Connectivity

In addition, the exact and asymptotic outage probability of SCo (e.g., $L = 1$ for (5.17) and (5.18)) are given as a baseline by

$$P_{\mathrm{SCo}}^{\mathrm{out}} = 1 - \exp\left(-\frac{A_1(R_{\mathrm{c}})}{\bar{\Gamma}}\right) \tag{5.30}$$

$$\approx \frac{A_1(R_{\mathrm{c}})}{\bar{\Gamma}}, \tag{5.31}$$

from which $G_{\mathrm{c,SCo}} = 1/A_1(R_{\mathrm{c}})$ is the coding gain of SCo.

5.5 Throughput

The throughput captures how much information is received at the destination on average per transmission, depending on the SNR. To capture this, following the standard approach in the literature [Mol12], we define the throughput T as the product of the bandwidth B, spectral efficiency R_c, and the non-outage probability $(1 - P^{\text{out}})$, i.e.,

$$T = BR_c(1 - P^{\text{out}}) \text{ in bit/s.} \tag{5.32}$$

To evaluate (5.32), we require the achieved spectral efficiency R_c for the different combining schemes ($j \in \{\text{JD}, \text{SC}, \text{MRC}\}$) for a given number of links L, outage probability P^{out}, and average received SNRs $\{\bar{\Gamma}_l\}_{l \in [1:L]}$.

Now, by reformulating (5.11) to express the achieved spectral efficiency in terms of a given outage probability, we obtain a high-SNR asymptotic expression for the throughput of JD as

$$T_{\text{JD},L} \approx BA_L^{-1}\left(P^{\text{out}} \prod_{l \in [1:L]} \bar{\Gamma}_l\right)(1 - P^{\text{out}}) \text{ in bit/s.} \tag{5.33}$$

Here, $A_L^{-1}(\cdot)$ is the inverse function of $A_L(\cdot)$. Unfortunately, the inverse function $A_L^{-1}(\cdot)$ does not have a closed-form solution. However, we give a good approximation. At high SNR, the achieved spectral efficiency for a given outage probability is $R_c \gg 1$. In this case, the inverse function can be given by use of an approximation of the asymptotic Lambert W function [HH07] by

$$A_L^{-1}\left(P^{\text{out}} \prod_{l \in [1:L]} \bar{\Gamma}_l\right) = R_c \approx \frac{L-1}{\ln(2)}\left[\ln(\zeta) - \ln(\ln(\zeta))\right], \tag{5.34}$$

where

$$\zeta = \frac{\sqrt[L-1]{(L-1)! P^{\text{out}} \prod_{l \in [1:L]} \bar{\Gamma}_l}}{L-1}. \tag{5.35}$$

For more details, we refer to the derivations in Appendix A.4. The asymptotic throughputs for SC and MRC can be given based on (5.18) and (5.29) as

$$T_{\text{SC},L} \approx B \operatorname{ld} \left(\sqrt[L]{P^{\text{out}} \prod_{l \in [1:L]} \bar{\Gamma}_l} + 1 \right) (1 - P^{\text{out}}) \text{ in bit/s}, \qquad (5.36)$$

$$T_{\text{MRC},L} \approx B \operatorname{ld} \left(\sqrt[L]{L! \cdot P^{\text{out}} \prod_{l \in [1:L]} \bar{\Gamma}_l} + 1 \right) (1 - P^{\text{out}}) \text{ in bit/s}, \qquad (5.37)$$

respectively. In addition, we give the asymptotic throughput of SCo (e.g., from $L = 1$ in (5.36)):

$$T_{\text{SCo}} \approx B \operatorname{ld} \left(P^{\text{out}} \bar{\Gamma} + 1 \right) (1 - P^{\text{out}}) \text{ in bit/s}. \qquad (5.38)$$

5.6 Multi-Connectivity Gain

In this section, we quantify the performance gain of MCo over SCo in terms of transmit power reduction. For MCo we consider the optimal combining scheme, i.e., JD. To ensure a fair comparison between different setups, we equally allocate the total transmit power P_{T} to all channels, such that $P_l = P_{\text{T}}/L, \forall l \in [1:L]$. However, this assumption is non-essential, and other system setups can be evaluated from our formulas with some effort.

We assume a target (fixed) spectral efficiency R_{c} (i.e., a certain throughput has to be guaranteed) and target (fixed) outage probability P^{out}, and evaluate the required total average SNR $\bar{\Gamma} = \sigma_{(\cdot)}(P^{\text{out}})$ in the high-SNR regime. The SNR gain is defined as the ratio of the required average SNR between SCo and MCo.

A reformulation of (5.11) yields

$$\sigma_{\text{JD}}(P^{\text{out}}) = \frac{P_{\text{T}}}{N_0} = L \sqrt[L]{\frac{A_L(R_{\text{c}})}{P^{\text{out}}}} \frac{1}{\sqrt[L]{\prod_{l \in [1:L]} d_l^{-\eta}}}, \qquad (5.39)$$

where $\sigma_{\text{JD}}(P^{\text{out}})$ is the required total average SNR for JD. The required total average SNR for SCo based on the reformulation of (5.31) is

$$\sigma_{\text{SCo}}(P^{\text{out}}) = \frac{P_{\text{T}}}{N_0} = \frac{A_1(R_{\text{c}})}{P^{\text{out}}} \frac{1}{d_1^{-\eta}}. \qquad (5.40)$$

The SNR gain is then given as the ratio between the required average SNRs for SCo and JD as

$$G_{\text{MCo,SCo}} = \frac{\sigma_{\text{SCo}}(P^{\text{out}})}{\sigma_{\text{JD}}(P^{\text{out}})} = \frac{A_1(R_{\text{c}})}{L \sqrt[L]{A_L(R_{\text{c}})}} \frac{1}{\sqrt[L]{(P^{\text{out}})^{L-1}}} \frac{\sqrt[L]{\prod_{l\in[1:L]} d_l^{-\eta}}}{d_1^{-\eta}}. \quad (5.41)$$

Based on (5.41), we answer fundamental questions, e.g., how much transmit power can be saved by MCo as compared with SCo depending on the number of links L, the spectral efficiency (corresponding to the throughput $T \approx BR_{\text{c}}$), the path loss $d_l^{-\eta}$ for $l \in [1:L]$, and the outage probability P^{out}.

5.7 Joint Decoding vs. Linear Combining

In this section, we evaluate the performance improvement of JD over SC and MRC. All combining schemes for MCo are superior to SCo, since the multiple diversity branches are exploited, i.e., the diversity gain is L. However, there exists a difference of the outage probabilities governed by the coding gains $G_{\text{c},(\cdot)}$ of each combining scheme ((5.11), (5.18), and (5.24)). Based on these equations, the performance improvement of JD over SC and MRC can be quantified in terms of the SNR gain, which is the ratio of the coding gains,

$$G_{\text{JD,SC}} = \frac{G_{\text{c,JD}}}{G_{\text{c,SC}}} = \frac{A_1(R_{\text{c}})}{\sqrt[L]{A_L(R_{\text{c}})}} > \sqrt[L]{L!}, \quad (5.42)$$

and

$$G_{\text{JD,MRC}} = \frac{G_{\text{c,JD}}}{G_{\text{c,MRC}}} = \frac{1}{\sqrt[L]{L!}} \cdot \frac{A_1(R_{\text{c}})}{\sqrt[L]{A_L(R_{\text{c}})}} > 1, \quad (5.43)$$

respectively. In Lemma 12 (see Appendix A.5) we prove that the SNR gain of JD over MRC is strictly larger than one, which implies that the SNR gain of JD over SC is strictly larger than $\sqrt[L]{L!}$.

5.8 SNR gain vs. Diversity-Multiplexing Tradeoff

In this section we relate the SNR gain to the DMT analysis. Note that the SNR gain in (5.41) can be separated into two parts, one depending on the spectral efficiency and the other depending on the outage probability. Both

parts are influenced by the number of links. As we can see, with a decreasing outage probability, the SNR gain increases, scaled by the power of $(L-1)/L$, i.e.,

$$\frac{\partial 10 \log_{10}\left(G_{\mathrm{MCo,SCo}}\right) \; \mathrm{dB}}{\partial P^{\mathrm{out}}} = -4.3 \frac{L-1}{L} \frac{1}{P^{\mathrm{out}}} \; \mathrm{dB}. \tag{5.44}$$

The dependency of the SNR gain in terms of the spectral efficiency cannot be seen that easily. However, similarly as for the throughput (cf. (A.36)) we simplify the SNR gain for sufficiently high spectral efficiencies, i.e., $R_{\mathrm{c}} \gg 1$, as

$$G_{\mathrm{MCo,SCo}} \approx \sqrt[L]{\frac{(L-1)!}{(\ln(2))^{L-1} L^{L}}} \frac{2^{R_{\mathrm{c}}\frac{L-1}{L}}}{R_{\mathrm{c}}^{\frac{L-1}{L}}} \frac{1}{\sqrt[L]{(P^{\mathrm{out}})^{L-1}}}. \tag{5.45}$$

Now, we see that with increasing spectral efficiency, the SNR gain increases, scaled by the factor $(L-1)/L$, i.e.,

$$\frac{\partial 10 \log_{10}\left(G_{\mathrm{MCo,SCo}}\right) \mathrm{dB}}{\partial R_{\mathrm{c}}} \approx 3 \frac{L-1}{L} \; \mathrm{dB}. \tag{5.46}$$

A similar analysis for the SNR gain of JD over SC and MRC in (5.42) and (5.43), respectively, leads to the same result as in (5.46) with respect to the spectral efficiency, while being insensitive to the target outage probability.

A factor of $(L-1)/L$ can be seen in (5.44) and (5.46). This factor can be related to the DMT analysis, as we show in the following. In the context of MIMO systems [ZT03], it is proven that for a multiplexing gain

$$G_{\mathrm{r}} = \lim_{\bar{\Gamma} \to \infty} \frac{R_c(\bar{\Gamma})}{\mathrm{ld}\left(L\bar{\Gamma}\right)}, \tag{5.47}$$

the diversity gain d will not exceed

$$G_{\mathrm{d}}(G_{\mathrm{r}}) = -\lim_{\bar{\Gamma} \to \infty} \frac{\mathrm{ld}\, P^{\mathrm{out}}_{\cdot,L}(G_{\mathrm{r}}, \bar{\Gamma})}{\mathrm{ld}\left(L\bar{\Gamma}\right)}, \tag{5.48}$$

for $\bar{\Gamma}_{1} = \ldots = \bar{\Gamma}_{L} = \bar{\Gamma}$, i.e., all distances are normalized to unit, and average system SNR $L\bar{\Gamma}$. By applying a singular value decomposition, the MIMO fading channel can also be formulated into a parallel fading channel in the space domain [TV05]. Thus, it is reasonable to relate the DMT with the SNR gain.
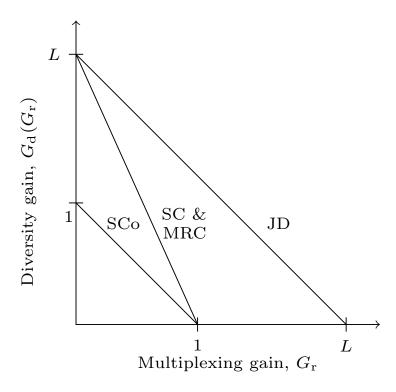
Fig. 5.2. Diversity-multiplexing tradeoff curves: JD outperforms SC and MRC, as it can flexibly trade diversity and multiplexing.

For JD, the diversity gain is a function of the multiplexing gain given by

$$G_{d,JD}(G_r) = L - G_r, \qquad G_r \in [0, L]. \qquad (5.49)$$

The DMT for SC and MRC is given by

$$G_{d,j}(G_r) = L \cdot (1 - G_r), \qquad G_r \in [0, 1], \qquad (5.50)$$

for $j \in \{SC, MRC\}$. For more details, we refer to the derivations in Appendix A.6.

The DMT of JD based on the lower bound in (5.13) given in [TV05, Ch. 9.1.3] is aligned with our results. It is not surprising that JD outperforms SC and MRC in terms of the multiplexing gain. Both SC and MRC perform a non-invertible linear transform on the received signal vector, collapsing the dimension from L to one. It is obvious that diversity can be maintained with SC and MRC, but both will suffer with respect to JD when the goal is to achieve multiplexing gain. Fig.5.2 illustrates the DMT for all combining schemes and SCo.

The SNR gain can be related to the corner cases of the DMT analysis, i.e., full diversity and full multiplexing. Tab 5.1 gives the maximum diversity gain

Tab. 5.1. Overview: full multiplexing and full diversity

	Maximum diversity gain $G_{\mathrm{d},(\cdot),\mathrm{max}}$	Maximum multiplexing gain $G_{\mathrm{r},(\cdot),\mathrm{max}}$
Joint decoding	L	L
Maximal-ratio combining	L	1
Selection combining	L	1
Single-connectivity	1	1

$G_{\mathrm{d},(\cdot),\mathrm{max}}$ and maximum multiplexing gain $G_{\mathrm{r},(\cdot),\mathrm{max}}$ for all considered schemes. Furthermore, we define the relative maximum diversity/multiplexing gain of JD to SCo, SC, and MRC as

$$\bar{G}_{\mathrm{d},\mathrm{max}} = \frac{G_{\mathrm{d,JD,max}} - G_{\mathrm{d},j,\mathrm{max}}}{G_{\mathrm{d,JD,max}}} \quad \text{and} \quad \bar{G}_{\mathrm{r},\mathrm{max}} = \frac{G_{\mathrm{r,JD,max}} - G_{\mathrm{r},j,\mathrm{max}}}{G_{\mathrm{r,JD,max}}}, \quad (5.51)$$

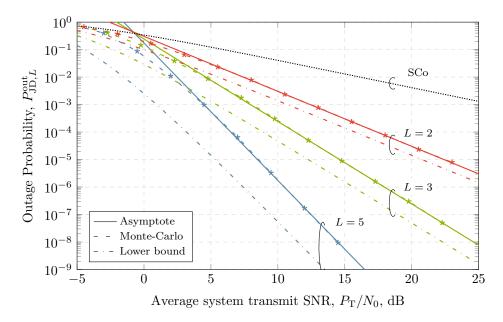for $j \in \{\mathrm{SCo}, \mathrm{SC}, \mathrm{MRC}\}$, respectively.

At full diversity (i.e., fixed spectral efficiency, $G_{\mathrm{r}} = 0$), the SNR gain increases by a factor proportional to $(L-1)/L$ with a decreasing outage probability (cf. (5.44)). The term $(L-1)/L$ is the relative maximum diversity gain of MCo (with JD) and SCo.

At full multiplexing (i.e., fixed outage probability, $G_{\mathrm{d}} = 0$), the SNR gain increases by a factor proportional to $(L-1)/L$ with an increasing spectral efficiency (cf. (5.46)). Similar to the full diversity, the term $(L-1)/L$ is the relative maximum multiplexing gain of MCo (with JD) and SCo.

In summary, both performance improvements are governed by the relation of the maximum diversity and maximum multiplexing gains of MCo (with JD) and SCo. The same line of argument can be used to relate the SNR gain of JD over SC and MRC to the DMT results.

In conclusion, one can give the slope of the SNR gain in the spectral efficiency and outage probability, based on the DMT analysis, but not the SNR gain itself. Furthermore, the slope in the spectral efficiency is merely valid for sufficiently high values, as we discuss in the next section.

5.9 Numerical Examples

(a)

(b)
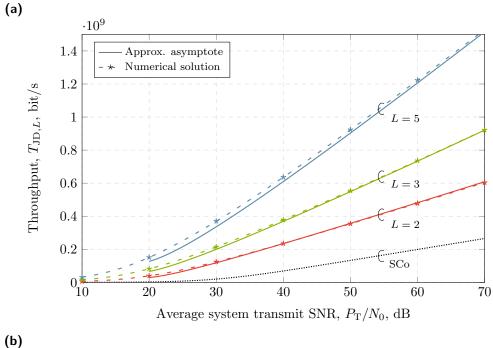
Fig. 5.3. (a) JD outage probability for Monte-Carlo simulation, asymptote, and lower bound, with $L \in \{2, 3, 5\}$ and, $R_c = 0.5$, and (b) JD throughput Monte-Carlo simulation, approximated asymptote with $L \in \{2, 3, 5\}$, $B = 20\,\text{MHz}$, and $P^{\text{out}} = 10^{-3}$. The outage probability and throughput of SCo are depicted for comparison.

In this section, we illustrate and discuss the exact, asymptotic, and the lower bound outage probabilities of JD as well as the exact and asymptotic throughput of JD. Furthermore, we illustrate and discuss the corresponding SNR gain. We equally allocate the total transmit power P_T to all channels,

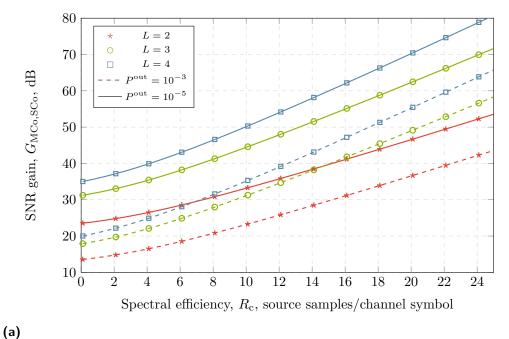such that $P_l = P_\mathrm{T}/L, \forall l \in [1:L]$. Furthermore, we normalize all distances to one. We define the average system transmit SNR as P_T/N_0.

Fig. 5.3a depicts the outage probability of JD (Monte-Carlo simulation of (5.9), our asymptote in (5.11), and the existing lower bound in (5.13)) versus the average system transmit SNR P_T/N_0. For comparison, we include the SCo outage probability in (5.30). We show results for $L \in \{2, 3, 5\}$ and a constant spectral efficiency of $R_\mathrm{c} = 0.5$. We observe the following: (i) the asymptote is very tight at medium and high SNR; (ii) with every additional link the diversity gain $G_{\mathrm{d,JD}}(r)$ increases by one with constant spectral efficiency, i.e., the multiplexing gain is $r = 0$; and (iii) the SNR offset of the lower bound increases with the number of links. At this point, we would like to clarify our assumptions on the SNR range. It is noteworthy that, even though our outage analysis is based on high SNR, it leads to accurate results in the low-to-medium SNR region as well. In Fig. 5.3a, for instance, the asymptotic outage probability with five links is already tight for an outage probability of $P_{\mathrm{JD},5}^{\mathrm{out}} = 10^{-3}$. The corresponding average system transmit SNR is then $P_\mathrm{T}/N_0 = 5\,\mathrm{dB}$. That means that the average transmit SNR per link is $P_l/N_0 = -2\,\mathrm{dB}$, which falls in the low-to-medium SNR region.

Remark: The lower and upper bounds based on the outage exponent analysis in (5.14) are tight, cf. [Bai+13, Fig. 3 - Fig. 7], but require heavy computation to be evaluated over the entire SNR range. Especially for the class of URLLC applications, the low-SNR range is not of interest, as the region of the required outage probabilities is at medium to high SNR.

Fig. 5.3b depicts the throughput for JD (numerical solution of (5.32) and our asymptote in (5.33) with the approximation of the asymptotic inverse function in (5.34)) versus the average system transmit SNR P_T/N_0. For comparison, we illustrate the SCo throughput in (5.38). We show results for $L \in \{2, 3, 5\}$, $B = 20\,\mathrm{MHz}$, and an outage probability of $P^{\mathrm{out}} = 10^{-3}$. The following can be observed: (i) the approximated asymptote is very tight at high SNR; and (ii) for increasing SNR, the JD throughput increases asymptotically with $L \cdot 20\,\mathrm{Mbit\,s^{-1}}$ per $3\,\mathrm{dB}$, whereas the SCo throughput increases asymptotically with $1 \cdot 20\,\mathrm{Mbit\,s^{-1}}$ per $3\,\mathrm{dB}$.

In the following, we show numerical results for the SNR gain with $P^{\mathrm{out}} \in \{10^{-3}, 10^{-5}\}$ and $L \in \{2, 3, 4\}$. As shown in Fig. 5.3a, the asymptotic outage probability is very tight within this range, i.e., the following numerical results based on the asymptotic outage probability barely differ from the numerical results based on the exact outage probability.

(a)

(b)
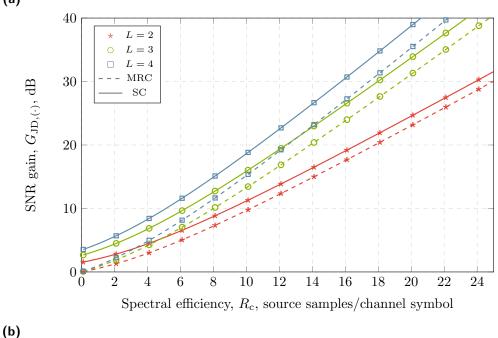
Fig. 5.4. (a) SNR gain of MCo (with JD) over SCo, with $L \in \{2, 3, 4\}$ and $P^{\text{out}} \in \{10^{-3}, 10^{-5}\}$ and (b) SNR gains of JD over SC and MRC, with $L \in \{2, 3, 4\}$.

Fig. 5.4a depicts the SNR gain of MCo over SCo —$G_{\text{MCo,SCo}}$ in (5.41)— versus the spectral efficiency R_{c} (corresponding to the throughput $T \approx BR_{\text{c}}$). We show results with $L \in \{2, 3, 4\}$ number of links and an outage probability of $P^{\text{out}} \in \{10^{-3}, 10^{-5}\}$. The following can be observed: (i) the SNR gain increases with the number of links, spectral efficiency, and decreasing outage probability; (ii) a decrease in outage probability manifests itself as a vertical

shift of the respective SNR gain, e.g., for an outage probability shift from 10^{-3} to 10^{-5}, we calculate the corresponding SNR gain shift from (5.41) as

$$\Delta G_{\text{MCo,SCo}} = G_{\text{MCo,SCo}}(P^{\text{out}} = 10^{-5}) - G_{\text{MCo,SCo}}(P^{\text{out}} = 10^{-3})$$
$$= \frac{A_1(R_{\text{c}})}{L \sqrt[L]{A_L(R_{\text{c}})}} \left(\left(10^{-5}\right)^{\frac{L}{L-1}} - \left(10^{-3}\right)^{\frac{L}{L-1}} \right)$$

which yields $\Delta G_{\text{MCo,SCo}} = 2 \cdot 10 \frac{L-1}{L}$ dB, corresponding to the results in (5.44); and (iii) for sufficiently high spectral efficiencies, the SNR gain increases by $3(L-1)/L$ dB per source sample/channel symbol (cf. (5.46)).
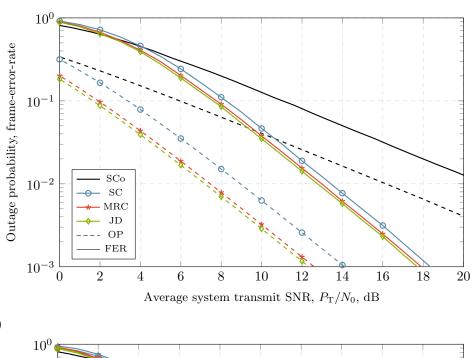
Fig. 5.4b depicts the SNR gain of JD —$G_{\text{JD},(\cdot)}$ given in (5.42) and (5.43)— over SC and MRC, respectively, versus the spectral efficiency R_{c}. The following can be observed: (i) the SNR gain of JD is greater than one, as proven in Lemma 12; (ii) the SNR gain of JD increases with L and R_c; (iii) the SNR gain of JD with respect to MRC differs from the SNR gain of JD with respect to SC by $\frac{1}{\sqrt[L]{L!}}$; (iv) for very low spectral efficiencies the SNR gain of JD over MRC vanishes; and (iv) for sufficiently high spectral efficiencies, the SNR gain increase by $3(L-1)/L$ dB per source sample/channel symbol (cf. (5.46)).

Note that the range of practical spectral efficiencies is within $R_{\text{c}} \in [0.5, 4.\bar{6}]$ (e.g., $1/2$ channel code rate and BPSK, or $2/3$ channel code rate and 128-QAM). However, we illustrate spectral efficiency up to $R_{\text{c}} = 25$, in order to show the asymptotic slope of the SNR gain.

Finally, in Fig. 5.5, we evaluate the FERs of the combining schemes, versus the average system transmit SNR, as achieved by the DTC in [AM12] (see Section 2.7). For meaningful comparison of the combining schemes, we use the turbo decoder also for SC and MRC, i.e., decoding of the already combined LLRs of SC and MRC corresponds to executing the DTC for just one link. We used the following simulation parameters:

- Frame length: $n = 1000$ channel symbols

- Generator polynomial of SNRCC: $G_{\text{SNRCC}} = ([3,1])_8$

- Generator polynomial of SRCC: $G_{\text{SRCC}} = ([3,1]3)_8$

- Doping ratio of ACC: $P_{\text{ACC}} = 1$

- Local iterations: 15

- Global iterations: 3

We compare the simulated FERs to the analytical outage probabilities given in (5.17), (5.23), and (5.9). The figures attest that JD scheme outperforms MRC and SC in terms of both outage probability and FER, becoming more advantageous as the number of increases. From Fig. 5.5a we conclude that the coding structure in [AM12] is clearly suboptimal, since the FER curves are loosely above the outage ones. Nevertheless, the gains of practical MCo systems over practical SCo systems are significant, and therefore justify the additional complexity of MCo networks.
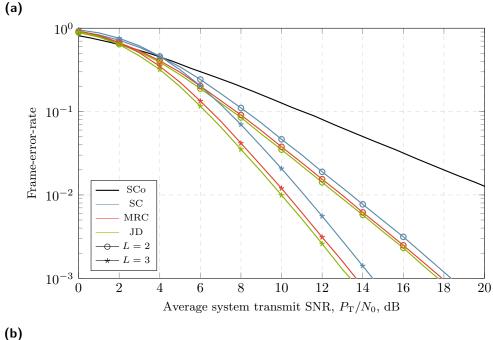

(a)

(b)

Fig. 5.5. (a) Outage probabilities vs. FERs for two links ($L = 2$), and (b) FERs with $L \in \{2, 3\}$.

5.10 Summary

MCo is seen as a key concept to enable URLLC applications in 5G networks, as it provides multiple links from source to destination yielding an increased reliability at low latency. In this chapter, we answered fundamental questions regarding the performance improvement of MCo over SCo. For doing so, we derived fundamental limits for optimal and suboptimal receiver schemes, namely, JD, SC, and MRC.

For JD, we showed that the Slepian-Wolf rate region simplifies to one rate constraint. Based on this simplified Slepian-Wolf rate region we derived results for the exact outage probability in integral form and closed-form solutions for the asymptotic outage probability at high SNR. It turned out that the simple asymptotic outage probability leads to accurate results in the low-to-medium SNR region as well. Thus, we concluded that the asymptotic analysis is well suited to characterize the performance limits of JD in light of URLLC applications.

Based on these findings, we compared the performance improvement of JD over SCo, SC, and MRC by the SNR gain. We found that the SNR gain of JD over SCo increases at a rate of around $3(L-1)/L \, \mathrm{dB}$ with respect to the target spectral efficiency (i.e., per source sample/channel symbol) and decreases at a rate of $4.3(L-1)/L \cdot 1/P^{\mathrm{out}} \, \mathrm{dB}$ with respect to the target outage probability. The comparison between JD and SC/MRC revealed that the SNR gain increases at a rate of around $3(L-1)/L \, \mathrm{dB}$ with respect to the target spectral efficiency (i.e., per source sample/channel symbol), while being insensitive to the target outage probability.

In a nutshell, JD proved to be an excellent concept to achieve URLLC in MCo networks and it becomes more advantageous in terms of the SNR gain as the spectral efficiency and the number of links increases. Furthermore, our results do not only quantify the performance improvement of JD but also are suitable for assessment or optimization of practical MCo deployments, i.e., the system configurations, namely, the number of links, the modulation scheme, the code rate, the bandwidth, and the SNR, can be instantly adjusted according to the user requirements. Insights on practical transmission models will be given in Section 6.2.

In addition to our outage probability results, we derived fundamental limits for the throughput of MCo networks. The throughput captures how much information is received at the destination on average per transmission. We were

able to find good approximations of the throughput at high SNR, offering an accurate characterization of the MCo performance's general trend.

Finally, we compared our analytical results to FERs of a practical DTC. The numerical examples showed that practical DTCs can fully exploit the diversity gain, but not the coding gain. In all numerical examples, the FER curves were loosely above the outage probability ones.

Further Practical Constraints

<div style="text-align: right">**6**</div>

So far, our results were based on some fundamental assumptions, e.g.,

- Independent fading, i.e., the pdf of the fading coefficients can be factorized,

- Perfect SNR estimation and packet detection at the receiver.

These assumptions were made to make mathematical derivations feasible. However, in practical systems, these assumptions might not be accurate. Therefore, it is of interest to evaluate the performance impairment if these assumptions do not hold. In this chapter, we address these issues and present results for MCo (see Chapter 5). This chapter is an important first step towards an extension of the methodology presented in Chapter 2.

In addition, we illustrate the potential of MCo for established wireless standards and cellular networks. For doing so, we evaluate the error-rate performance of an advanced WLAN physical layer with MCo and we apply our outage analysis, given in Chapter 5, to real field channel measurements.

6.1 Correlated Fading

The performance analysis so far, has been based on the assumption, that the quasi-static Rayleigh fading is independent for each channel. However, correlation among channels can arise when the antennas are in close proximity due to space limitations of arrays or insufficiently large guard bands between adjacent frequency channels due to bandwidth limitations. In this section, we are interested in the performance loss for MCo due to correlation. For doing so, we derive the exact and asymptotic outage probability for JD, where we model the correlated Rayleigh fading based on a simple mathematical form generated from the Gaussian distribution. These are our main contributions: (1) finding the exact coding gain of the outage probability for parallel AWGN channels with quasi-static correlated Rayleigh fading; and (2) quantifying the performance loss due to correlation in terms of SNR offset.

6.1.1 Related Work

For correlated fading, the absolute value of the complex channel gain $|A_l|$ (see Section 2.4.2) must be described by multivariate distributions. In [DRT07; CT05], tri- and quadrivariate Rayleigh and Nakagami-m distributions are given for arbitrary correlations. But the pdfs are expressed by multiple nested infinite summations, which leads to significant complexity (computational effort). On the other hand, Beaulieu and Hemachandra presented in [BH11] a simple mathematical form for a vast class of multivariate distributions generated from the Gaussian distribution. The advantage of the new approach in [BH11] is that only a single integral computation is needed.

Based on a large range of correlated fading distributions (Rayleigh, Rician, Nakagami-m, etc.), the performance of linear diversity combining schemes, such as SC and MRC, has been studied in numerously publications, e.g., [MW02; ZB06b; ZB06a; Zhu+15]. However, the JD scheme, which is optimum, remains open for investigation.

6.1.2 Channel Model

Recall the system model from Chapter 5. We are interested in the lossless transmission of a BMS S transmitted over parallel AWGN channels with quasi-static fading. Distinct from the system model in Chapter 5, we assume correlated fading, which we introduce in the following.

The channel model, introduced in Section 2.4.2, is defined as

$$Y_l^n = A_l \cdot X_l^n + N_l^n, \tag{6.1}$$

where X_l^n is the transmit sequence, Y_l^n is the received sequence, N_l^n the random Gaussian noise sequence, and A_l represents the complex channel gain. So far, the channel gain was modelled as a zero-mean, circularly symmetric complex Gaussian RV with unit variance, i.e., $A_l = A_{l,\mathrm{r}} + jA_{l,\mathrm{i}}$, where $\sqrt{j} = -1$ and $A_{l,\mathrm{r}}, A_{l,\mathrm{i}}$ are independent and $\mathcal{N}(0, 1/2)$ for $l \in [1 : L]$. To model correlated fading, Beaulieu and Hemachandra introduce correlated Gaussian RVs as [BH11, (1)]

$$A_l = \left(\sqrt{1 - \lambda_l^2} A_{l,\mathrm{r}} + \lambda_l A_{0,\mathrm{r}} \right) + j \left(\sqrt{1 - \lambda_l^2} A_{l,\mathrm{i}} + \lambda_l A_{0,\mathrm{i}} \right) \tag{6.2}$$

where $A_{0,\mathrm{r}}, A_{0,\mathrm{i}}$ are independent and $\mathcal{N}(0, 1/2)$ auxiliary RVs, and $\lambda_k \in (-1, 1)$ is the correlation coefficient. Note that A_l remains a zero-mean, circularly

symmetric complex Gaussian RV with unit variance. It can be shown, that the correlation coefficient between any A_l and A_k, for $l \neq k$, is given by

$$\rho_{l,k} = \frac{\mathbb{E}[A_l A_k^*] - \mathbb{E}[A_l]\mathbb{E}[A_k^*]}{\sqrt{\text{Var}[A_l]\text{Var}[A_k]}} = \lambda_l \lambda_k. \qquad (6.3)$$

Note that $|A_l|$ follows a Rayleigh distribution with unit variance, where the pdf of $|A_l|$ conditioned on the auxiliary RVs $\{A_{0,\text{r}}, A_{0,\text{i}}\}$ can be given by [BH11, (33a)]

$$f_{|A_l||A_{0,\text{r}}A_{0,\text{i}}}(r_l|a_{0,\text{r}}, a_{0,\text{i}}) = \frac{r_l}{\Omega_l^2} \exp\left(-\frac{r_l^2 + \mu_l^2}{2\Omega_l^2}\right) \text{I}_0\left(\frac{r_l \mu_l}{\Omega_l^2}\right), \qquad (6.4)$$

with

$$\mu_{l,\text{r}} = \lambda_l a_{0,\text{r}}, \quad \mu_{l,\text{i}} = \lambda_l a_{0,\text{i}}, \quad \mu_l^2 = \mu_{l,\text{r}}^2 + \mu_{l,\text{i}}^2, \quad \Omega_l^2 = (1 - \lambda_l^2)/2, \qquad (6.5)$$

and $\text{I}_0(\cdot)$ denotes the modified Bessel function of the first kind and order zero. As defined in Section 2.4.2, the received SNR is given by $\Gamma_l := |A_l|^2 \bar{\Gamma}_l$ with the average SNR $\bar{\Gamma}_l$ being obtained as $\bar{\Gamma}_l = (P_l/N_0) \cdot d_l^{-\eta}$. By use of $r_l = \sqrt{\gamma_l/\bar{\Gamma}_l}$, $\text{d}r_l/\text{d}\gamma_l = 1/(2\sqrt{\gamma_l \bar{\Gamma}_l})$, and some reformulations, the pdf of the received SNR conditioned on the auxiliary RVs $\{A_{0,\text{r}}, A_{0,\text{i}}\}$ can be given by

$$f_{\Gamma_l|A_{0,\text{r}}A_{0,\text{i}}}(\gamma_l|a_{0,\text{r}}, a_{0,\text{i}}) = \frac{1}{2\Omega_l^2 \bar{\Gamma}_l} \exp\left(-\frac{\gamma_l/\bar{\Gamma}_l + \mu_l^2}{2\Omega_l^2}\right) \text{I}_0\left(\frac{\sqrt{\gamma_l/\bar{\Gamma}_l}\mu_l}{\Omega_l^2}\right). \qquad (6.6)$$

Next, we give the joint pdf of the received SNRs conditioned on the auxiliary RVs $\{A_{0,\text{r}}, A_{0,\text{i}}\}$ as

$$f_{\Gamma_1...\Gamma_L|A_{0,\text{r}}A_{0,\text{i}}}(\gamma_1, ..., \gamma_L|a_{0,\text{r}}, a_{0,\text{i}}) = \prod_{l \in [1:L]} f_{\Gamma_l|A_{0,\text{r}}A_{0,\text{i}}}(\gamma_l|a_{0,\text{r}}, a_{0,\text{i}}). \qquad (6.7)$$

The joint pdf of the received SNRs is then given by integration over $\{A_{0,\text{r}}, A_{0,\text{i}}\}$ as

$$\begin{aligned} f_{\Gamma_1...\Gamma_L}(\gamma_1, ..., \gamma_L) &= \int_{a_{0,\text{r}}} \int_{a_{0,\text{i}}} \prod_{l \in [1:L]} f_{\Gamma_l|A_{0,\text{r}}A_{0,\text{i}}}(\gamma_l|a_{0,\text{r}}, a_{0,\text{i}}) \\ &\quad \times \frac{1}{\pi} \exp\left(-(a_{0,\text{r}}^2 + a_{0,\text{i}}^2)\right) \text{d}a_{0,\text{i}} \text{d}a_{0,\text{r}} \qquad (6.8) \\ &= \int_{t=0}^{\infty} \exp(-t) \prod_{l \in [1:L]} \frac{1}{2\Omega_l^2 \bar{\Gamma}_l} \exp\left(-\frac{\gamma_l/\bar{\Gamma}_l + \lambda_l^2 t}{2\Omega_l^2}\right) \text{I}_0\left(\frac{\sqrt{\gamma_l \lambda_l^2 t/\bar{\Gamma}_l}}{\Omega_l^2}\right) \text{d}t, \end{aligned}$$

$$(6.9)$$

where $a_{0,\mathrm{r}} = \sqrt{t}\cos(\theta)$ and $a_{0,\mathrm{i}} = \sqrt{t}\sin(\theta)$. The steps in (6.7)-(6.9) can be similarly justified as in [BH11, (14)].

6.1.3 Outage Probability

Following the same approach as in Section 5.4, (5.6), the outage probability of JD is given by

$$P_{\mathrm{JD},L}^{\mathrm{out}} = \Pr\left[\sum_{l\in[1:L]} \psi(\Gamma_l) < R_{\mathrm{c}}\right] \tag{6.10}$$

$$= \int_{t=0}^{\infty} \exp(-t) \int_{\gamma_1=0}^{2^{R_{\mathrm{c}}}-1} \int_{\gamma_2=0}^{2^{R_{\mathrm{c}}-\psi(\gamma_1)}-1} \cdots \int_{\gamma_L=0}^{2^{R_{\mathrm{c}}-\psi(\gamma_1)-\ldots-\psi(\gamma_{L-1})}-1}$$

$$\times \prod_{l\in[1:L]} \frac{1}{2\Omega_l^2 \bar{\Gamma}_l} \exp\left(-\frac{\gamma_l/\bar{\Gamma}_l + \lambda_l^2 t}{2\Omega_l^2}\right) \mathrm{I}_0\left(\frac{\sqrt{\gamma_l \lambda_l^2 t/\bar{\Gamma}_l}}{\Omega_l^2}\right) \mathrm{d}\gamma_L...\mathrm{d}\gamma_2 \mathrm{d}\gamma_1 \mathrm{d}t. \tag{6.11}$$

The steps can by similarly justified as (5.6)-(5.9). Note that in difference to (5.9) an additional integration over t is required to model the correlation. Although the outage expression in (6.11) cannot be solved in closed form, an asymptotic solution can be derived at high SNR, equal correlation $\lambda = \lambda_l$, and equal average SNR $\bar{\Gamma} = \bar{\Gamma}_l$ for $l \in [1:L]$ as

$$P_{\mathrm{JD},L}^{\mathrm{out}} \approx \frac{1}{\left(2\Omega^2\bar{\Gamma}\right)^L} \int_{t=0}^{\infty} \exp\left(-t\left(1 + \frac{L\lambda^2}{2\Omega^2}\right)\right) C_L(R_{\mathrm{c}},t)\mathrm{d}t \tag{6.12}$$

$$= \left(\frac{1+\Theta}{\bar{\Gamma}}\right)^L (1+L\Theta)^{-1} A_L(R_{\mathrm{c}})$$

$$+ \Theta\left(\frac{1+\Theta}{\bar{\Gamma}}\right)^{L+1} (1+L\Theta)^{-2} B_L(R_{\mathrm{c}}), \tag{6.13}$$

where

$$\Theta = \frac{\lambda^2}{1-\lambda^2}, \qquad C_L(R_{\mathrm{c}}) = A_L(R_{\mathrm{c}}) + \frac{1}{4}\frac{\lambda^2 t}{\bar{\Gamma}\Omega^4}B_L(R_{\mathrm{c}}), \tag{6.14}$$

with $A_L(R_{\mathrm{c}})$ given in (5.12), and

$$B_L(R_{\mathrm{c}}) = \begin{cases} \left(2^{2R_{\mathrm{c}}} + (-1)^{L+1}\right)\dfrac{L}{2} - 2^{R_{\mathrm{c}}}L\displaystyle\sum_{k=[1:l]}\dfrac{(R_{\mathrm{c}}\ln(2))^{L-2k+1}}{(L-2k+1)!} & \text{for } L = 2l, \\ \left(2^{2R_{\mathrm{c}}} + (-1)^{L+1}\right)\dfrac{L}{2} - 2^{R_{\mathrm{c}}}L\displaystyle\sum_{k=[1:(l+1)]}\dfrac{(R_{\mathrm{c}}\ln(2))^{L-2k+1}}{(L-2k+1)!} & \text{for } L = 2l+1. \end{cases} \tag{6.15}$$

For more details, we refer to the derivations in [Che19]. Note that for $\lambda = 0$, the asymptotic solution for correlated fading in (6.13) collapses to the one for independent fading in (5.11).

6.1.4 Correlation Loss

Similar to the SNR gain, we are interested in the SNR offset caused by correlation. The loss due to correlation can be defined as the corresponding asymptotic reduction in SNR while achieving the same outage probability. Thus, we equate the outage probabilities with and without correlation in (6.13) and reformulate the equation to the ratio between the required average SNRs, $\bar{\Gamma}_{\lambda=0}$ and $\bar{\Gamma}_\lambda$, respectively, i.e.,
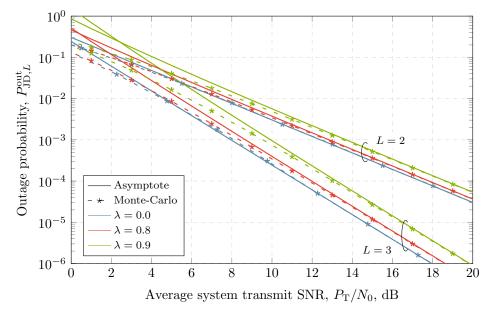
$$
\frac{A_L(R_\mathrm{c})}{\left(\bar{\Gamma}_{\lambda=0}\right)^L} = \left(\frac{1+\Theta}{\bar{\Gamma}_\lambda}\right)^L (1+L\Theta)^{-1} A_L(R_\mathrm{c})
$$

$$
+ \Theta \left(\frac{1+\Theta}{\bar{\Gamma}_\lambda}\right)^{L+1} (1+L\Theta)^{-2} B_L(R_\mathrm{c}) \tag{6.16}
$$

$$
\Leftrightarrow L_{\mathrm{JD}}(\lambda) = \frac{\bar{\Gamma}_\lambda}{\bar{\Gamma}_{\lambda=0}} = \sqrt[L]{\frac{(1+\Theta)^L}{1+L\Theta}\left(1+\Theta\frac{1+\Theta}{1+L\Theta}\frac{B_L(R_\mathrm{c})}{A_L(R_\mathrm{c})}\frac{1}{\bar{\Gamma}_\lambda}\right)} \tag{6.17}
$$

$$
= \sqrt[L]{\frac{(1+\Theta)^L}{1+L\Theta}}. \tag{6.18}
$$

The reformulation in (6.18) is based on the asymptotic assumption, i.e., $\lim_{\bar{\Gamma}\to\infty} 1/\bar{\Gamma} = 0$.

6.1.5 Numerical Examples

In this section, we illustrate and discuss the exact and asymptotic outage probabilities of JD with and without correlated fading. Furthermore, we illustrate and discuss the corresponding correlation loss. We equally allocate the total transmit power P_T to all channels, such that $P_l = P_\mathrm{T}/L, \forall l \in [1:L]$, and assume identical correlation coefficients $\lambda_l = \lambda$ for $l \in [1:L]$. Furthermore, we normalize all distances to one and define the average system transmit SNR as P_T/N_0.

Fig. 6.1a depicts the outage probability of JD (Monte-Carlo simulation of (6.11) and our asymptote in (6.13)) versus the average system transmit SNR P_T/N_0. We show results for $L \in \{2, 3\}$, correlation coefficient $\lambda \in \{0.0, 0.8, 0.9\}$ and a constant spectral efficiency of $R_\mathrm{c} = 0.5$. We observe the following: (i) the asymptote is very tight at medium and high SNR; (ii) the
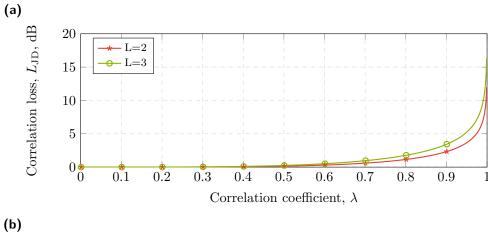
(a)

(b)

Fig. 6.1. (a) Exact and asymptotic outage probability with $\lambda \in \{0, 0.8, 0.9\}$, and (b) correlation loss with $\lambda \in [0, 1]$.

correlation loss increases with λ and the number of links L, and (iii) the diversity gain can be maintained even for larger correlation coefficients.

Fig. 6.1b depicts the correlation loss of JD —L_{JD} given in (6.18) — versus the correlation coefficient λ. We observe that the correlation loss increases significantly if the correlation coefficient approaches one.

6.2 Channel Estimation and Packet Detection in WLAN

In this section, we are interested to assess the impact of channel estimation and packet detection as examples of imperfections in typical receiver implementations, in addition to the coding performance. For doing so, we simulate FERs via a link-level Monte-Carlo framework built on the "MATLAB WLAN System Toolbox". The "MATLAB WLAN System Toolbox" implements functions and models to simulate the physical layer of WLAN as defined in the standards IEEE 802.11{a,ac,ad,ah,b,g,n,j,p} [Mat17].

6.2.1 Related Work

In [AT06], FERs were analyzed for a single link orthogonal frequency-division multiplexing (OFDM) system such as in WLAN for frequency selective fading channels. The gain of SC in terms of achievable data rates was evaluated in [PD16] for a stochastic MIMO channel system modelling frequency selective fading. In [Ehr+17], a link-level simulation of WLAN for up to four frequency selective channels was conducted. At the receiver side, SC was considered as combining algorithm. However, the aforementioned studies did not take imperfections of a complete physical layer implementation into account. Furthermore, since the authors did not present results for a well-known reference channel model such as Rayleigh fading, it is difficult to determine the impact of the WLAN implementation and channel conditions on the FER separately.

6.2.2 Transmission Model

Fig. 6.2 highlights the relevant WLAN processing blocks of the sender and the receiver, and the wireless channel for a single link. Next, we outline each block of the transmission chain.
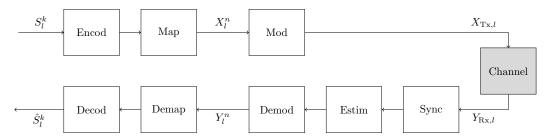
Fig. 6.2. Transmission chain of a single link, depicting the considered processing blocks in transmitter (top), channel (right), and receiver (bottom).

Transmitter   The binary source sequence S_l^k is processed as follows:

- *Encod*: Convolutional channel encoding (see Section 2.7.1);

- *Map*: Mapping to complex-valued symbols, collected in X_l^n;

- *Mod*: OFDM modulation to (time-continuous) baseband signal $X_{\text{Tx},l}$, including inverse fast Fourier transform (IFFT), cyclic prefix, and preamble.

The modulation block was configured with the "High Throughput" profile of IEEE 802.11a and $20\,\text{MHz}$ channel bandwidth. The "High Throughput" profile comprises 52 OFDM subcarriers of which 48 carry data and 4 are used as pilots. Each OFDM symbol is $3.2\,\mu\text{s}$ long, plus a $0.8\,\mu\text{s}$ cyclic prefix. The preamble includes signalling information and multiple training fields, including 2 symbols of 12 subcarriers for packet detection and coarse carrier frequency offset (CFO) correction (short training field (STF)) and 2 symbols using all 52 subcarriers for fine time synchronization, channel estimation and fine CFO correction (long training field (LTF)).

Channel   The channel models available in the "MATLAB WLAN System Toolbox" reach from quasi-static, non-frequency selective Rayleigh fading to realistic frequency selective fading. The channel models are defined in [ESK04] as part of the IEEE 802.11a WLAN standard.

Receiver   The received baseband signal $Y_{\text{Rx},l}$ is processed as follows:

- *Sync*: Packet detection, coarse and fine CFO correction, and fine time synchronization is performed using the STF and the LTF;

- *Estim*: Channel estimation for sampling frequency offset (SFO) correction, channel equalization, and coherent SNR weighting of the links (required for combining schemes);

- *Demod*: Demodulation, including cyclic prefix removal, fast Fourier transform (FFT), SFO correction and channel equalization, to complex-valued symbols, collected in Y_l^n;

- *Demap*: Symbol demapping to LLR values with coherent SNR weighting of the links;

- *Decod*: (Joint) turbo decoding to binary source sequence estimate $\hat{S}_l^k$ (see Section 2.7.2).

The decoding block differs depending on the combing scheme. For SC and MRC the already combined LLR values are decoded by the JTD for just one link. For JD the individual LLR values of each link are correspondingly forwarded to the JTD.

For a detailed review of the simulation framework, the author refers to [Sch17].
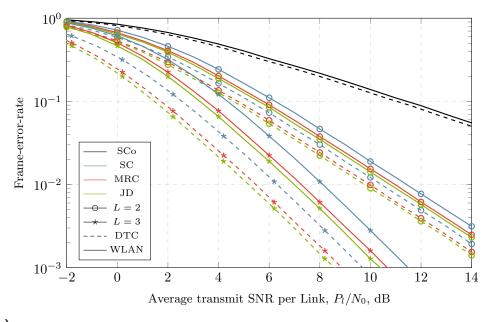
6.2.3 Numerical Examples

Based on the following questions, we evaluate the performance improvement of MCo over SCo in WLAN and the impact of receiver imperfections:

1. What is the performance degradation caused by realistic WLAN base-band processing (*Sync* except for packet detection, *Demod*, and *Demap*)?

2. How sensitive are the combining schemes to unavailable SNR esti-mates?

3. What is the impact of packet detection?

For doing so, we simulate FERs for quasi-static, non-frequency selective Rayleigh fading and BPSK (for a meaningful comparison to the results presented in Section 5.9). Note that regardless of the channel model, the "MATLAB WLAN System Toolbox" executes all transmitter and receiver blocks introduced above.

At first, we address question 1. by comparison of FER curves from the DTC (presented in Section 5.9) and FER curves when the DTC is embedded into the WLAN simulation framework, see Fig. 6.3a. We assume that the accurate SNR knowledge is available to the combining schemes and that all packets are detected. We see a degradation of the performance, which increases with the number of links. This degradation is caused by the imperfect CFO and SFO correction, and channel equalization.
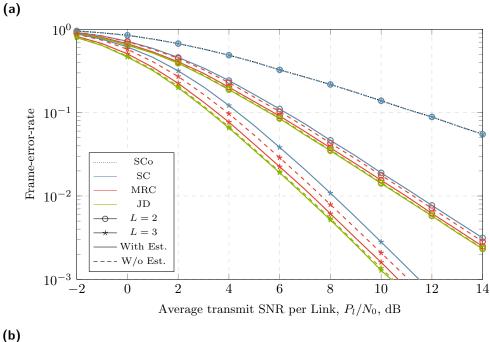
(a)

(b)

Fig. 6.3. (a) Impact of WLAN implementation, and (b) penalty of unavailable SNR estimation while combining.

Secondly, we evaluate the impact of SNR estimation, which is not necessarily perfect. In Fig. 6.3b, we consider the worst case, i.e., no SNR estimate is available for the combining schemes. Without SNR knowledge, SC can not maintain the diversity gain, since the algorithm randomly selects a link, thereby falling back to the performance of SCo. If the links are combined at the symbol level, without SNR weighting before averaging, MRC becomes equal gain combining [Gol05], causing a slight SNR degradation of less than
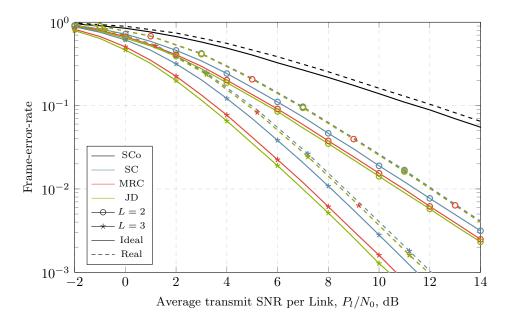
Fig. 6.4. Performance difference between ideal and real packet detection.

$1\,\mathrm{dB}$ but retaining its diversity gain. On the other hand, JD is almost not affected by missing SNR weighting, which can be reasoned based on the DTC scheme. Each turbo decoder maintains separate LLR vectors for each link evaluating the reliability of the received codeword. Thus, if the received codewords seems unreliable, its LLR values are decreased and visa versa. Thus, the DTC inherently contains an SNR estimator.

Thirdly, likewise dependent on preamble design, packet detection is a major concern for WLAN receivers, especially in frequency selective channels [HET97]. Fig. 6.4 shows FER results for the impact of packet detection, where we compare the FERs with ideal and real packet detection[1]. We see an increasing performance degradation with the number of links. This result is reasonable, since the probability that all links are detected decreases with the number of links. Furthermore, the performance differences between the combining schemes diminishes, since the probability of detection error is dominant.

For additional simulation results with frequency selective fading channels, the reader is referred to [Sch17; Sch+18].

Even though the WLAN standard (we consider IEEE 802.11a to be a representative example for an OFDM system) does not exploit the entire potential

---

[1]Ideal packet detection: all packets are detected; real packet detection: some packets cannot be detected due to the limited preamble size (STF and LTF).
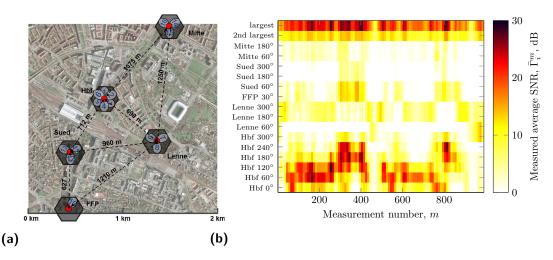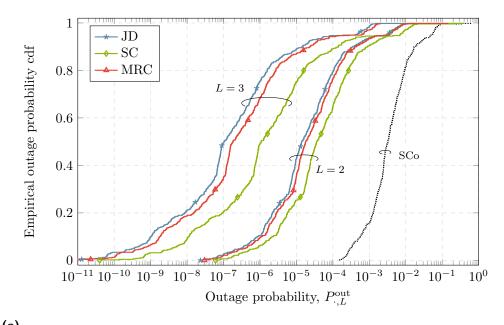
Fig. 6.5. (a) Testbed deployment, and (b) measured average SNR $\bar{\Gamma}_i^m$ achieved at all base station (BS)s of the testbed during the complete field trial. (Source: [Wol+19] © 2019 IEEE).

of MCo, due to suboptimal synchronization, estimation and demodulation, the findings above demonstrate the potential of MCo in wireless systems.

6.3 Cellular Field Trial

In this section, we investigate the potential of MCo in a real cellular network. Fortunately, we have access to field trial measurement data from downtown Dresden (Germany). The measurements were carried out by Michael Grieger et al [Gri14] to evaluate the potential of uplink joint detection in a real cellular network. We reuse the measurement data to generate empirical cumulative distribution functions (cdfs) of the outage probability and the throughput, using the analytical framework from Chapter 5. Our results elaborate on the following points: (i) the achievable performance improvement of MCo over SCo in a real cellular network and (ii) the performance gain of JD in comparison to SC and MRC. Next we shortly introduce the field trial setup and measurement data from Michael Grieger et al and then present the approach to generate the empirical cdfs of the outage probability and the throughput with our analytical framework.

(a)

(b)
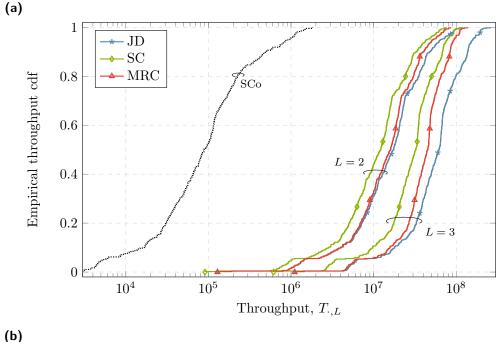
Fig. 6.6. Empirical cdf of the outage probability ($L \in \{2,3\}$, $R_c = 1$), and (d) empirical cdf of the throughput ($L \in \{2,3\}$, $P^{\text{out}} = 10^{-5}$) for JD, SC, and MRC.

6.3.1 Field Trial Setup

The field trial testbed, deployed in Dresden downtown, is depicted in Fig. 6.5a. In total, 16 BS located on five sites with up to six-fold sectorization were used for the measurements. During the field trial, two UEs were moved on a measurement bus in $5\,\mathrm{m}$ distance while transmitting on the same time and frequency resources employing one dipole antenna each. The super-imposed signal is jointly received by all BS, which took snapshots of 80

ms (corresponding to 80 transmit time intervals) every $10\,\text{s}$. In total, about 1900 such measurements were taken in order to observe a large number of different transmission scenarios. In Fig. 6.5b the measured average SNR $\bar{\Gamma}_i^m$ values for around 1000 measurements observed at all BS and locations are shown, where m denotes the measurement number and i the BS index, $i \in \{\text{Hbf}\,0°, \text{Hbf}\,60°, ...\}$. The two largest average SNRs measured at any BS for each measurement are depicted in the upper part of the figure. An interesting result is that multiple relatively high average SNR values of two different BS are observed at each location of the UEs. Since combining algorithms are particularly beneficial in scenarios with multiple relatively high average SNR values, this result indicates that cooperation among BS can provide a much more reliable data transmission, as confirmed next. For more details on this field trial setup, please refer to [Gri14].

6.3.2 Empirical CDFs for Outage Probability and Throughput

With the measured average SNR $\bar{\Gamma}_i^m$ in Fig. 6.5b we generate an empirical cdfs of the outage probability and the throughput based on the analysis presented in Chapter 5. For each measurement we consider the L strongest links, i.e., the largest measured average SNRs $\bar{\Gamma}_i^m$. The outage probability can be assessed with (5.11), (5.17) and (5.28) for JD , SC, and MRC, respectively, for each measurement. Similarly, the throughput is given by (5.33), (5.36), and (5.37) for JD, SC, and MRC, respectively.

Fig. 6.6a and Fig. 6.6b depict the empirical cdf of the outage probability the throughput, respectively. We show results for $L \in \{2, 3\}$ number of links, a spectral efficiency of $R_\text{c} = 1$ (Fig. 6.6a), and an outage probability of $P^\text{out} = 10^{-5}$ (Fig. 6.6b). The following can be observed: (i) MCo is much superior to SCo and (ii) JD outperforms SC and MRC, the performance gain increasing with the number of links from source to destination.

6.3.3 Discussion

Based on the field trial setup, we conclude that MCo can achieve a substantial performance improvement in real cellular networks. The measurement data at hand documents that multiple relatively high average SNR values frequently occur, for which combining algorithms are particularly beneficial. From the uplink measurement data we also draw conclusions for the

downlink. Under the assumption that the statistical properties of the link model are identical for the up- and downlinks, it is reasonable to assume that multiple relatively high average SNR values frequently occur in the downlink as well. Based on this, MCo can also achieve low outage probabilities and high throughput in the downlink of real cellular networks.

6.4 Summary

In this chapter, we questioned some fundamental assumptions from the preceding chapters. In a nutshell, we gave answers to the following questions for the MCo network:

- How does correlation of the fading channels degrade the performance?

  We derived the correlation loss, i.e., the SNR offset between the outage probability curves depending on the correlation coefficient between the complex channel gains. From our analytical results, we concluded the following: i) an increased correlation coefficient yields an increased correlation loss; ii) for moderate correlation, the correlation loss is marginal, and iii) even though the diversity gain can be maintained whatever the correlation, the performance improvement of MCo in regard to SCo vanishes if the correlation coefficient approaches one.

- What is the impact of typical receiver imperfections such as SNR estimation and packet detection?

  We implemented optimal and suboptimal combining schemes into the WLAN standard and simulated error-rates of the physical layer. We found that DTC is tolerant of unavailable SNR estimation as opposed to the other combining schemes. An advantage not known from theoretical work before. We identified packet detection as a major concern as its performance degradation increased with the number of links. Nevertheless, we concluded that MCo is a suitable technology to enable ultra-reliable communications in WLAN.

- How realistic are the theoretical performance improvements in real cellular networks?

  We applied our analytical framework from Chapter 5 to real cellular networks. Based on the measurement data recorded in a field trial, we evaluated the achievable performance improvement by the use of MCo. The measurement data documented that multiple relatively

high average SNR values frequently occur, in which case MCo proves particularly beneficial.

Conclusions and Outlook | 7

7.1 Conclusions

This thesis laid theoretical foundations for understanding the performance of MSCCs in three cooperative communication networks in light of ultra-reliable communications. The ultimate performance limit for wirelesses communications over fading channels can be assessed by the outage analysis. Ultimately, we derived results on the exact outage probability and the asymptotic outage probability at high SNR. It turned out that the simple asymptotic outage probability leads to accurate results in the low-to-medium SNR region. Thus, we concluded that the asymptotic analysis is well suited to characterize the performance limits of cooperative communication networks for ultra-reliable communications. For the cooperative communication networks under investigation, we found that MSCCs significantly improved the reliability in regard to other (non-)communication concepts. Therefore, this thesis sees practical schemes based on MSCCs as a strong candidate to achieve the stringent ultra-reliable communication requirements in upcoming wireless networks. Furthermore, the practical relevance of our results is threefold: i) optimality of practical schemes can be evaluated in regard to our results; ii) practical deployments of communication networks can be assessed or optimized, i.e., the system configurations, namely, the number of links, the modulation scheme, the code rate, the bandwidth, and the SNR, can be instantly adjusted according to the user requirements; and iii) the complexity of network-level simulations can be reduced by using our results for link-level abstraction.

The MSCC outage analysis over quasi-static fading channels in this thesis was based on two steps:

1. We evaluated the communication performance of the MSCC for a set of fixed channel realizations. For doing so, we decoupled the MSCC into a multiterminal source code and multiple point-to-point channel codes, an approach which is known to be optimum for infinite block-length. The advantage is that we can easily adjust the multiterminal source code to the desired cooperative communication network. The multiterminal source code defines the minimum set of rates for reliable communication (i.e., perfect reconstruction of the sources). The derivation of the corresponding rate regions was our first major contribution

Tab. 7.1. Overview: key findings

	Relay network	Wireless sensor network	Multi-connectivity network
Rate region	Inner bound on $\mathcal{R}_{\text{GP}}$ given in (3.18)	$\mathcal{R}_{\text{SW}}$ given in (4.7)	$\mathcal{R}_{\text{SW}}$ given in (5.5)
Exact outage probability	Upper bound for $P_{\text{LF},L}^{\text{out}}$ given in (3.28)	$P_{\text{WSN},L}^{\text{out}}$ given in (4.11)	$P_{\text{JD},L}^{\text{out}}$ given in (5.9)
Asymptotic outage probability	remains unknown	$P_{\text{WSN},L}^{\text{out}}$ $\approx \sum_{l \in [1:L]} \frac{A_l(R_{\text{c}})}{\overline{\Gamma}_i}$	$P_{\text{JD},L}^{\text{out}}$ $\approx \frac{A_L(R_{\text{c}})}{\prod_{l \in [1:L]} \overline{\Gamma}_l}$
Coding gain	remains unknown	$G_{\text{C,WSN}} = 1/A_l(R_{\text{c}})$	$G_{\text{C,JD}} = 1/\sqrt[L]{A_L(R_{\text{c}})}$
Diversity gain	$L+1$ (One source and L helpers)	1	L
SNR gain	Quantified by numerical example	G_{WSN} $= \frac{\sum_{l \in [1:L]} B(R_{\text{c}}) \cdot d_l^\eta}{\sum_{l \in [1:L]} A_l(R_{\text{c}}) \cdot d_l^\eta}$	$G_{\text{MCo,SCo}} = \frac{A_1(R_{\text{c}})}{L\sqrt[L]{A_L(R_{\text{c}})}}$ $\times \frac{\sqrt[L]{\prod_{l \in [1:L]} d_l^{-\eta}}}{\sqrt[L]{(P^{\text{out}})^{L-1} \cdot d_1^{-\eta}}}$

(see Tab. 7.1). If the set of fixed channel capacity realizations is not inside the rate region, an outage event occurs and vice versa.

2. By integration over all channel realizations we obtained the average performance, i.e., the exact outage probability. This constitutes our second major contribution (see Tab. 7.1).

At high SNR, the exact outage probability can be described by its asymptote, which consists of the coding and diversity gain. For WSN and MCo we found the asymptotic outage probability, which is another major contribution of this thesis (see Tab. 7.1). Unfortunately, the asymptotic outage probability of LF remains unknown. Based on the asymptotic outage probability, we were able to quantify the SNR gain of the MSCC under investigation over other (non-)cooperative communication concepts. Finally, by evaluation of FERs, we demonstrated that similar gains can be obtained for practical implementations based on DTCs.

Moreover, for MCo networks, we presented results including further practical constraints. In particular, we analyzed the performance impairment of correlated fading and practical receiver imperfections in terms of the correlation loss and error-rates in physical layer simulations of WLAN (as defined in IEEE 802.11a), respectively. Our results revealed that the loss is marginal for moderate correlation, that the DTC is tolerant of unavailable SNR estimation, and that performance degradation caused by packet detection increased with

the number of links. However, our findings provide a strong argument for using MCo in wireless systems exposed to adverse channel conditions. Lastly, we applied our analytical framework to real cellular networks. We analyzed the potential performance improvement of MCo over SCo based on measurement data recorded in a field trial. The measurement data documented that multiple relatively high average SNR values frequently occur, in which case MCo proves particularly beneficial.

7.2 Outlook

Finally, we like to discuss several topics that were not addressed so far but could be of interest for future work.

Finite Blocklength Performance   Note that the fundamental limits in Sections 2.1-2.3 are derived based on the assumption of infinite blocklength $(k, n \rightarrow \infty)$. However, for low-latency communications, the length of the data packet is rather short, and thus, the outage analysis based on infinite blocklength is not necessarily a valid criterion [Yan+14].

During the last few years, significant progress has been made in the field of finite blocklength analysis. For the AWGN channel, the finite blocklength performance was characterized by Hayashi [Hay09] and Polyanskiy, Poor, and Verdú [PPV10]. In addition to channel coding, new fundamental limits for the problem of lossy source coding [Sha59a] have been derived by Kostina and Verdú [KV12] in the finite blocklength regime. Subsequently, Kostina and Verdú [KV13] also derived the finite blocklength performance for the lossy joint source-channel coding problem [Sha59a]. In [KV13], Kostina and Verdú showed that the source-channel separation is suboptimal in the finite blocklength regime.

Therefore, in future work a finite blocklength analysis of MSCCs is of interest to assess their suitability for short-packet communication.

In [ZWM19], we made a first important step towards the finite blocklength analysis of MSCCs. Based on the latest advances in information theory, we derived fundamental limits for the finite blocklength performance of MSCCs in MCo networks. Our results demonstrate that the outage analysis (based on infinite blocklength) is still a valid criterion even in the finite blocklength scenario with negligible loss of performance. Furthermore, we showed that MSCCs are suitable for URLLC and short-packet communication, and their

performance limit can be well approximated by the simple outage analyses in Chapter 5.

Extended Analysis of Correlated Fading   In Sections 6.1, we considered the topics of correlated fading for MCo. The presented results are the basis to extend the methodology in Chapter 2 and derive similar results for relay networks and WSNs.

Imperfection of Packet Detection and Channel Estimation   In Section 6.2, the influence of packet detection and channel estimation are evaluated for WLAN. However, the results are simulation based and thus the fundamental relationship between performance and packet detection/channel estimation remains open. It would be of interest to analyze the impairment of the outage probability due to imperfect channel estimation. Furthermore, the probability of the packet detection error has to be embedded into an overall outage probability.

Code Optimization   From the numerical results in Chapters 3-5 we conclude that the DTC [AM12] (see Section 2.7) is clearly suboptimal, since the FER curves are loosely above the outage probability ones. The performance might be improved by modification of some decoding parameters, such as coding rate, frame length, generate polynomial, doping ratio, and iterations rounds. On the other hand, the suboptimal performance could also be caused by the coding family and coding structure itself.

Two other prominent coding families are low-density parity-check (LDPC) codes [Gal62] and Polar codes [Ari09]. Both coding families are known to be (almost) capacity-achieving. Distributed coding schemes exploiting both coding concepts have been proposed in [Bou+10; JYY18]. The investigation of these coding concepts in the context of cooperative communications could be of interest for future works.

We made first trials to improve the DTCs performance by modifying the decoding parameters, which showed an improved performance. However, the gains ahighly depend on the channel model and the network topology. So far, we could not identify an optimum set of DTC decoding parameters that outperformed other sets for any possible channel model and network topology. Furthermore, we substituted the turbo codes with LDPC codes in the distributed coding scheme (see Section 2.7). Our results showed no significant performance improvement. Therefore, we concluded that the

decoding structure (i.e., separate channel decoders exchanging LLRs via a variable node) is suboptimal.

Correlation in Time, Frequency, and Information In this thesis, we mainly exploit the correlation of sources to increase the spectral efficiency of the wireless communication system. On the other hand, wireless fading channels are impaired by correlation in the frequency and the time domain. We presented and evaluated some result for the correlation in the frequency domain for MCo. In future work a general system model which combines all three dimensions of correlation in time, frequency, and information, would be of interest.

Appendix

<div style="text-align: right; font-size: 3em;">A</div>

A.1 Proof of Theorem 8

The conditional entropy in Theorem 4 can be given by

$$H\left(S_0|\{U_l\}_{l\in[1:L]}\right) = H\left(S_0, \{U_l\}_{l\in[1:L]}\right) - H\left(\{U_l\}_{l\in[1:L]}\right) \tag{A.1}$$

$$= \sum_{l\in[1:L]} H(U_l|S_0) - H\left(\{U_l\}_{l\in[2:L]}|U_1\right) \tag{A.2}$$

$$= \sum_{l\in[1:L]} h\left(\epsilon_l * \kappa_l\right) - \eta(\{\epsilon_l * \kappa_l\}_{l\in[1:L]}) \tag{A.3}$$

for $L \geq 2$. The steps are justified as follows: (A.1) is the chain rule of entropy; for (A.2), the entropy of the primary source and the auxiliary RVs can be partitioned by the chain rule and simplified by the fact that $(U_1, ..., U_L)$ are conditionally independent given S_0, i.e., $H(U_l|S_0, U_1, ..., U_{l-1}) = H(U_l|S_0)$, and the entropy of the auxiliary RVs can be reformulated by the chain rule; and (A.3) follows from the properties $H(S_0) = H(S_l) = H(U_l) = 1$, $H(U_l|S_0) = H(S_0|U_l)$, and $H(U_l|U_{\bar{l}}) = H(U_{\bar{l}}|U_l)$ for $l \in [1:L]$, $l \neq \bar{l}$, the Markov chain, i.e., $H(U_l|S_0) = h(\epsilon_l * \kappa_l)$, and

$$H\left(\{U_l\}_{l\in[2:L]}|U_1\right) = -\sum_{u_1\in\{0,1\}} p_{U_1}(u_1) \sum_{\{u_l\}_{l\in[2:L]}\in\{0,1\}^{L-1}} p_{U_2...U_L|U_1}(u_2, ..., u_l|u_1)$$

$$\times \operatorname{ld} p_{U_2...U_L|U_1}(u_2, ..., u_l|u_1) \tag{A.4}$$

$$= -\sum_{\{u_l\}_{l\in[2:L]}\in\{0,1\}^{L-1}}$$

$$\times \left(\sum_{s_0\in\{0,1\}} p_{U_2...U_L|S_0}(u_2, ..., u_l|s_0)p_{S_0|U_1}(s_0|0)\right)$$

$$\times \operatorname{ld}\left(\sum_{s_0\in\{0,1\}} p_{U_2...U_L|S_0}(u_2, ..., u_l|s_0)p_{S_0|U_1}(s_0|0)\right) \tag{A.5}$$

$$\triangleq \eta(\{\epsilon_l * \kappa_l\}_{l\in[1:L]}) \tag{A.6}$$

for $L \geq 2$, with

$$p_{U_2...U_L|S_0}(u_2, ..., u_l|s_0) = \prod_{l\in[2:L]} p_{U_l|S_0}(u_l|s_0) \tag{A.7}$$

$$= \prod_{l\in[2:L]} [(1 - \epsilon_l * \kappa_l)\,\mathbb{1}(u_l = s_0) + (\epsilon_l * \kappa_l)\,\mathbb{1}(u_l \neq s_0)], \tag{A.8}$$

and

$$p_{S_0|U_1}(s_0|0) = \left[(1 - \epsilon_1 * \kappa_1) \, \mathbb{1}(s_0 = 0) + (\epsilon_1 * \kappa_1) \, \mathbb{1}(s_0 \neq 0) \right]. \qquad \text{(A.9)}$$

For $L < 2$ we have $\eta(\{\epsilon_l * \kappa_l\}_{l \in [1:L]}) = 0$. In (A.8) and (A.9), $\mathbb{1}(\cdot)$ is the indicator function. The steps are justified as follows: (A.5) follows from the law of total probability, the Markov chain $U_1 \to S_0 \to U_2...U_L$, and the symmetric properties of the primary source and channels; and (A.7) follows from the Markov chain $U_l \to S_0 \to U_{\bar{l}}$, for $l, \bar{l} \in [1:L]$ and $l \neq \bar{l}$. The conditional mutual information in Theorem 4 can be given by

$$I\left(\{S_l\}_{l \in \mathcal{V}}; \{U_l\}_{l \in \mathcal{V}} | \{U_l\}_{l \in \mathcal{V}^c}\right)$$
$$= H\left(\{U_l\}_{l \in \mathcal{V}} | \{U_l\}_{l \in \mathcal{V}^c}\right) - H\left(\{U_l\}_{l \in \mathcal{V}} | \{S_l\}_{l \in \mathcal{V}}\right) \qquad \text{(A.10)}$$
$$= H\left(\{U_l\}_{l \in [1:L]}\right) - H\left(\{U_l\}_{l \in \mathcal{V}^c}\right) - \sum_{l \in \mathcal{V}} H(U_l | S_l) \qquad \text{(A.11)}$$
$$= \eta(\{\epsilon_l * \kappa_l\}_{l \in [1:L]}) - \eta(\{\epsilon_l * \kappa_l\}_{l \in \mathcal{V}^c}) - \sum_{l \in \mathcal{V}} h(\kappa_l), \qquad \text{(A.12)}$$

$\forall \mathcal{V} \subset [1:L]$ and $\mathcal{V}^c = [1:L] \backslash \mathcal{V}$. The steps can be justified similarly as (A.1)-(A.3). In particular, for $\mathcal{V} = [1:L]$, we have

$$I\left(\{S_l\}_{l \in [1:L]}; \{U_l\}_{l \in [1:L]}\right) = H\left(\{U_l\}_{l \in [1:L]}\right) - H\left(\{U_l\}_{l \in [1:L]} | \{S_l\}_{l \in [1:L]}\right)$$

$$\text{(A.13)}$$

$$= 1 + \eta(\{\epsilon_l * \kappa_l\}_{l \in [1:L]}) - \sum_{l \in [1:L]} h(\kappa_l). \qquad \text{(A.14)}$$

The inner bound is then generated by ranging the auxiliary parameters over $\{\kappa_l\}_{l \in [1:L]} \in [0, 0.5]^L$. This completes the proof.

A.2 Asymptotic Outage Probability

The asymptotic outage probability can be obtained as

$$P_{\cdot,L}^{\text{out}} = \int_{\gamma_1=0}^{2^{R_c}-1} \int_{\gamma_2=0}^{2^{R_c-\psi(\gamma_1)}-1} ... \int_{\gamma_L=0}^{2^{R_c-\psi(\gamma_1)-\psi(\gamma_2)-...-\psi(\gamma_{L-1})}-1}$$
$$\frac{1}{\bar{\Gamma}_1} \exp\left(-\frac{\gamma_1}{\bar{\Gamma}_1}\right) \frac{1}{\bar{\Gamma}_2} \exp\left(-\frac{\gamma_2}{\bar{\Gamma}_2}\right) ... \frac{1}{\bar{\Gamma}_L} \exp\left(-\frac{\gamma_L}{\bar{\Gamma}_L}\right) \mathrm{d}\gamma_L...\mathrm{d}\gamma_2 \mathrm{d}\gamma_1$$
$$\text{(A.15)}$$

$$\approx \int_{\gamma_1=0}^{2^{R_c}-1} \int_{\gamma_2=0}^{2^{R_c-\psi(\gamma_1)}-1} ... \int_{\gamma_L=0}^{2^{R_c-\psi(\gamma_1)-\psi(\gamma_2)-...-\psi(\gamma_{L-1})}-1}$$

$$\frac{1}{\bar{\Gamma}_1}\left(1 - \frac{\gamma_1}{\bar{\Gamma}_1}\right)\frac{1}{\bar{\Gamma}_2}\left(1 - \frac{\gamma_2}{\bar{\Gamma}_2}\right)...\frac{1}{\bar{\Gamma}_L}\left(1 - \frac{\gamma_L}{\bar{\Gamma}_L}\right)\mathrm{d}\gamma_L...\mathrm{d}\gamma_2\mathrm{d}\gamma_1 \quad \text{(A.16)}$$

$$\approx \frac{1}{\bar{\Gamma}_1\bar{\Gamma}_2...\bar{\Gamma}_L}\int_{\gamma_1=0}^{2^{R_c}-1}\int_{\gamma_2=0}^{2^{R_c-\psi(\gamma_1)}-1}...\int_{\gamma_L=0}^{2^{R_c-\psi(\gamma_1)-\psi(\gamma_2)-...-\psi(\gamma_{L-1})}-1}\mathrm{d}\gamma_L...\mathrm{d}\gamma_2\mathrm{d}\gamma_1$$

<div align="right">(A.17)</div>

$$= \frac{A_L(R_c)}{\bar{\Gamma}_1\bar{\Gamma}_2...\bar{\Gamma}_L}. \quad \text{(A.18)}$$

The steps are justified as follows: (A.16) MacLaurin series for exponential function $\exp(-x_l) \approx 1 - x_l$ for $x_l \to 0$, (A.17) expanding the resulting product as $\prod_l(1-x_l) \approx 1$ for $x_l \to 0$; (A.18) is proven in Lemma 10 and the assumption that the received SNRs are independently distributed, thus we can interchange the integral bounds.

Lemma 10. *For any $L \in \mathbb{N}\backslash\{1\}$,*

$$A_L(x) = \int_{\gamma_L=0}^{2^x-1}\int_{\gamma_{L-1}=0}^{2^{x-\psi(\gamma_L)}-1}...\int_{\gamma_1=0}^{2^{x-\psi(\gamma_L)-...-\psi(\gamma_2)}-1}\mathrm{d}\gamma_1...\mathrm{d}\gamma_{L-1}\mathrm{d}\gamma_L \quad \text{(A.19)}$$

$$=(-1)^L\left(1 - 2^x \cdot e_L\left(-x\ln(2)\right)\right). \quad \text{(A.20)}$$

Here, $e_L(y) = \sum_{l\in[0:L-1]}\frac{y^l}{l!}$ is the exponential sum function.

Proof. Base case: If $L = 2$, then (A.19) is

$$A_2(x) = \int_{\gamma_2=0}^{2^x-1}\int_{\gamma_1=0}^{2^{x-\psi(\gamma_2)}-1}\mathrm{d}\gamma_1\mathrm{d}\gamma_2 = \int_{\gamma_2=0}^{2^x-1}\left[\frac{2^x}{1+\gamma_2}-1\right]\mathrm{d}\gamma_2$$

$$= 2^x\left(x\cdot\ln(2) - 1\right) + 1, \quad \text{(A.21)}$$

which is (A.20) for $L = 2$. So, the theorem holds for $L = 2$.
Inductive hypothesis: Suppose the theorem holds for all values of L up to some $K \geq 2$.
Inductive step: Let $L = K + 1$, then (A.19) is

$$A_{K+1}(x) = \int_{\gamma_{K+1}=0}^{2^x-1}\underbrace{\int_{\gamma_K=0}^{2^{x-\psi(\gamma_{K+1})}-1}...\int_{\gamma_1=0}^{2^{x-\psi(\gamma_{K+1})-...-\psi(\gamma_2)}-1}\mathrm{d}\gamma_1...\mathrm{d}\gamma_K}_{A_K(x-\psi(\gamma_{K+1}))}\mathrm{d}\gamma_{K+1}$$

<div align="right">(A.22)</div>

$$= \int_{\gamma_{K+1}=0}^{2^x-1}\left[(-1)^K + \frac{2^x}{1+\gamma_{K+1}}\right.$$

$$\times \sum_{l\in[0:K-1]} (-1)^{K+l+1}\frac{1}{l!}\left(x-\psi(\gamma_{K+1})\right)^l\left(\ln(2)\right)^l\Bigg]\mathrm{d}\gamma_{K+1} \tag{A.23}$$

$$= \int_{\gamma_{K+1}=0}^{2^x-1}\left[(-1)^K + \frac{2^x}{1+\gamma_{K+1}}\sum_{l\in[0:K-1]}(-1)^{K+l+1}\frac{1}{l!}\left(\ln(2)\right)^l\right.$$

$$\left.\times \sum_{k\in[0:l]}(-1)^k\binom{l}{k}x^{l-k}\psi(\gamma_{K+1})^k\right]\mathrm{d}\gamma_{K+1} \tag{A.24}$$

$$= (-1)^K\gamma_{K+1} + 2^x\sum_{l\in[0:K-1]}(-1)^{K+l+1}\frac{1}{l!}\left(\ln(2)\right)^l$$

$$\times \sum_{k\in[0:l]}(-1)^k\binom{l}{k}x^{l-k}\frac{\left(\ln(1+\gamma_{K+1})\right)^{k+1}}{(k+1)\left(\ln(2)\right)^k}\Bigg|_{\gamma_{K+1}=0}^{2^x-1} \tag{A.25}$$

$$= (-1)^K\left(2^x - 1 - 2^x\sum_{l\in[0:K-1]}(-1)^l\frac{1}{l!}x^{l+1}\left(\ln(2)\right)^{l+1}\underbrace{\sum_{k\in[0:l]}(-1)^k\binom{l}{k}\frac{1}{k+1}}_{\frac{1}{(l+1)}}\right)$$

$$\tag{A.26}$$

$$= (-1)^{K+1}\left(1 - 2^x\cdot e_{K+1}\left(-x\ln(2)\right)\right). \tag{A.27}$$

The steps are justified as follows: (A.23) is our inductive hypothesis; for (A.24) we have used the binomial formula; (A.27) we have used the following

$$\sum_{k\in[0:l]}(-1)^k\binom{l}{k}\frac{1}{k+1} = \frac{1}{l+1}\sum_{k\in[0:l]}(-1)^k\binom{l+1}{k+1} \tag{A.28}$$

$$= \frac{-1}{l+1}\left[\underbrace{\sum_{k\in[l+1]}(-1)^k\binom{l+1}{k}}_{\sum_{k\in[0:l+1]}(-1)^k\binom{l+1}{k}=(1-1)^{l+1}=0} + \binom{l+1}{0} - \binom{l+1}{0}\right] = \frac{1}{l+1} \tag{A.29}$$

and carried out some algebraic manipulations. Equation (A.27) corresponds to (A.20) for $L = K + 1$. So, the theorem holds for $L = K + 1$. Hence, by the principle of mathematical induction, the theorem holds for all $L \in \mathbb{N}\backslash\{1\}$. $\square$

A.3 Lemma 11

Lemma 11. *For any $L \in \mathbb{N}$, $R_c > 0$, and RVs $\Gamma_l \in \mathbb{R}_+, \forall l \in [1:L]$,*

$$\Pr\left[0 \leq \sum_{l\in[1:L]}\Gamma_l \leq A_1(R_c)\right] \leq \frac{1}{L!}\frac{\left(A_1(R_c)\right)^L}{\prod_{l\in[1:L]}\bar{\Gamma}_l}, \tag{A.30}$$

where $A_1(R_c) = 2^{R_c} - 1$ *and pdf* $f_{\Gamma_l}(\gamma_l) = \frac{1}{\bar{\Gamma}_l} \exp\left(-\frac{\gamma_l}{\bar{\Gamma}_l}\right), \forall i \in [1:L].$

Proof. Let us define a L-fold simplex as

$$\mathcal{S}_L := \left\{ (x_1, ..., x_L) \in \mathbb{R}^L : x_l \geq 0, \sum_{l \in [1:L]} \bar{\Gamma}_l x_l \leq A_1(R_c) \right\}. \qquad \text{(A.31)}$$

The geometric simplex volume is [Ell76]

$$\text{Vol}\,(\mathcal{S}_L) := \int \cdots \int_{\mathcal{S}_L} \mathrm{d}x_L...\mathrm{d}x_1 = \frac{1}{L!} \frac{(A_1(R_c))^L}{\prod_{l \in [1:L]} \bar{\Gamma}_l}. \qquad \text{(A.32)}$$

Now, the left hand side of Lemma 11 can be rewritten as

$$\Pr\left[0 \leq \sum_{l \in [1:L]} \Gamma_l \leq A_1(R_c) \right] = \Pr\left[0 \leq \sum_{l \in [1:L]} \bar{\Gamma}_l X_l \leq A_1(R_c) \right] \qquad \text{(A.33)}$$

$$= \int \cdots \int_{\mathcal{S}_L} \prod_{l \in [1:L]} \exp(-x_l)\mathrm{d}x_L...\mathrm{d}x_1 \qquad \text{(A.34)}$$

$$\leq \int \cdots \int_{\mathcal{S}_L} \mathrm{d}x_L...\mathrm{d}x_1. \qquad \text{(A.35)}$$

The steps can be justified as follows: in (A.33) and (A.34) we introduce the RV $X_l = \frac{\Gamma_l}{\bar{\Gamma}_l}$, with pdf $f_{X_l}(x_l) = \exp\left(-x_l\right), \forall i \in [1 : L]$; in (A.35) the exponential function can be upper-bounded by $\exp(-x) \leq 1$ for $x \geq 0$; (A.35) is the geometric simplex volume in (A.32). $\qquad \square$

A.4 Inverse Function

For $R_c \gg 1$, the term of the exponential sum function with the highest order in (5.12) is dominant. Thus, we approximate $A_L(R_c = x) \approx y = f(x)$ to

$$y = 2^x x^{(L-1)} \frac{(\ln(2))^{L-1}}{(L-1)!} = 2^x x^a b. \qquad \text{(A.36)}$$

We reformulate (A.36) as follows

$$2^x x^a = \frac{y}{b} \quad \Leftrightarrow \quad \frac{x}{a} 2^{\frac{x}{a}} = \frac{1}{a} \sqrt[a]{\frac{y}{b}} \quad \Leftrightarrow \quad \frac{x \ln(2)}{a} \exp\left(\frac{x \ln(2)}{a}\right) = \frac{\ln(2)}{a} \sqrt[a]{\frac{y}{b}}$$

(A.37)

$$\Leftrightarrow \quad z \exp(z) = \frac{\ln(2)}{a} \sqrt[a]{\frac{y}{b}} \quad \Leftrightarrow \quad x = \frac{az}{\ln(2)} = \frac{a}{\ln(2)} W\left(\frac{\ln(2)}{a} \sqrt[a]{\frac{y}{b}}\right),$$

(A.38)

where $W(\cdot)$ is the Lambert W function, i.e., $z = g^{-1}(z \exp(z)) = W(z \exp(z))$ is the inverse function of $g(z) = z \exp(z)$, for $z \geq -1$. For $z \geq e$, the Lambert W function is bounded by [HH07, Theorem 2.7]

$$W(z) = \ln(z) - \ln(\ln(z)) + \Theta\left(\frac{\ln(\ln(z))}{\ln(z)}\right).$$

(A.39)

Finally, with (A.38) and (A.39) we give an approximation of the inverse function as

$$A_L^{-1}(A_L) = R_c \approx \frac{L-1}{\ln(2)} \left[\ln(\zeta) - \ln(\ln(\zeta))\right], \quad \text{where } \zeta = \frac{\sqrt[L-1]{(L-1)! A_L}}{L-1}.$$

(A.40)

A.5 Lemma 12

Lemma 12. *For any $L \in \mathbb{N}\backslash\{1\}$ and $x > 0$,*

$$X_L(x) = (A_1(x))^L > L! \cdot A_L(x) = Y_L(x),$$

(A.41)

where $A_L(x)$ is given in Lemma 10.

Proof. For $x = 0$ we have $X_L(0) = 0$ and $Y_L(0) = 0$ in (A.41). Next, show that the slope of $X_L(x)$ is larger than the slope of $Y_L(x)$ for $x > 0$ and thus $X_L(x) > Y_L(x)$, $x \geq 0, \forall L$.

$$\frac{\mathrm{d}}{\mathrm{d}x} X_L(x) = \frac{\mathrm{d}}{\mathrm{d}x}\left[(2^x - 1)^L\right] = L 2^x \ln(2) (2^x - 1)^{L-1},$$

(A.42)

$$\frac{\mathrm{d}}{\mathrm{d}x} Y_L(x) = \frac{\mathrm{d}}{\mathrm{d}x}\left[L!(-1)^L\left(1 - 2^x \sum_{l \in [0:L-1]} \frac{1}{l!}(-x \ln(2))^l\right)\right]$$

(A.43)

$$= L! \ln(2) 2^x (-1)^{L+1}\left(\sum_{l \in [0:L-1]} (-1)^l \frac{1}{l!}(x \ln(2))^l\right)$$

$$+ \underbrace{\sum_{l \in [L-1]} (-1)^l \frac{1}{(l-1)!} (x \ln(2))^{l-1}}_{-\sum_{l \in [0:L-2]} (-1)^l \frac{1}{l!} (x \ln(2))^l}\Bigg) \tag{A.44}$$

$$= L! \ln(2) 2^x (-1)^{2L} \frac{1}{(L-1)!} (x \ln(2))^{L-1} = L 2^x \ln(2) (x \ln(2))^{L-1}. \tag{A.45}$$

We have to show that

$$(2^x - 1)^{L-1} > (x \ln(2))^{L-1} \quad \text{for } x > 0. \tag{A.46}$$

Since both sides in (A.46) are equal for $x = 0$ and have the same exponent, it is sufficient to show

$$\frac{\mathrm{d}}{\mathrm{d}x} (2^x - 1) > \frac{\mathrm{d}}{\mathrm{d}x} (x \ln(2)) \tag{A.47}$$

$$\ln(2) 2^x > \ln(2). \tag{A.48}$$

(A.48) holds for $x > 0$. $\qquad\square$

A.6 Derivation of Diversity-Multiplexing Tradeoff

Based on the outage probability analysis considered before the diversity gains for JD, SC, and MRC are given by

$$G_{\mathrm{d,JD}}(G_{\mathrm{r}}) = -\lim_{\bar{\Gamma} \to \infty} \frac{\mathrm{ld}\left(A_L(G_{\mathrm{r}}, \bar{\Gamma})\right) - L \, \mathrm{ld}\left(\bar{\Gamma}\right)}{\mathrm{ld}\left(L\bar{\Gamma}\right)} \tag{A.49}$$

$$= -\lim_{\bar{\Gamma} \to \infty} \left(G_{\mathrm{r}} \frac{\mathrm{ld}\left(L\bar{\Gamma}\right)}{\mathrm{ld}\left(L\bar{\Gamma}\right)} + \frac{\mathrm{ld}\left(\frac{1}{(L-1)!} \left(r \, \mathrm{ld}(L\bar{\Gamma})\right)^{(L-1)} (\ln(2))^{(L-1)}\right)}{\mathrm{ld}\left(L\bar{\Gamma}\right)} - \frac{L \, \mathrm{ld}\left(\bar{\Gamma}\right)}{\mathrm{ld}\left(L\bar{\Gamma}\right)} \right) \tag{A.50}$$

$$= L - G_{\mathrm{r}}, \tag{A.51}$$

$$G_{\mathrm{d,SC}}(G_{\mathrm{r}}) = -\lim_{\bar{\Gamma} \to \infty} \frac{L \, \mathrm{ld}\left(A_1(G_{\mathrm{r}}, \bar{\Gamma})\right) - L \, \mathrm{ld}\left(\bar{\Gamma}\right)}{\mathrm{ld}\left(L\bar{\Gamma}\right)} \tag{A.52}$$

$$= -L \lim_{\bar{\Gamma} \to \infty} \left(G_{\mathrm{r}} \frac{\mathrm{ld}\left(\bar{\Gamma}\right)}{\mathrm{ld}\left(L\bar{\Gamma}\right)} - \frac{\mathrm{ld}\left(\bar{\Gamma}\right)}{\mathrm{ld}\left(L\bar{\Gamma}\right)} \right) \tag{A.53}$$

$$= L \cdot (1 - G_{\mathrm{r}}), \quad \text{and} \tag{A.54}$$

$$G_{\mathrm{d,MRC}}(G_{\mathrm{r}}) = -\lim_{\bar{\Gamma} \to \infty} \frac{L \, \mathrm{ld}\left(A_1(G_{\mathrm{r}}, \bar{\Gamma})\right) - \mathrm{ld}\left(L!\right) - L \, \mathrm{ld}\left(\bar{\Gamma}\right)}{\mathrm{ld}\left(L\bar{\Gamma}\right)} \tag{A.55}$$

$$= -L \lim_{\bar{\Gamma}\to\infty} \left(G_{\mathrm{r}} \frac{\mathrm{ld}\left(\bar{\Gamma}\right)}{\mathrm{ld}\left(L\bar{\Gamma}\right)} - \frac{\mathrm{ld}\left(L!\right)}{L\,\mathrm{ld}\left(L\bar{\Gamma}\right)} - \frac{\mathrm{ld}\left(\bar{\Gamma}\right)}{\mathrm{ld}\left(L\bar{\Gamma}\right)} \right) \tag{A.56}$$

$$= L \cdot (1 - G_{\mathrm{r}}), \tag{A.57}$$

respectively. The steps can be justified as follows: (A.49), (A.52), and (A.55) are given by substituting (5.11), (5.18), (5.24) into (5.48); in (A.50) we use the infinite SNR properties of $A_L\left(G_{\mathrm{r}}, \bar{\Gamma}\right)$ in (A.60) and some algebraic manipulations; for infinite SNR the properties (A.61) hold which yields (A.51); in (A.53) and (A.56) we use the infinite SNR property of $A_1\left(G_{\mathrm{r}}, \bar{\Gamma}\right)$ in (A.58) and some algebraic manipulations; for infinite SNR the properties in (A.61) hold which yields (A.54) and (A.57).

Substituting (5.47) into (5.12) the constants $A_L(G_{\mathrm{r}}, \bar{\Gamma})$ and its special case $A_1(G_{\mathrm{r}}, \bar{\Gamma})$ can be given depending on the multiplexing gain r by

$$\lim_{\bar{\Gamma}\to\infty} A_1(G_{\mathrm{r}}, \bar{\Gamma}) = \lim_{\bar{\Gamma}\to\infty} \left(2^{G_{\mathrm{r}}\,\mathrm{ld}\left(\bar{\Gamma}\right)} - 1 \right) = \lim_{\bar{\Gamma}\to\infty} 2^{G_{\mathrm{r}}\,\mathrm{ld}\left(\bar{\Gamma}\right)}, \tag{A.58}$$

$$\lim_{\bar{\Gamma}\to\infty} A_L(G_{\mathrm{r}}, \bar{\Gamma}) = \lim_{\bar{\Gamma}\to\infty} \left((-1)^L + 2^{G_{\mathrm{r}}\,\mathrm{ld}\left(L\bar{\Gamma}\right)} \right.$$

$$\left. \times \sum_{l\in[0:L-1]} (-1)^{L+l+1} \frac{1}{l!} \left(r\,\mathrm{ld}(L\bar{\Gamma}) \right)^l (\ln(2))^l \right) \tag{A.59}$$

$$= \lim_{\bar{\Gamma}\to\infty} 2^{G_{\mathrm{r}}\,\mathrm{ld}\left(L\bar{\Gamma}\right)} \frac{1}{(L-1)!} \left(r\,\mathrm{ld}(L\bar{\Gamma}) \right)^{(L-1)} (\ln(2))^{(L-1)}, \tag{A.60}$$

where (A.60) can be justified with the infinite SNR properties in (A.62). Further properties for infinite SNR are:

$$\lim_{\bar{\Gamma}\to\infty} \frac{\mathrm{ld}\left(\bar{\Gamma}\right)}{\mathrm{ld}\left(L\bar{\Gamma}\right)} = 1, \quad \lim_{\bar{\Gamma}\to\infty} \frac{(L-1)\,\mathrm{ld}\left(\mathrm{ld}\left(L\bar{\Gamma}\right)\right)}{\mathrm{ld}\left(L\bar{\Gamma}\right)} = 0, \quad \lim_{\bar{\Gamma}\to\infty} \frac{\mathrm{ld}(L!)}{L\,\mathrm{ld}\left(L\bar{\Gamma}\right)} = 0, \tag{A.61}$$

$$\lim_{\bar{\Gamma}\to\infty} \left(\mathrm{ld}(L\bar{\Gamma})\right)^{(L-1)} \gg \lim_{\bar{\Gamma}\to\infty} \left(\mathrm{ld}(L\bar{\Gamma})\right)^{(L-l)} \text{ for } l = [2 : L]. \tag{A.62}$$

List of Abbreviations

5G	fifth-generation mobile networks
AWGN	additive white Gaussian noise
BAC	binary asymmetric channel
BS	base station
BMS	binary memoryless source
BPSK	binary phase shift keying
BSC	binary symmetric channel
CFO	carrier frequency offset
cdf	cumulative distribution function
CEO	chief executive officer
CI	conditionally independent
CSI	channel state information
D2D	device to device
DF	decode-and-forward
DLC	distributed lossless compression
DMS	discrete memoryless source
DMC	discrete memoryless channel
DMT	diversity-multiplexing tradeoff
DTC	distributed turbo code
FFT	fast Fourier transform
FER	frame-error-rate
IFFT	inverse fast Fourier transform
IE	intra-link error
FC	fusion center
i.i.d.	independent and identically distributed
IoT	internet of things
IoV	internet of vehicles
JD	joint decoding
JTD	joint turbo decoder
LDPC	low-density parity-check
LF	lossy forwarding

LLR log likelihood ratio
LTF long training field
M2M machine to machine
MCo multi-connectivity
MIMO multiple-input multiple-output
MRC maximal-ratio combining
MSCC multiterminal source-channel code
MSE mean square error
OFDM orthogonal frequency-division multiplexing
pdf probability density function
pmf probability mass function
RV random variable
SFO sampling frequency offset
SC selection combining
SCo single-connectivity
SNR signal-to-noise ratio
STF short training field
SNRCC systematic non-recursive convolutional code
SRCC systematic recursive convolutional code
URLLC ultra-reliable low latency communications
WLAN wireless local area network
WSN wireless sensor network

List of Symbols

Symbols

A	Channel gain
B	Bandwidth
C	Capacity
d	Distance
G	SNR gain
G_c	Coding gain
G_d	Diversity gain
$\bar{G}_d$	Relative diversity gain
G_r	Multiplexing gain
$\bar{G}_r$	Relative multiplexing gain
G_{SNRCC}	Generator polynomial of SNRCC
G_{SRCC}	Generator polynomial of SRCC
H	Entropy
I	Mutual information
k	Length of source sequence
L	Link/node number
L_a	A priori LLR
L_{ch}	Channel LLR
L_e	Extrinsic LLR
L_{JD}	Correlation Loss
L_p	Posteriori LLR
M	Message size
n	Length of channel codeword sequence
N	Noise
N_0	Noise power
P	Power constraint, transmit power
P_{ACC}	Doping ratio
P_e	Probability of error
P^{out}	Outage probability

$\tilde{P}^{\text{out}}$	Asymptotic outage probability
R	Rate
R_{c}	Spectral efficiency
R_{cu}	Channel usage
S	Source
$\hat{S}$	Source estimate
T	Throughput
U	Auxiliary RV
X	Transmitted channel codeword
Y	Received channel codeword
$\mathcal{C}$	Capacity region
$\mathcal{D}$	Distortion constraint
$\mathcal{R}_{\text{GP}}$	Gelfand-Pinsker rate region
$\mathcal{R}_{\text{SW}}$	Slepian-Wolf rate region
Γ	Signal-to-noise ratio
ϵ	Crossover probability
η	Path-loss exponent
κ	Auxiliary variable
ρ	Correlation coefficient
σ	Variance

Functions

$d(\cdot, \cdot)$	Distortion measure
$f(\cdot)$	Encoder
$f_{\text{c}}(\cdot)$	Update function
$\text{ld}(\cdot)$	Binary logarithm
$h(\cdot)$	Binary entropy function
$h^{-1}(\cdot)$	Inverse binary entropy function
$\ln(\cdot)$	Natural logarithm
$Q(\cdot)$	Gaussian complementary cdf
$Q^{-1}(\cdot)$	Inverse Gaussian complementary cdf
$\mathbb{E}$	Expectation
$\mathcal{N}(\cdot, \cdot)$	Normal distribution
$\Re(\cdot)$	Real part

$\delta(\cdot)$	Indicator function
$\rho(\cdot)$	Cost function
$\phi(\cdot)$	Decoder
$\psi(\cdot)$	Capacity of complex Gaussian channel

List of Figures

List of Tables

Bibliography

[AK75]   R. Ahlswede and J. Körner. „Source coding with side information and a converse for degraded broadcast channels". In: *IEEE Trans. Inf. Theory* 21.6 (Nov. 1975), pp. 629–637 (cit. on pp. 10, 13, 31).

[AM12]   Khoirul Anwar and Tad Matsumoto. „Accumulator-Assisted Distributed Turbo Codes for Relay Systems Exploiting Source-Relay Correlation". In: *IEEE Commun. Letters* 16.7 (July 2012), pp. 1114–1117 (cit. on pp. 2, 22, 23, 25, 26, 31, 49, 50, 53, 61, 62, 84, 85, 108).

[Ari09]   E. Arikan. „Channel Polarization: A Method for Constructing Capacity-Achieving Codes for Symmetric Binary-Input Memoryless Channels". In: *IEEE Trans. Inf. Theory* 55.7 (July 2009), pp. 3051–3073 (cit. on p. 108).

[ARS16]   M. Agiwal, A. Roy, and N. Saxena. „Next Generation 5G Wireless Networks: A Comprehensive Survey". In: *IEEE Commun. Surveys Tutorials* 18.3 (Mar. 2016), pp. 1617–1655 (cit. on p. 1).

[AT06]   Olufunmilola Awoniyi and Fouad A. Tobagi. „Packet Error Rate in OFDM-based Wireless LANs Operating in Frequency Selective Channels". In: Barcelona, Spain, Apr. 2006, pp. 1–13 (cit. on p. 95).

[AY07]   Ameer. Ahmed. Abbasi and Mohamed. Younis. „A Survey on Clustering Algorithms for Wireless Sensor Networks". In: *Elsevier Journal of Computer Communications* 30 (Oct. 2007), pp. 2826–2841 (cit. on p. 1).

[Bah+74]   L. Bahl, J. Cocke, F. Jelinek, and J. Raviv. „Optimal Decoding of Linear Codes for Minimizing Symbol Error Rate (Corresp.)" In: *IEEE Trans. Inform. Theory* 20.2 (Mar. 1974), pp. 284–287 (cit. on p. 23).

[Bai+13]   B. Bai, W. Chen, K. B. Letaief, and Z. Cao. „Outage Exponent: A Unified Performance Metric for Parallel Fading Channels". In: *IEEE Trans. Inf. Theory* 59.3 (Mar. 2013), pp. 1657–1677 (cit. on pp. 68, 70–72, 82).

[Ber77]   Toby Berger. „Multiterminal source coding". In: *Lectures presented at CISM Summer School on the Information Theory Approach to Communications* 229 (1977), pp. 171–231 (cit. on pp. 10, 18).

[BH06]   Norman C Beaulieu and Jeremiah Hu. „A closed-form expression for the outage probability of decode-and-forward relaying in dissimilar Rayleigh fading channels". In: *IEEE Commun. Letters* 10.12 (Dec. 2006), pp. 813 –815 (cit. on pp. 2, 31, 42).

[BH11]   N. C. Beaulieu and K. T. Hemachandra. „Novel Simple Representations for Gaussian Class Multivariate Distributions With Generalized Correlation". In: *IEEE Trans. Inf. Theory* 57.12 (Dec. 2011), pp. 8072–8083 (cit. on pp. 90–92).

[Bou+10] J. J. Boutros, A. Guillen i Fabregas, E. Biglieri, and G. Zemor. „Low-Density Parity-Check Codes for Nonergodic Block-Fading Channels". In: *IEEE Trans. Inf. Theory* 56.9 (Sept. 2010), pp. 4286–4300 (cit. on p. 108).

[BPS98]   E. Biglieri, J. Proakis, and S. Shamai. „Fading channels: information-theoretic and communications aspects". In: *IEEE Trans. Inf. Theory* 44.6 (Oct. 1998), pp. 2619–2692 (cit. on p. 18).

[CAM13a] M. Cheng, K. Anwar, and T. Matsumoto. „Outage probability of a relay strategy allowing intra-link errors utilizing Slepian-Wolf theorem". In: *EURASIP J. Adv. Signal Process* 1 (Feb. 2013), pp. 1–12 (cit. on pp. 4, 21).

[CAM13b] Meng Cheng, Khoirul Anwar, and Tad Matsumoto. „Outage based power allocation: Slepian-Wolf relaying viewpoint". In: *Proc. IEEE Global Communications Conference Workshops (GCW)*. Atlanta, GA, USA, Dec. 2013, pp. 807–811 (cit. on p. 53).

[Che19]   Yuhou Chen. *Outage Analysis and Code Design for Multi-Connectivity for Correlated Fading Channels*. Diploma thesis. Germany, 2019 (cit. on pp. 28, 93).

[Cov75]   T. Cover. „A proof of the data compression theorem of Slepian and Wolf for ergodic sources (Corresp.)" In: *IEEE Trans. Inf. Theory* 21.2 (Mar. 1975), pp. 226–228 (cit. on pp. 10, 12).

[CT05]   Yunxia Chen and C. Tellambura. „Infinite series representations of the trivariate and quadrivariate Rayleigh distribution and their applications". In: *IEEE Trans. Commun.* 53.12 (Dec. 2005), pp. 2092–2101 (cit. on p. 90).

[CT06]   Thomas M. Cover and Joy A. Thomas. *Elements of Information Theory*. 2. ed. Wiley-Interscience, 2006 (cit. on pp. 58, 72).

[CYV05]   Zhuo Chen, Jinhong Yuan, and Branka Vucetic. „Analysis of transmit antenna selection/maximal-ratio combining in Rayleigh fading channels". In: *IEEE Trans. Veh. Technol.* 54.4 (Apr. 2005), pp. 1312–1321 (cit. on pp. 70, 73).

[DG08]   Tolga M Duman and Ali Ghrayeb. *Coding for MIMO Communication Systems*. John Wiley & Sons, 2008 (cit. on pp. 70, 72, 73).

[DRT07]   P. Dharmawansa, N. Rajatheva, and C. Tellambura. „Infinite series representations of the trivariate and quadrivariate Nakagami-m distributions". In: *IEEE Trans. Wireless Commun.* 6.12 (Dec. 2007), pp. 4320–4328 (cit. on p. 90).

[DZ10]   Amir Dembo and Ofer Zeitouni. *Large deviations techniques and applications, volume 38 of Stochastic Modelling and Applied Probability*. Springer-Verlag, Berlin, 2010 (cit. on p. 72).

[EGK11]   Abbas El Gamal and Young-Han Kim. *Network Information Theory*. Cambridge University Press, 2011 (cit. on pp. 12, 18, 31, 34, 40).

[Ehr+17]   Marcus Ehrig, Markus Petri, Vladica Sark, et al. „Reliable Wireless Communication and Positioning enabling Mobile Control and Safety Applications in Industrial Environments". In: Toronto, Canada, Mar. 2017 (cit. on pp. 1, 95).

[Ell76]   Richard S Ellis. „Volume of an N-Simplex by multiple Integration." In: *Elemente der Mathematik* 31 (1976), pp. 57–59 (cit. on p. 115).

[ESK04]   Vinko Erceg, Laurent Schumacher, and Persefoni Kyritsi. „TGn Channel Models". In: *IEEE 802.11-03/940r4* (2004) (cit. on p. 96).

[Gal62]   Robert Gallager. „Low-density parity-check codes". In: *IRE Trans. Inf. Theory* 8.1 (July 1962), pp. 21–28 (cit. on p. 108).

[GFZ05]   J. Garcia-Frias and Ying Zhao. „Near-Shannon/Slepian-Wolf Performance for Unknown Correlated Sources Over AWGN Channels". In: *IEEE Trans. Commun.* 53.4 (Apr. 2005), pp. 555–559 (cit. on pp. 2, 31).

[Gol05]   Andrea Goldsmith. *Wireless Communications*. Cambridge University Press, 2005 (cit. on p. 98).

[GP79]   Sergei Izrail'evich Gelfand and Mark Semenovich Pinsker. „Coding of sources on the basis of observations with incomplete information". In: *Problemy Peredachi Informatsii* 15.2 (Feb. 1979), pp. 45–57 (cit. on pp. 13, 14, 32).

[GR14]   Izrail Solomonovich Gradshteyn and Iosif Moiseevich Ryzhik. *Table of integrals, series, and products*. Academic press, 2014 (cit. on p. 72).

[Gri14]   Michael Grieger. „Uplink Joint Detection in a Realistic Macro Cellular Environment". PhD thesis. Germany: TU Dresden, 2014 (cit. on pp. 100, 102).

[Gu+07]   W. Gu, R. Koetter, M. Effros, and T. Ho. „On Source Coding with Coded Side Information for a Binary Source with Binary Side Information". In: *Proc. IEEE International Symposium on Information Theory (ISIT)*. Nice, France, June 2007, pp. 1456–1460 (cit. on pp. 32, 35, 36).

[Hay09]   Masahito Hayashi. „Information spectrum approach to second-order coding rate in channel coding". In: *IEEE Trans. Inf. Theory* 55.11 (2009), pp. 4947–4966 (cit. on p. 107).

[He+18]   J. He, V. Tervo, X. Zhou, et al. „A Tutorial on Lossy Forwarding Cooperative Relaying". In: *IEEE Communications Surveys Tutorials* (Aug. 2018), pp. 1–22 (cit. on p. 31).

[HET97]   L. Hazy and M. El-Tanany. „Synchronization of OFDM systems over frequency selective fading channels". In: *Proc. IEEE Vehicular Technology Conference (VTC)*. Phoenix, AZ, USA, May 1997, pp. 2094–2098 (cit. on p. 99).

[HH07]   Abdolhossein Hoorfar and Mehdi Hassani. „Approximation of the Lambert W function and hyperpower function". In: *Research report collection* 10.2 (Feb. 2007) (cit. on pp. 75, 116).

[Jan09]   S. Jana. „Alphabet sizes of auxiliary random variables in canonical inner bounds". In: *Proc. 43rd Annual Conference on Information Sciences and Systems (CISS)*. Baltimore, MD, USA, Mar. 2009, pp. 67–71 (cit. on pp. 32, 35).

[JP04]   A. Jindal and K. Psounis. „Modeling spatially-correlated sensor network data". In: *Proc. IEEE Sensor and Ad Hoc Communications and Networks (SECON)*. Santa Clara, CA, USA, Oct. 2004, pp. 162–171 (cit. on p. 3).

[JYY18]   L. Jin, P. Yang, and H. Yang. „Distributed Joint Source-Channel Decoding Using Systematic Polar Codes". In: *IEEE Commun. Lett.* 22.1 (Jan. 2018), pp. 49–52 (cit. on p. 108).

[Kir+15]   F. Kirsten, D. Öhmann, M. Simsek, and G. P. Fettweis. „On the utility of macro- and microdiversity for achieving high availability in wireless networks". In: *Proc. IEEE International Symposium on Personal, Indoor, and Mobile Radio Communications (PIMRC)*. Hong Kong, Aug. 2015, pp. 1723–1728 (cit. on p. 67).

[KM79]   J. Körner and K. Marton. „How to encode the modulo-two sum of binary sources (Coresp.)" In: *IEEE Trans. Inf. Theory* 25.2 (Mar. 1979), pp. 219–221 (cit. on p. 32).

[KV12]   V. Kostina and S. Verdú. „Fixed-Length Lossy Compression in the Finite Blocklength Regime". In: *IEEE Trans. Inf. Theory* 58.6 (June 2012), pp. 3309–3338 (cit. on p. 107).

[KV13]   V. Kostina and S. Verdú. „Lossy Joint Source-Channel Coding in the Finite Blocklength Regime". In: *IEEE Trans. Inf. Theory* 59.5 (May 2013), pp. 2545–2575 (cit. on p. 107).

[Li09]   Y. Li. „Distributed coding for cooperative wireless networks: An overview and recent advances". In: *IEEE Communications Magazine* 47.8 (Aug. 2009), pp. 71–77 (cit. on p. 2).

[Mal16]   K. Mallinson. *The path to 5G: as much evolution as revolution*. May 2016. URL: http://www.3gpp.org/news-events/3gpp-news/1774-5g_wiseharbour (cit. on p. 1).

[Mol12]   Andreas F. Molisch. *Wireless Communications*. John Wiley & Sons, 2012 (cit. on pp. 2, 67, 75).

[MW02]   R. K. Mallik and M. Z. Win. „Analysis of hybrid selection/maximal-ratio combining in correlated Nakagami fading". In: *IEEE Trans. Commun.* 50.8 (Aug. 2002), pp. 1372–1383 (cit. on p. 90).

[Nar06]   R. Narasimhan. „Finite-SNR Diversity-Multiplexing Tradeoff for Correlated Rayleigh and Rician MIMO Channels". In: *IEEE Trans. Inf. Theory* 52.9 (Sept. 2006), pp. 3965–3979 (cit. on p. 68).

[NFR07]   K. D. Nguyen, A. G. i. Fabregas, and L. K. Rasmussen. „Analysis and Computation of the Outage Probability of Discrete-Input Block-Fading Channels". In: *Proc. IEEE International Symposium on Information Theory (ISIT)*. Nice, France, June 2007, pp. 1196–1200 (cit. on p. 22).

[NP16]   Jimmy J Nielsen and Petar Popovski. „Latency analysis of systems with multiple interfaces for ultra-reliable M2M communication". In: *Proc. IEEE 17th International Workshop on Signal Processing Advances in Wireless Communications (SPAWC)*. Edinburgh, UK, July 2016, pp. 1–6 (cit. on p. 67).

[Ooh05]   Y. Oohama. „Rate-distortion theory for Gaussian multiterminal source coding systems with several side informations at the decoder". In: *IEEE Trans. Inf. Theory* 51.7 (July 2005), pp. 2577–2593 (cit. on p. 32).

[Ooh08]   Yasutada Oohama. „Multiterminal source coding problem with several side informations at the decoder". In: *Proc. IEEE International Symposium on Information Theory (ISIT)*. Toronto, Canada, July 2008, pp. 687–691 (cit. on pp. 13, 32).

[Ooh97]   Y. Oohama. „Gaussian multiterminal source coding". In: *IEEE Trans. Inf. Theory* 43.6 (Nov. 1997), pp. 1912–1923 (cit. on p. 18).

[PD16]   A. Panajotović and D. Drača. „Capacity of OFDM-based WLAN system with SC diversity". In: *Proc. IEEE International Symposium on Industrial Electronics (INDEL)*. Banja Luka, Bosnia Herzegovina, Nov. 2016, pp. 1–6 (cit. on p. 95).

[Poc+15]   Guillermo Pocovi, Beatriz Soret, Mads Lauridsen, Klaus I Pedersen, and Preben Mogensen. „Signal quality outage analysis for ultra-reliable communications in cellular networks". In: *Proc. IEEE Global Communications Conference Workshops (GCW)*. San Diego, CA, USA, Dec. 2015, pp. 1–6 (cit. on p. 67).

[PPV10]   Yury Polyanskiy, H Vincent Poor, and Sergio Verdú. „Channel coding rate in the finite blocklength regime". In: *IEEE Trans. Inf. Theory* 56.5 (May 2010), pp. 2307–2359 (cit. on p. 107).

[PS06]   S. Pfletschinger and F. Sanzi. „Error Floor Removal for Bit-Interleaved Coded Modulation with Iterative Detection". In: *IEEE Trans. Wireless Commun.* 5.11 (Nov. 2006), pp. 3174–3181 (cit. on p. 23).

[RA12]   Abolfazl Razi and Ali Abedi. „Adaptive Bi-Modal Decoder for Binary Source Estimation with Two Observers". In: Princeton, NJ, USA, Mar. 2012, pp. 1–5 (cit. on p. 25).

[RG07]   A. Roumy and D Gesbert. „Optimal Matching in Wireless Sensor Networks". In: *IEEE Journal of Selected Topics in Signal Processing* 4.1 (Dec. 2007), pp. 725–735 (cit. on p. 53).

[Sch+17]   P. Schulz, M. Matthe, H. Klessig, et al. „Latency Critical IoT Applications in 5G: Perspective on the Design of Radio Interface and Network Architecture". In: *IEEE Communications Magazine* 55.2 (Feb. 2017), pp. 70–78 (cit. on p. 1).

[Sch17]   Nick Schwarzenberg. *A Simulation Framework for Error Rates of Multi-Connectivity Considering Multiplexing Diversity Trade-Off*. Diploma thesis. Germany, 2017 (cit. on pp. 28, 97, 99).

[Sha48]   Claude Elwood Shannon. „A mathematical theory of communication". In: *Bell System Technical Journal* 27 (1948), pp. 379–423 (cit. on pp. 16, 19, 40).

[Sha59a]   Claude E Shannon. „Coding theorems for a discrete source with a fidelity criterion". In: *IRE Nat. Conv. Rec* 4.142-163 (1959), p. 1 (cit. on pp. 40, 107).

[Sha59b]   Claude E Shannon. „Probability of error for optimal codes in a Gaussian channel". In: *Bell System Technical Journal* 38.3 (1959), pp. 611–656 (cit. on p. 19).

[SW73]   D. Slepian and J.K. Wolf. „Noiseless Coding of Correlated Information Sources". In: *IEEE Trans. Inf. Theory* 19.4 (July 1973), pp. 471–480 (cit. on pp. 10, 11, 42, 53).

[Tun78]   Sui-Yin Tung. „Multiterminal source coding". PhD thesis. Cornell Univ., School of Elect. Eng., Ithaca, 1978 (cit. on pp. 10, 18).

[TV05]   David Tse and Pramod Viswanath. *Fundamentals of Wireless Communi-cation*. Cambridge University Press, 2005 (cit. on pp. 68, 70, 71, 78, 79).

[TVW10]   S. Tavildar, P. Viswanath, and A. B. Wagner. „The Gaussian Many-Help-One Distributed Source Coding Problem". In: *IEEE Trans. Inf. Theory* 56.1 (Jan. 2010), pp. 564–581 (cit. on p. 32).

[WG03]   Zhengdao Wang and Georgios B Giannakis. „A simple and general parameterization quantifying performance in fading channels". In: *IEEE Trans. Commun.* 51.8 (Aug. 2003), pp. 1389–1398 (cit. on pp. 22, 57, 71).

[Wyn73]   A. Wyner. „A theorem on the entropy of certain binary sequences and applications: part II". In: *IEEE Trans. Inf. Theory* 19.6 (Nov. 1973), pp. 769–772 (cit. on p. 38).

[Wyn75]   A.D. Wyner. „On source coding with side information at the decoder". In: *IEEE Trans. Inf. Theory* 21.3 (May 1975), pp. 294–300 (cit. on pp. 10, 13, 31).

[WZ76]   A. Wyner and J. Ziv. „The rate-distortion function for source coding with side information at the decoder". In: *IEEE Trans. Inf. Theory* 22.1 (Jan. 1976), pp. 1–10 (cit. on p. 10).

[XL07]   J. J. Xiao and Z. Q. Luo. „Multiterminal Source-Channel Communication Over an Orthogonal Multiple-Access Channel". In: *IEEE Trans. Inf. Theory* 53.9 (Sept. 2007), pp. 3255–3264 (cit. on pp. 4, 17, 18).

[XLC04]   Z. Xiong, A.D. Liveris, and S. Cheng. „Distributed source coding for sensor networks". In: *IEEE Signal Processing Magazine* 21.5 (Sept. 2004), pp. 80–94 (cit. on p. 53).

[Yan+14]   Wei Yang, Giuseppe Durisi, Tobias Koch, and Yury Polyanskiy. „Quasi-static multiple-antenna fading channels at finite blocklength". In: *IEEE Trans. Inf. Theory* 60.7 (June 2014), pp. 4232–4265 (cit. on p. 107).

[ZA06]   Guang-Chong Zhu and F. Alajaji. „Joint source-channel turbo coding for binary Markov sources". In: *IEEE Trans. Wireless Commun.* 5.5 (May 2006), pp. 1065–1075 (cit. on p. 40).

[ZB06a]   X. Zhang and N. C. Beaulieu. „Outage Probability of MRC Corrupted by Multiple Unequal-Power Interferers and Correlated Rayleigh Fading". In: *Proc. IEEE Annual Wireless and Microwave Technology Conference (WAMICON)*. Clearwater Beach, FL, USA, Dec. 2006, pp. 1–4 (cit. on p. 90).

[ZB06b]   X. Zhang and N. C. Beaulieu. „Performance Analysis of Generalized Selection Combining in Generalized Correlated Nakagami-m Fading". In: *IEEE Trans. Commun.* 54.11 (Nov. 2006), pp. 2103–2112 (cit. on p. 90).

[Zho+14]   Xiaobo Zhou, Meng Cheng, Xin He, and Tad Matsumoto. „Exact and Approximated Outage Probability Analyses for Decode-and-Forward Relaying System Allowing Intra-Link Errors". In: *IEEE Trans. Wireless Commun.* 13.12 (Dec. 2014), pp. 7062–7071 (cit. on pp. 4, 21, 31, 40, 53).

[Zho13]   Xiaobo Zhou. „Multi-dimensional correlation exploited cooperative wireless communications". PhD thesis. Japan: JAIST, 2013 (cit. on p. 1).

[Zhu+15]   B. Zhu, J. Cheng, N. Al-Dhahir, and L. Wu. „Bounds on outage probabilities for diversity receptions over arbitrarily correlated Rician channels". In: *Proc. IEEE International Conference on Computing, Networking and Communications (ICNC)*. Garden Grove, CA, USA, Feb. 2015, pp. 972–976 (cit. on p. 90).

[ZT03]   Lizhong Zheng and D. N. C. Tse. „Diversity and multiplexing: a fundamental tradeoff in multiple-antenna channels". In: *IEEE Trans. Inf. Theory* 49.5 (May 2003), pp. 1073–1096 (cit. on pp. 68, 78).

[Bib13]   M. Bibinger. „Notes on the sum and maximum of independent exponentially distributed random variables with different scale parameters". In: (2013) (cit. on p. 74).

[Mat17]   MathWorks Inc. *WLAN system toolbox - MATLAB*. 2017. URL: `https://web.archive.org/web/20170718214413/https://www.mathworks.com/products/wlan-system.html` (cit. on p. 95).

[Öhm17]   David Öhmann. „High Reliability in Wireless Networks Through Multi-Connectivity". PhD thesis. Germany: TU Dresden, 2017 (cit. on pp. 4, 67).

Publications of the Author

Journal Publications

[Gon+17]   D. C. González, A. Wolf, L. L. Mendes, J. C. S. Santos Filho, and G. Fettweis. „An Efficient Power Allocation Scheme for Multirelay Systems with Lossy Intra-Links“. In: *IEEE Trans. Commun.* 65.4 (Apr. 2017), pp. 1549–1560 (cit. on p. 29).

[Gon+18]   D. C. González, A. Wolf, L. L. Mendes, et al. „Allocating Power to Lossy-Forward Relays“. In: *IEEE Commun. Lett.* 22.7 (June 2018), pp. 1502–1505 (cit. on p. 29).

[Sch+19a] P. Schulz, A. Wolf, G. Fettweis, et al. „Efficient and Flexible Network Architectures for Demanding Performance Requirements in 5G“. In: *IEEE Vehicular Technology Magazine* 14.2 (June 2019), pp. 33–43 (cit. on p. 29).

[Wol+16]   A. Wolf, D. C. González, J. C. S. Santos Filho, and G. Fettweis. „Asymptotically Optimal Power Allocation for WSNs With Mutually Correlated Sensing Data“. In: *IEEE Commun. Lett.* 20.7 (July 2016), pp. 1317–1320 (cit. on p. 28).

[Wol+17b] A. Wolf, D. C. González, M. Dörpinghaus, et al. „Outage Analysis for Decode-and-Forward Multirelay Systems Allowing Intra-Link Errors“. In: *IEEE Wireless Commun. Lett.* 6.6 (Dec. 2017), pp. 758–761 (cit. on p. 28).

[Wol+19]   A. Wolf, P. Schulz, M. Dörpinghaus, J. C. S. Santos Filho, and G. Fettweis. „How Reliable and Capable is Multi-Connectivity?“ In: *IEEE Trans. Commun.* 67.2 (Feb. 2019), pp. 1506–1520 (cit. on pp. 28, 100).

[ZWM19]   L. Zhou, A. Wolf, and M. Motani. „On Lossy Multi-Connectivity: Finite Blocklength Performance and Second-Order Asymptotics“. In: *IEEE Journal on Selected Areas in Communications* 37.4 (Apr. 2019), pp. 735–748 (cit. on pp. 29, 107).

[San+18] J. C. S. Santos Filho, D. C. González, A. Wolf, et al. „SNR-Aware Power Allocation Scheme for Lossy-Forward Relaying Systems". In: *IEEE Wireless Commun. Lett.* 7.6 (Dec. 2018), pp. 1018–1021 (cit. on p. 29).

Conference Publications

[Gon+16] D. C. González, A. Wolf, J. C. S. Santos Filho, and G. Fettweis. „Efficient Power Allocation for Multiple Relays with Lossy Intra-Links and Distributed Source Coding". In: *Proc. the Brazilian Telecommunications and Signal Processing Symposium (SBrT)*. Santarém-PA, Brazil, Sept. 2016 (cit. on p. 29).

[Sch+18] N. Schwarzenberg, A. Wolf, N. Franchi, and G. Fettweis. „Quantifying the Gain of Multi-Connectivity in Wireless LAN". In: *Proc. IEEE European Conference on Networks and Communications (EuCNC)*. Ljubljana, Slovenia, June 2018, pp. 1–5 (cit. on pp. 28, 99).

[Sch+19b] N. Schwarzenberg, F. Burmeister, A. Wolf, N. Franchi, and G. Fettweis. „Joint Synchronization in Macro-Diversity Multi-Connectivity Networks". In: *Proc. IEEE 90th Vehicular Technology Conference (VTC) (accepted)*. Honolulu, HI, USA, Sept. 2019, pp. 1–6 (cit. on p. 29).

[Ter+16] V. Tervo, X. He, X. Zhou, et al. „An error rate model of relay communications with lossy forwarding and joint decoding". In: *Proc. IEEE International Conference on Communications (ICC)*. Kuala Lumpur, Malaysia, May 2016, pp. 528–533 (cit. on p. 29).

[WMF15]   A. Wolf, M. Matthé, and G. Fettweis. „Improved source correlation estimation in wireless sensor networks". In: *Proc. IEEE International Conference on Communications Workshop (ICCW)*. London, UK, June 2015, pp. 2121–2126 (cit. on p. 29).

[Wol+15] A. Wolf, M. Matthé, A. Festag, and G. Fettweis. „Outage based power allocation for a lossy forwarding two-relaying system". In: *2015 IEEE 20th International Workshop on Computer Aided Modelling and Design of Communication Links and Networks (CAMAD)*. Surrey, UK, Sept. 2015 (cit. on p. 29).

[Wol+17a] A. Wolf, P. Schulz, D. Öhmann, M. Dörpinghaus, and G. Fettweis. „On The Gain of Joint Decoding for Multi-Connectivity". In: *Proc. IEEE Global Communications Conference (GC)*. Singapore, Dec. 2017 (cit. on p. 28).

[Wol+18a] A. Wolf, D. C. González, M. Dörpinghaus, J. C. S. Santos Filho, and G. Fettweis. „On The Binary Lossless Many-Help-One Problem with Independently Degraded Helpers". In: *Proc. IEEE 56th Annual Allerton Conference on Communication, Control, and Computing (Allerton)*. Monticello, IL, USA, Oct. 2018 (cit. on p. 28).

[Wol+18b] A. Wolf, P. Schulz, D. Öhmann, M. Dörpinghaus, and G. Fettweis. „Rate-Reliability Tradeoff for Multi-Connectivity". In: *Proc. IEEE Wireless Communications and Networking Conference (WCNC)*. Barcelona, Spain, Apr. 2018 (cit. on p. 29).

[ZWM18] L. Zhou, A. Wolf, and M. Motani. „On the Finite Blocklength Performance of Lossy Multi-Connectivity". In: *Proc. IEEE Global Communications Conference (GC)*. Abu Dhabi, UAE, Dec. 2018 (cit. on p. 29).